Tucholke, B.E., Sibuet, J.-C., and Klaus, A. (Eds.)
Proceedings of the Ocean Drilling Program, Scientific Results Volume 210

9. Evidence of Continental Breakup from the Newfoundland Rifted Margin (Ocean Drilling Program Leg 210): Lower Cretaceous Seafloor Formed by Exhumation of Subcontinental Mantle Lithosphere and the Transition to Seafloor Spreading[1]

Alastair H.F. Robertson[2]

ABSTRACT

Drilling of the distal Newfoundland margin at Ocean Drilling Program Site 1277 recovered part of the transition between exhumed subcontinental mantle lithosphere and normal mid-ocean-ridge basalt (N-MORB) volcanism perhaps related to the initiation of seafloor spreading, which may have occurred near the Aptian/Albian boundary, coincident with the final separation of subcontinental mantle lithosphere. Subcontinental mantle lithosphere was recovered near the crest of a basement high, the Mauzy Ridge. This ridge lies near magnetic Anomaly M1 and is inferred to be of Barremian age. The recovered section is dominated by serpentinized spinel harzburgite, with subordinate dunite and minor gabbroic intrusives, and it includes inferred high-temperature ductile shear zones. The serpentinite is capped by foliated gabbro cataclasite that is interpreted as the product of a major seafloor extensional detachment. The serpentinized harzburgite beneath is highly depleted subcontinental mantle lithosphere that was exhumed to create new seafloor within the ocean–continent transition zone. After inferred

[1]Robertson, A.H.F., 2007. Evidence of continental breakup from the Newfoundland rifted margin (Ocean Drilling Program Leg 210): Lower Cretaceous seafloor formed by exhumation of subcontinental mantle lithosphere, and the transition to seafloor spreading. *In* Tucholke, B.E., Sibuet, J.-C., and Klaus, A. (Eds.), *Proc. ODP, Sci. Results,* 210: College Station, TX (Ocean Drilling Program), 1–69. doi:10.2973/odp.proc.sr.210.104.2007
[2]Grant Institute of Earth Science, School of GeoSciences, University of Edinburgh, West Mains Road, Edinburgh EH9 3JW, United Kingdom.
Alastair.robertson@ed.ac.uk

Initial receipt: 07 January 2006
Acceptance: 09 July 2007
Web publication: 26 July 2007
Ms 210SR-104

removal of overlying brittle crust, the detachment was eroded, producing multiple mass flows that were dominated by clasts of serpentinite and gabbro in a lithoclastic and calcareous matrix. Basaltic lavas were erupted spasmodically, mainly as sheet flows, with subordinate lava breccia, hyaloclastite, and possible pillow lava. The sedimentary-volcanic succession and the exhumed mantle lithosphere experienced later high-angle extensional fracturing and probably faulting. Extensional fissures opened incrementally and were filled with silt-sized carbonate, basalt-derived clastic sediment, and hyaloclastite, forming neptunian dykes and geopetal structures.

Chemical analysis of representative basalts for major elements and trace elements were made using a high-precision, high-accuracy X-ray fluorescence method (utilizing increased count times) and by whole-rock inductively coupled plasma–mass spectrometry that yielded additional evidence for rare earth elements. The analyses indicate N-MORB to slightly enriched compositions. The MORB was produced by relatively high degree melting of a fertile mantle source that differed strongly from the cored serpentinized peridotites. The basalts exhibit a distinct negative Nb anomaly on MORB-normalized plots that can be explained by prior extraction of melt from upper mantle that had previously been affected by subduction, possibly during closure of the Iapetus or Rheic oceans.

In the proposed interpretation, mantle lithosphere was exhumed to the seafloor and experienced mass wasting to form serpentinite-rich mass flows. The interbedded MORB records the beginning of a transition to "normal" seafloor spreading. This interpretation takes into account drilling results from the Iberia-Galicia margin and the Jurassic Alps-Apennines.

INTRODUCTION

One of the outstanding discoveries of the Ocean Drilling Program (ODP) in the North Atlantic Ocean is that a broad strip of seafloor parallel to both rifted margins can no longer be considered simply as oceanic crust formed by spreading at a mid-ocean ridge. This seafloor instead originated, at least partially, from subcontinental mantle lithosphere that was exhumed during the latest stages of continental breakup. This seafloor is equivalent to the Zone of Exhumed Continental Mantle of Whitmarsh et al. (2001). Basement ridges drilled within the ocean–continent transition zone on the Iberia-Galicia margin were initially identified as serpentinized peridotite of apparently subcontinental origin, based on geophysical, petrological, geochemical, and dating studies (e.g., Boillot et al., 1980). The zone of exhumed subcontinental mantle lithosphere between definite continental crust and inferred "normal" oceanic crust is estimated as 150–180 km wide for the restored Iberia-Newfoundland conjugate (Tucholke et al., 2007). This zone may include thinned continental crust on both the Iberia margin (Reston et al., 1995) and the Newfoundland margin (Van Avendonk et al., 2006). Possible ocean crust on this conjugate traverse is located in the vicinity of magnetic Anomaly M3 on the Iberia margin and probably oceanward of this on the Newfoundland margin. The age of the oldest "normal" oceanic crust on the Iberia-Newfoundland conjugate is inferred to be latest Aptian–earliest Aptian (Tucholke et al., 2007).

The zone of subcontinental mantle lithosphere on both margins of the Atlantic is presently one of the most poorly known regional tec-

tonic settings on Earth. ODP Leg 210 provided an opportunity to sample this intermediate zone between continental crust and "normal" oceanic crust at Site 1277. This site is located directly oceanward of a magnetic anomaly identified as M1 (late Barremian) and is assumed to lie between the rifted Newfoundland margin and the oldest "normal" oceanic crust (Shillington et al., 2006; Tucholke et al., 2007). A basement composed of serpentinized peridotite is overlain by a cover of serpentinite-rich mass flows interbedded with basaltic lava flows. This succession was recovered near the summit of a basement ridge, known as the Mauzy Ridge (Fig. F1). Drilling at Site 1277 recovered coherent lava flows for the first time within the ocean–continent transition zone, with important implications for continental breakup and the initiation of seafloor spreading.

This paper provides a detailed description and interpretation of the sedimentary, volcanic, and tectonized rocks overlying exhumed mantle at Site 1277. It also compares these with the previously well-documented recovery of lithologies and structures from the Iberia-Galicia conjugate and with the classic Jurassic land exposure in the Alps-Apennines region.

GEOLOGICAL SETTING

Mauzy Ridge is 21 nmi southeast of Site 1276 on the lower continental rise of the Newfoundland margin (Fig. F2). Drilling at Site 1276 (Figs. F1, F2) terminated in Lower Cretaceous alkaline basalt/diabase sills that are believed to be located several tens of meters above a subsediment basement, which could be either attenuated continental crust or subcontinental mantle. The sedimentary cover of Mauzy Ridge at Site 1277 was not sampled because of time constraints at the end of Leg 210. Core recovery began with pieces of micaceous sediment (in a wash core) and fossiliferous, ferromanganiferous crust directly above basement-related rocks and sediments. Beneath this, two contrasting units were recovered, as shown in Figure F3 (Tucholke, Sibuet, Klaus, et al., 2004).

Unit 1 (less than ~104–142.10 meters below seafloor [mbsf]) consists of basalt and is estimated to make up ~50% of the succession as lava flows and intercalated coarse clastic sediments. The sediments contain abundant clasts of serpentinite and lesser amounts of gabbro, together with minor amounts of finer grained clastic and ferruginous sediments. The relative proportions of these constituents vary within the succession, as discussed below. Relatively low recovery of most lithologies allows only estimates of the thicknesses of individual basaltic flows and clastic intervals to be made. The coarse-grained clastic sediments were initially interpreted as slumps, slides, and debris flows (see Shipboard Scientific Party, 2004b).

By contrast, Unit 2 (142.10–180.30 mbsf) is dominated by strongly deformed and altered serpentinized harzburgite and some dunite, together with minor gabbroic injections. The top of the unit is characterized by a gabbro cataclasite, and several thin zones of foliated cataclasite occur beneath this. The shear zones were interpreted by the Shipboard Scientific Party as products of an extensional detachment system related to the exhumation of subcontinental mantle to the seafloor. The serpentinized peridotite is cut by millimeter- to centimeter-wide hydrothermal veins that are mainly composed of talc, magnetite, and calcite. The foliated serpentinite is interpreted as strongly deformed mantle peridotite that was cut by small gabbroic intrusions and then

F1. Sites 1276 and 1277, p. 42.

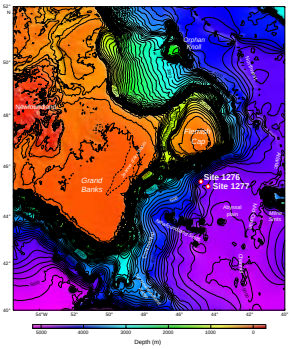

F2. Seismic profile, p. 43.

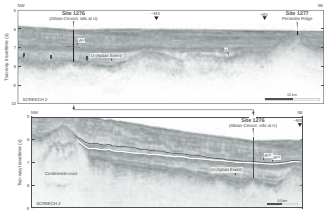

F3. Site 1277 lithology summary, p. 44.

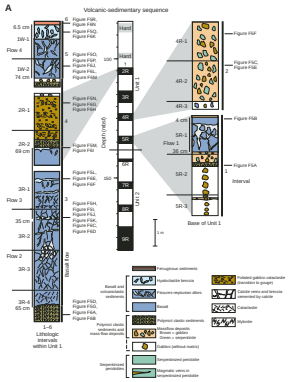

exhumed to the seafloor in response to an advanced stage of rifting and continental breakup (Shipboard Scientific Party, 2004b). Details of the mineralogy and petrogenesis of the plutonic rocks of lithologic Unit 2 have been given by Müntener and Manatschal (2006). In general, the composition of the spinel within the serpentinized peridotite is indicative of a relatively high degree of melting (14%–25%). Gabbroic to monzonitic veins are also present in the basement, and gabbroic clasts ranging from gabbros and gabbronorites to oxide gabbros and anorthosites are present as clasts (Müntener and Manatschal, 2006). An Ar-Ar age of 126.5 ± 0.1 Ma was obtained from biotite crystals that were separated from gabbroic veins (G. Manatschal, pers. comm., 2006). This is the same age as the nearby M1 anomaly (late Barremian) and suggests that gabbro intrusion was approximately contemporaneous with basement exhumation.

NOMENCLATURE

There is currently no general agreement concerning the meaning of such terms as "rifting" and "continental breakup." The following definitions are used here:

1. *Ocean–continent transition zone*. This refers to crust located between well-defined continental crust (as indicated mainly by seismic refraction studies) and "normal" oceanic crust with an assumed well-layered stratigraphy.
2. *Continental rifting*. This refers generally to the complete sequence of events involving crustal extension, beginning with initial faulting of preexisting continental crust and ending with final separation of subcontinental mantle lithosphere to form new oceanic crust. Continental breakup refers in general to the disintegration of continental crust but is only meaningful if the nature of the rifted lithosphere is specified (e.g., upper crust or mantle lithosphere).
3. *Break up of continental crust*. This refers to the complete separation of the brittle upper crust, which may be associated with the exhumation of subcontinental mantle lithosphere to form new seafloor. Fragments of brittle continental crust may persist above the subcontinental mantle lithosphere and remain stranded within the ocean–continent transition zone as "extensional allochthons."
4. *Break up of subcontinental mantle lithosphere*. This refers to the final and complete separation of the previously exhumed subcontinental mantle lithosphere, which is replaced by juvenile asthenosphere as "normal" seafloor spreading begins.
5. *"Normal" seafloor spreading*. This is regarded as oceanic lithosphere with a well-defined layered stratigraphy, as inferred mainly from the study of certain ophiolites (e.g., Troodos and Vourinos ophiolites) (Anonymous, 1972). However, many ophiolites are now known to be of suprasubduction zone type and their stratigraphies are unlikely to be representative of most oceanic lithosphere formed at mid-ocean ridges (e.g., Robertson, 2002). The stratigraphy of the early ("normal") oceanic lithosphere that was formed by seafloor spreading adjacent to the Newfoundland rifted margin remains unknown, as it has not been drilled. This "normal oceanic crust" is assumed to differ

from the earlier crust that was formed by mantle exhumation, as sampled at Site 1277.

6. *Timescale*. The timescale used here is that of Gradstein et al. (2004).

VOLCANIC-SEDIMENTARY SUCCESSION

To supplement the brief summary in the "Site 1277" chapter of the Leg 210 *Initial Reports* volume (Shipboard Scientific Party, 2004b), a detailed description and local interpretation is given for lithologic Unit 1 together with a summary of lithologic Unit 2. To aid interpretation of the temporal evolution of Site 1277 the lithologies are discussed in stratigraphic order from the base upward (rather than as summarized collectively from the top downwards as in the *Initial Reports* volume).

Lithologic Unit 2: Serpentinized Ultramafic Basement

The lithologic boundary between Unit 2 and Unit 1 (Fig. **F3**) was placed by the Shipboard Scientific Party above the highest serpentinite that shows a pervasive nonsedimentary fabric (i.e., the lower part of Section 210-1277A-6R-1) and beneath the lowest sedimentary breccia-conglomerate formed by sedimentary processes (Sample 210-1277A-5R-3, 75.5 cm). However, the contact itself was not recovered.

In general, the top of the basement unit is interpreted as the eroded surface of a presently low-angle fault, possibly a detachment fault that exposed serpentinized mantle lithosphere on the seafloor, where it was covered by basalt and polymict sediments (Shipboard Scientific Party, 2004b).

Most of Unit 2 is dominated by serpentinized harzburgite, which ranges from homogeneous serpentinite, through a tectonic breccia composed of interlocking jigsaw-type clasts, to a well-foliated porphyroclastic serpentinized peridotite. Subordinate dunite is also present. Many of the harzburgite pieces that were recovered exhibit well-developed spinel foliation that is typical of serpentinized upper mantle that has undergone ductile deformation as a result of asthenosphere flow prior to exhumation. This foliation is steeply inclined (>80°) in many intact pieces of core recovered. The more massive serpentinized harzburgite lower in the section is locally cut by gabbroic segregations. A network of calcite- and talc-filled veins is also present. These observations indicate that the peridotite experienced high-temperature deformation, injection of small volumes of gabbroic melt, and later low-temperature tectonic fracturing and veining. The serpentinized peridotite includes several intervals of serpentinite mylonite and foliated mylonite, which are interpreted to be the result of ductile (high-temperature) shearing related to exhumation of the mantle to the seafloor.

Postcruise geochemical studies of the plutonic rocks (Müntener and Manatschal, 2006) show that the sepentinized spinel peridotites from Unit 2 occurring as clasts in Unit 1 are strongly depleted, similar to the most depleted abyssal peridotites and to the tectonite (depleted mantle) of typical "suprasubduction zone ophiolites."

The gabbro breccia recovered from just beneath the contact between Units 2 and 1 was determined to be a cataclasite because the clasts are angular and exhibit an interlocking jigsaw-type fabric without any evidence of a sedimentary matrix (Fig. **F4A**). Tectonic clasts within the cataclasite range from angular to subrounded and vary from medium-

F4. Core photographs, Unit 2, p. 46.

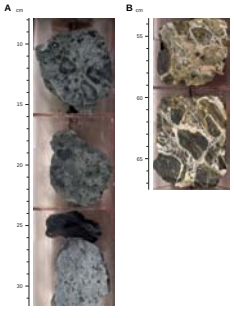

grained to pegmatitic. One piece is foliated with asymmetric porphyroblasts, whereas another is a cataclasite with angular interlocking clasts. Calcite-filled veins and fractures are common. The directly underlying harzburgite shows similar tectonic brecciation (Fig. F4B). It should be noted that all of the plutonic rocks of Unit 2 form parts of a coherent "basement" and as such they differ in setting from basalts that were erupted as flows within the overlying clastic sediments of Unit 1, as discussed below.

Lithologic Unit 1: Igneous-Sedimentary Cover

Six main sedimentary or volcanic intervals are recognized, specifically consisting of three basaltic layers and three main occurrences of polymict sediments dominated by detrital serpentinite and gabbro (Fig. F3A).

Interval 1: Heterogeneous Basal Section

The lowermost recovery above Unit 2 consists of pieces of brecciated gabbro, polymict serpentinite-rich breccia, and basalt (Fig. F3A). The gabbro pieces range from medium grained to coarse grained and include gabbro pegmatite.

A single sandstone piece (interval 210-1277A-5R-2, 33–42 cm) was described on the ship as finely laminated pink, purple, and gray graded ferruginous sandstone (Fig. F5A). The well-sorted texture and fine grain size of this sedimentary rock differ from the other clastic lithologies recovered at Site 1277. In hand specimen, the lower part of this interval is pale orange and passes upward through a purple-red interval into a bright red, strongly oxidized uppermost interval. A thin section studied after the cruise shows that this sediment is strongly altered, although primary grading and a primary planar lamination are clearly visible. This sediment appears to have been eroded from a lava flow, as it includes highly altered basalt clasts and volcanic glass. In common with the other sediments, it shows evidence of fracturing and calcite veining after cementation.

The recovered basalt above this interval (210-1277A-5R-1, 5–135 cm) shows evidence of strong tectonic brecciation. High-angle fractures are partly infilled with volcaniclastic silt and were later partially cemented by calcite spar. Some unfilled fractures are lined with prismatic calcite spar (Fig. F5B).

Interpretation

The nature of the lowermost interval suggests that deposition began with sedimentary breccias rich in clasts of brecciated gabbro. These clasts are likely to have been eroded from fault gouge, and it is therefore inferred that an extensional detachment fault is present between Unit 2 peridotites and the base of the overlying clastic section. The intense fracturing of sedimentary rock clasts indicates that they were deformed after lithification, similar to other sedimentary lithologies recovered from higher in the succession (see below). The graded volcaniclastic sandstone is likely to represent a sand turbidite, derived from erosion of basalt in an upslope area. This was distinct from the more local setting that is inferred for the clastic debris and basaltic volcanics. The different provenances are particularly suggested by the strong contrast between the well-sorted, graded, laminated sediment and the typically much coarser, poorly sorted mass flows that were cored at Site 1277. Assuming

F5. Core photographs, Unit 1, p. 47.

that the basaltic sands are turbidites, a supply of basaltic material must have been available some distance from Site 1277 (i.e., hundreds of meters to kilometers away). This would further imply that basalts were erupted more widely than the lava flows locally cored at Site 1277. The basalt above the recovered clastic sediment could be as thick as several meters, and it is interpreted as the lowermost lava flow that was cored (marked as Flow 1 on Fig. F3A). This flow was strongly fractured and veined.

Interval 2: Polymict Breccia-Conglomerate

The lowermost heterogeneous interval is overlain by a distinctive interval that is composed of reddish brown, matrix-supported, poorly sorted breccia-conglomerate, estimated to be as thick as 30 m (intervals 210-1277A-4R-1, 1 cm, through 5R-1, 25 cm). This interval (Fig. F3A) includes angular clasts and is termed "breccia-conglomerate," in contrast to polymict breccia higher in the succession, in which the clasts are generally more rounded ("conglomerate-breccia"). Clasts of serpentinite and gabbro, mostly <5 cm in size, comprise ~30% of this interval (Fig. F5C, F5D–F5F). Occasional large clasts of gabbro (e.g., Fig. F5E) and serpentinite (e.g., Fig. F5F) are present within a finer grained matrix.

Thin sections of the polymict breccia-conglomerate confirm the predominance of serpentinite clasts set in a fine-grained calcareous matrix. Where little altered, the serpentinite clasts range from massive to foliated to mylonitic. Several clasts of massive serpentinite retain a primary magmatic foliation as defined by preferential orientation of spinel grains (e.g., interval 210-1277A-4R-1, 7–15 cm). Remnants of a ductile foliation are also preserved in several mylonite clasts. In the most highly altered clasts, serpentinite is mainly replaced by coarsely crystalline calcite. Gabbro clasts are locally present; these clasts range from little-altered gabbro to occasional clasts in which the gabbro is largely altered to blue chlorite. In addition, several clasts of recrystallized biotite-rich metabasic rocks were observed in thin section and these appear to have metamorphosed basic igneous rocks as their protoliths (e.g., interval 210-1277A-4R-1R, 39–43 cm).

The matrix, ~70% of the rock, is reddish brown silty sandstone cemented by calcite spar (e.g., Fig. F5E) and locally shows a vague subhorizontal lamination defined by coarser grains. Sand-sized grains are mainly subangular to subrounded serpentinite and gabbro of the same composition as the larger clasts.

The polymict breccia-conglomerate is cut by numerous calcite veins (e.g., Figs. F5E, F5F, F6A). Steeply inclined fractures (Fig. F5E) are as wide as 2 cm and in some cases show evidence of several generations of carbonate precipitation. Some of the widest veins cut even the largest clasts and their enclosing matrix, showing that the entire unit was relatively well cemented before fracturing and cementation took place. Many of the larger clasts are rimmed by carbonate cement (e.g., Fig. F5F), possibly because cracks preferentially opened along the interfaces between clasts and matrix. In some samples several phases of crosscutting veins are visible (Fig. F6A).

Above the breccia-conglomerate is a distinctive interval of graded granulestone (Fig. F5G) cemented by calcite spar (Fig. F6A, F6B). This clastic sediment retains a primary contact with overlying lava, described in the next section.

F6. Thin sections, p. 53.

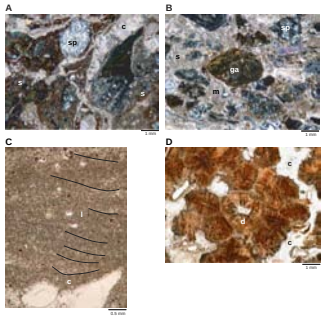

Interpretation

The matrix-supported breccia-conglomerate, characterized by mostly angular clasts, was mainly derived from serpentinized peridotite and, to a lesser extent, from gabbro. The material includes serpentinite mylonite and gabbro cataclasite, which were probably derived from an underlying inferred extensional detachment fault zone, as outlined earlier. The serpentinite mylonite was veined by carbonate spar before being incorporated into the breccia. The matrix of finer grained material was derived from the same lithologies. The matrix-supported fabric and angular clasts are suggestive of an origin as cohesive mass flows in which little abrasion and rounding of clasts took place during local transport. This material is unlikely to have experienced more than one cycle of gravity emplacement because there are no signs of mixing of clasts of differing roundness or of reworking of previously deposited sediment. This texture contrasts with more texturally mature conglomerate-breccias higher in the succession that are interpreted as less cohesive pebbly debris flows that were reworked before final emplacement. The breccia-conglomerate shows evidence of high-angle fracturing that created a network of cracks that were infilled with calcareous sediment and cemented by calcite spar. This suggests that the entire recovered interval experienced horizontal axis extension that took place after emplacement and substantial lithification. The well-sorted granulestone above this polymict interval possibly represents material from the underlying, relatively cohesive serpentinite-rich debris flow that was reworked as a noncohesive pebbly debris flow before being overridden by a basaltic sheet flow.

Interval 3: Massive Basalt Flows

An interval of internally brecciated massive basalt (Fig. **F3A**) is inferred to represent two lava flows, with a total thickness estimated at as much as 15 m (interval 210-1277A-2R-2, 69 cm, through 3R-4, 65 cm) (Fig. **F5H, F5I, F5J, F5K, F5L, F5M**), although the recovery was incomplete.

The base of the thicker, lower flow (marked as Flow 2 on Fig. **F3A**) exhibits a primary eruptive contact with clastic sediment, as noted above (Fig. **F5G**). Also, the top of the lower flow (interval 210-1277A-3R-2, 35 cm) is marked by a well-preserved chilled margin (Fig. **F3A**). The lower flow begins with an interval of massive basalt interspersed with minor amounts of concentrically laminated, angular to elliptical hyaloclastite cemented by coarse calcite spar. Localized reworking of basaltic material is present, but nonvolcanic clasts (e.g., gabbro or serpentinite) do not occur. The grain size of the lower flow gradually decreases upward from medium grained to very fine grained. The flow finally passes upward through an interval of vesicular basalt (1 cm thick) and green, crustose, laminar hyaloclastite (as thick as 0.9 cm). A devitrified glass texture was observed locally near the top of this flow (Fig. **F6D**).

The upper flow (interval 210-1277A-2R-2, 69 cm, through 3R-2, 37 cm) (Flow 3 on Fig. **F3A**) is uniformly fine grained. Its upper surface is brecciated, and spaces between clasts contain subrounded pebbles of calcite-cemented hyaloclastite (<1 cm) and angular basalt clasts (Fig. **F5M**). This basalt includes several thin intervals (several centimeters) of well-cemented medium-grained volcaniclastic sandstone containing small (centimeter sized) pebbles of green hyaloclastite (Figs. **F5L, F6E, F6F**).

Both basalt flows are cut by irregular fractures, as wide as ~1 cm, and are mainly filled with calcite spar. Partly cemented veins are lined with dogtooth spar. Larger fractures, as much as 3–4 cm wide, are infilled with poorly sorted silt-sized carbonate sediment and basaltic detritus (Fig. **F5H, F5I, F5J, F5K**). Weak planar lamination is defined by the input of fine sand-sized to granule-sized basalt and hyaloclastite (Fig. **F5H**). Small pebbles of concentrically laminated hyaloclastite show little sign of fracturing or abrasion and were cemented in place after percolating downward into open fractures (Fig. **F5K, F5L**). In one interval the basalt clasts and the matrix are stained a reddish color, especially along the margins of clasts. This possibly reflects the flow of oxidizing seawater after deposition (Fig. **F5J**).

Several samples of the sediment-filled fractures were studied in thin section. The "internal sediment" shows weakly developed parallel lamination highlighted by small basalt and hyaloclastite particles. In one clear example, primary sedimentary laminae are deflected over small projections in the surface of the cavity and ponded into small (millimeter sized) depressions (Fig. **F6C**). This internal lamination is subhorizontal, indicating that little tilting took place after the sediment was deposited.

Interpretation

The two lava flows (2 and 3) were perhaps emplaced quite rapidly as they are internally massive and show no evidence of pillow structure. This in turn suggests that the local seafloor was gently inclined, at least locally, and possibly resulted in ponding of lava. The breccia at the top of the upper flow resulted from a primary eruptive process to create hyaloclastite, coupled with some reworking of cooler basalt and hyaloclastite. Minor hyaloclastite is also present within Flow 2, suggesting that eruption was spasmodic. Both of these lava flows have been tectonically brecciated and contain subvertical neptunian fissures. This brecciation occurred after eruption, as many of the clasts are angular to subrounded, retain a jigsaw-type fabric, and lack glassy selvages. Exotic material (e.g., serpentinite) and evidence of sedimentary reworking are absent from within, or between, the two lava flows. This suggests that all of the breccia material was derived locally from the two lava flows. The relatively rounded nature of some basalt clasts probably reflects abrasion that resulted from faulting or gravity collapse.

After cooling and initial cementation, the tectonic fracturing of the lava flows allowed calcareous sediment, together with basalt and hyaloclastite grains, to filter downward through open cracks and fractures (Fig. **F5H, F5I**). This sediment can be compared with well-known geopetal fabrics that have formed as infills within cavities in lithologies such as carbonate rocks (e.g., Bathurst, 1971). Such "internal sediment" is a good indicator of the paleohorizontal (e.g., in carbonate reef complexes). The neptunian fissures are subvertical, whereas the lamination within the internal sediment is gently inclined (e.g., Fig. **F5H;** 104–107.5 cm). In places, the lamination is concave downward because of differential compaction (Fig. **F6C**); however, it is subhorizontal within the largest fissures. The basalt flows, therefore, cannot have been tilted significantly (less than ~10°) after the fissures opened on the seafloor. The fact that the volcanic-sedimentary succession was not significantly tilted at a later stage places constraints on the tectonic history of the site after volcanism and sedimentation ended, as discussed later in this paper.

Interval 4: Polymict Conglomerate-Breccia with a Large Sheared and Brecciated Gabbro Clasts

At the base of this distinctive interval is a conglomerate-breccia that was termed "serpentinite breccia" in the Leg 210 *Initial Reports* volume (Shipboard Scientific Party, 2004b). It is composed of granule- to pebble-sized material (interval 210-1277A-2R-2, 40 cm, through 2R-2, 66 cm) (Fig. F3A). Clasts of serpentinite and gabbro (as long as 1.5 cm) are set in a poorly sorted fine-grained carbonate matrix of siltstone to sandstone (Fig. F6I). These clasts range from subangular to subrounded and are cemented by sparry calcite.

A notable interval, >1.6 m thick, of greenish cataclastic gabbro was recovered above this interval (210-1277A-2R-1, 12 cm, through 2R-2, 40 cm) (Fig. F5N). Crude foliation is defined by the preferred orientation of a chloritic matrix and by crude subparallel alignment of small (<2 cm) elongate gabbro clasts. Many individual gabbroic clasts are typically strongly altered. By contrast, larger, more equidimensional gabbroic clasts retain a primary magmatic fabric and show little or no preferred orientation. Thin sections show that variably altered, highly angular plagioclase and pyroxene crystals, and also gabbro fragments, are aligned within a foliated chloritic matrix (Fig. F6G, F6H). This entire rock was formed by tectonic fragmentation of gabbro (i.e., as porphyroclastic gabbro) and is not considered to have a sedimentary origin.

Short intervals of basalt recovered above this interval (210-1277A-2R-1, 0–10 cm) were interpreted by the Shipboard Scientific Party as isolated basalt pebbles (Shipboard Scientific Party, 2004b) (Fig. F3A). However, it is also possible that they record an additional thin basalt flow that was mainly not recovered.

A piece of intact calcite-cemented polymict conglomerate-breccia was recovered from interval 210-1277A-1W-2, 91–105 cm (Fig. F5O). The clasts within this breccia as large as 2 cm and range from angular to subrounded to occasionally well rounded. This sediment is normally graded with the largest clasts at the base, passing upward from pebble to granule to coarse sand–sized material. Several unusually large, relatively well rounded clasts are present toward the top of this depositional unit. In thin section, mainly sand-sized lithoclasts, including gabbro and serpentinite, are set in a fine-grained carbonate matrix. The matrix includes small detrital grains of serpentinite and iron oxide together with later stage coarser calcite spar; however, basalt and hyaloclastite were not observed within the matrix.

Above the conglomerate-breccia, several small well-rounded pebbles of cemented coarse clastic sediment were recovered (interval 210-1277A-1W-2, 81–90 cm), followed upsection by several isolated angular fragments of strongly altered coarse-grained gabbro (5 cm in size) (interval 210-1277A-1W-2, 75–80 cm). The different pebbles show either primary sedimentary fabric (i.e., sedimentary lamination) or tectonic fabric (e.g., foliation), respectively. One pebble of conglomerate-breccia is dominated by subrounded to subangular detrital grains of altered serpentinite and gabbro set in a calcareous matrix. The calc-siltite matrix is partially recrystallized to microspar-sized carbonate and cut by calcite veins (Fig. F6J).

Interpretation

The polymict conglomerate-breccia is interpreted as one, or several, subaqueous mass flows that are dominated by clasts of serpentinite and gabbro within a calcite-cemented matrix. The well-rounded nature of

some of the clasts implies that extensive reworking occurred, in turn suggesting a significant distance of transport prior to final deposition (perhaps more than hundreds of meters). In the absence of evidence of rounding in a high-energy shallow-marine or nonmarine setting (i.e., neritic fossils are absent), it is probable that the rounding resulted from abrasion during subaqueous downslope sedimentary transport. The coexistence of both rounded clasts and angular clasts suggests sediment recycling, possibly involving reworking of preexisting debris flows. The source of the clastic material was mainly serpentinite and gabbro that experienced intense shearing beneath an inferred extensional detachment before being incorporated into the mass flows.

The angular, tectonically brecciated gabbro interval (>1.4 m thick) represents a block (i.e., an unusually large clast) that was derived from the inferred underlying extensional detachment that was originally exposed at the seafloor around Site 1277. The relatively large size of the block suggests a proximal source. The foliated cataclastic breccia originated as plagioclase-pyroxene gabbro that experienced subseafloor brecciation, shearing, and metamorphism prior to incorporation within this mass flow interval. The ductile matrix may have formed by a combination of cataclasis of gabbro and fluid-assisted alteration of the host gabbro to form chlorite and related hydrothermal and diagenetic minerals. The presence of a block of this size suggests that the exposed detachment was at least locally fractured to form more than meter-scale relief, thus providing an appropriate source.

The isolated pebbles of brecciated gabbro, serpentinite, and sedimentary conglomerate-breccia near the top of this interval probably represent clasts derived from one or more poorly cemented pebbly debris flows. These clasts may have been selectively recovered by drilling, whereas the enclosing matrix was lost. Some of these well-rounded pebbles are preserved within a matrix of carbonate cement, confirming that the rounding, where present, cannot be an artifact of drilling.

Interval 5: Basalt Flow Capped by Basaltic Breccia and Hyaloclastite and Later Fissured

The polymict breccia and its enclosed gabbro cataclasite block are overlain by a lava flow, marked as Flow 4 in Figure **F3A,** that is made up of medium-grained gray aphyric basalt. This is the uppermost of the three volcanic intervals recovered. Massive basalt at the base contains chilled selvages composed of variably altered green hyaloclastite (Fig. **F5P**) together with pockets of calcite-cemented hyaloclastite and pink fine-grained calcareous internal sediment (calc-siltite) (Fig. **F6L**). The carbonate sediment is locally recrystallized or partially dissolved to form cavities (vugs) that were later lined with calcite spar (Fig. **F6K, F6M**).

The basalt is cut by anatomizing veins, as long as tens of centimeters long and several centimeters wide. Two generations of millimeter-sized calcite veins are visible, commonly intersecting at high angles. Numerous hairline cracks are filled with calcite spar. Some of these cracks later widened, allowing hyaloclastite mixed with fine basaltic grains to fill cavities and be cemented by sparry calcite (e.g., interval 210-1277A-1W-2, 32–40 cm) (Fig. **F5P**). There are also numerous small irregular calcite-filled veins, as long as several millimeters, of uncertain relative time relations.

The massive basalt is overlain by an interval of altered basalt, lava breccia, brecciated basalt, and hyaloclastite, which contain subvertical

sediment-filled fissures (Fig. F5Q). This volcanic interval is dominated by greenish breccia composed of poorly sorted, well-indurated breccia and hyaloclastite (altered volcanic glass). Primary glass is commonly recrystallized or replaced by carbonate. The breccia includes angular fragments of aphyric basalt as large as tens of centimeters. The larger basalt clasts are randomly strewn through a matrix of greenish hyaloclastite sand to fine breccia. Clasts of variably altered basalt range in color from green to pale green through gray to black. Clasts of all sizes are cemented by calcite spar.

The brecciated basalt and lava breccias are cut by a prominent subvertical fissure (e.g., interval 210-1277A-1W-1, 40–60 cm) (Fig. F5Q). Part of this fill is shown on the left side of this core photograph. Two generations of sediment fill must have existed within the fissure. The first was soft, brownish, massive, fine-grained, apparently ferromanganiferous sediment. This is now mainly brecciated, but locally it remains in direct contact with coarse clastic host breccia (e.g., green reworked hyaloclastite in interval 210-1277A-1W-1, 56–58 cm). This shows that the host was consolidated and/or cemented at a relatively early stage and filled by the fine-grained sediment. After cementation, this first generation of sediment fill was brecciated and the preexisting fracture was reopened. A second generation of sediment (paler in color) then filtered in, composed of greenish gray calcite-cemented calcareous silt (calc-siltite) together with sand- to granule-sized grains of basalt and hyaloclastite. Some of these small detrital grains show evidence of abrasion and rounding.

Other fissures, in these cases cutting altered basalt, show evidence of filling with calc-siltite of similar composition to the pale second-stage clastic fill described above. These fills show a subhorizontal lamination defined by coarser and finer grains. One small, near-vertical, straight-sided vein, ~4 mm wide, is filled with fine-grained calc-siltite including hyaloclastite particles (Fig. F6N). Close inspection of the fine-grained sediment reveals gently tilted lamination (~20°) that could reflect tilting after deposition. Any pore space remaining after sediment filling, especially between hyaloclastite fragments, was filled with coarse carbonate spar.

Numerous millimeter-sized carbonate veins are continuous between the greenish volcaniclastic matrix and the basaltic clasts (i.e., they run from the one lithology into the other without a break and also cut the sediment infills). These veins indicate late-stage brittle fracturing that postdated the episodic filling of neptunian fissures.

The highest recovered interval of volcanic breccia consists of angular to subangular fragments of calcified basalt set within subrounded grains of green chloritic hyaloclastite (e.g., interval 210-1277A-1W-1, 10–28 cm; uppermost interval 5) (Fig. F5R).

Interpretation

These uppermost basalts (Flow 4) probably erupted episodically. The presence of inclined or curved glassy selvages might suggest the presence of pillow lavas; however, these features could simply represent cooling cracks. The presence of hyaloclastite reflects the interaction of hot lava with cold seawater. Hyaloclastite typically forms along the fronts of advancing lava flows that may then be overridden by lava or incorporated into lava flows. Hyaloclastite is, for example, abundant where lava is erupted on a sloping seafloor, increasing the rate and amount of interaction with cold seawater. In addition, lava breccias can form in a range of settings, which include gravity collapse of flow fronts

and breakup of the solidified crusts of lava flows (Fisher and Schmincke, 1984).

After initial accumulation of lava breccia and its cementation by hydrothermal calcite, fracturing took place, opening subvertical fissures that allowed mainly silt-sized carbonate sediment to percolate downward, creating neptunian dykes. The first generation of calcareous sediment infill includes an apparently Fe-Mn rich hydrothermal metaliferous component. Following infill and cementation, a second phase of fracturing widened the early fissures. These cracks were infilled by a more homogeneous, pale-colored calc-siltite that includes detrital basalt and hyaloclastite grains.

Four possible origins of the calc-siltite are considered. The first is from background pelagic calcareous sediment that filtered down into open cracks. This is unlikely because microfossils (e.g., foraminifers) were not observed. The sediments show little sign of recrystallization and so it is unlikely that microfossils were dissolved during diagenesis. The second alternative is that the carbonate sediment was derived from the Newfoundland continental margin. This is most unlikely, as the fissure-filling sediment lacks terrigenous components. A third possibility is that the fine carbonate sediment is a primary hydrothermal precipitate. However, this is clearly not the case because the sediment is finely laminated and shows other sedimentary features (e.g., compaction into small depressions). A fourth alternative, favored here, is that the carbonate sediment was derived by reworking of early calcite cement and calcite-cemented basalt associated with faulting. This carbonate material was derived from within the lava flows because there is no evidence of exotic material derived from above the lava flows. The initial carbonate could have been precipitated as veins and/or as calcite-cemented hyaloclastite. When faulting took place the early carbonate cement was comminuted and filtered down to deeper levels within neptunian fissures as carbonate silt. In one scenario, brittle fault-controlled fissures opened and were lined with carbonate cement. With further faulting the cement and the host volcanics were fragmented and abraded, creating fine-grained sediment composed of silt- to sand-derived carbonate, basalt, and hyaloclastite that filtered downward to create the observed neptunian infill.

Interval 6: Ferromanganese-Cemented Sedimentary Crust

A single piece of well-indurated brown ferromanganiferous clastic sediment at the top of the cored section is composed of poorly sorted medium- to coarse-grained sandstone and includes scattered granule-sized lithic grains (Sample 210-1277A-1W-1, 5–9 cm) (Fig. **F5R**). The clastic sediment includes variably altered basalt, gabbro, and carbonate, together with feldspar and rare spinel. In common with the underlying sediments at Site 1277, terrigenous sediment (e.g., detrital quartz and mica) is conspicuously absent. The clastic sediment forms a colloform-textured microlaminated ferromanganese crust, comprising centimeter-scale laterally linked domes. An orange botryoidal lamination appears to have formed initially (iron oxide rich), followed by darker and more regularly laminated material (manganese oxide rich). The crust contains agglutinated benthic foraminifers, encrusting wormlike tubes, and several tiny planktonic foraminifers, none of which were age diagnostic (Shipboard Scientific Party, 2004b).

The top of Core 210-1277A-1W (interval 1W-1, 1–3 cm) is a micaceous sandstone that may be lithified sediment from the overlying sedimentary section, or it may be a glacial dropstone (Fig. F5R).

Interpretation

This coarse, clastic, metal-rich sediment records a period of submarine erosion or nondeposition on the igneous basement. The clasts are similar to the composition of underlying coarser polymict sediments, including material derived from both mafic and ultramafic rocks. The poorly sorted nature of the ferromanganiferous sediment is consistent with a relatively local provenance from the crest of Mauzy Ridge. The presence of ferromanganese oxides suggests accumulation in a strongly oxidizing setting. The planktonic foraminifers indicate an open-marine setting that was possibly near the calcite compensation depth, in view of the paucity and poor preservation of the calcareous microfossils. The absence of terrigenous sediment suggests that the area was isolated from a supply of terrigenous turbidites of the type drilled closer to the Newfoundland margin at Site 1276.

GEOCHEMISTRY AND SIGNIFICANCE OF BASALT FLOWS

Samples taken from the three main basaltic intervals were chemically analyzed. The samples were taken from Cores 210-1277A-1W, 3R, 4R, and 5R at the positions listed in Tables T1 and T2. The sample from Core 210-1277A-1W is from an isolated piece of basalt (Flow 4). The samples from Core 210-1277A-3R are from the two massive lava Flows 2 and 3. The sample from Core 210-1277A-4R is a piece of basalt interpreted as part of the underlying lava Flow 1, from which another sample was taken in Core 210-1277A-5R. The samples were carefully selected to cover the vertical range of basalt and to exclude detrital sediment, as well as hydrothermally veined and oxidized intervals. All the basalt from Core 210-1277A-1W, however, is strongly altered and rich in secondary carbonate.

T1. Major and trace element analyses, p. 68.

T2. Major, trace, and rare earth element analyses, p. 69.

Primary Mineralogy and Alteration

Basalts were studied in six thin sections, representing a range of visible textures. Samples from Flow 4 are considerably more altered than those in the flows below. The uppermost sample (210-1277A-1W-1, 36–39 cm) exhibits a well-crystallized granular intersertal texture with microphenocrysts of plagioclase, together with small granules of opaque ore. Plagioclase crystals are relatively unaltered, whereas the mesostasis is mainly replaced by carbonate. Another sample from this flow (Sample 210-1277A-1W-1, 101–104 cm) is similar but contains occasional large plagioclase phenocrysts. Scattered small amygdules are dominantly carbonate and chlorite. A further sample from this core (Sample 210-1277A-1W-1, 38–41 cm) includes scattered microphenocrysts of augite partly replaced by calcite.

Samples from Flows 2 and 3 are less altered. The upper levels of Flow 3 (Samples 210-1277A-3R-1, 132–134 cm, and 3R-2, 36–39 cm) show devitrified glass (variolitic) texture with feathery plagioclase and rare ferromagnesian phenocrysts replaced by chlorite, carbonate, and opaque ore minerals. Beneath this, the basalt of Flow 2 (e.g., Sample 210-1277A-3R-2, 106–109 cm) is more crystalline, with a granular inter-

sertal texture defined by plagioclase and clinopyroxene (augite) microphenocrysts. Many individual plagioclase crystals are altered and the mesostasis is partly chloritized, but secondary carbonate is much less abundant than in the overlying flow. No basalts from Flow 1 were studied in thin section.

Analytical Methods and Results

Nine basalt samples were analyzed for major and trace elements by X-ray fluorescence (XRF) at the Grant Institute of Earth Science, University of Edinburgh (United Kingdom) using the method of Fitton et al. (1998) (Table T1). Loss on ignition varies from 3.43 to 26.37 wt%. High CaO values (e.g., 130 wt%) are attributed to the abundance of secondary calcite, as observed in thin sections (see below).

The precision and accuracy of chemical analysis by a standard XRF technique can be variable; however, high-precision data can be obtained, especially when using a specifically developed and tested XRF technique, as documented by Fitton et al. (1998). This method has been applied to basalts from a wide range of areas and ages including Iceland and the East Greenland rifted margin. Where samples are suspected to contain very low values of incompatible trace elements, the analytical conditions and calibrations for these elements are optimized for low concentrations, as appropriate. Background positions are placed as close as possible to peaks, and long count times are used at both peak and background positions. Where background count rates are measured on either side of the peak, as in most trace element determinations, the count time is divided equally between the two positions. Matrix corrections and spectrometer calibrations were carried out as specified by Fitton et al. (1998). Trace element precision has been previously estimated by repeatedly analyzing several samples from ODP Leg 152, yielding a precision of ±0.1 ppm for the critical element Nb. Comparisons of analytical values with published international standards indicate high levels of accuracy (Fitton et al., 1998). Comparisons show that precision and accuracy of basalt analyses using the above modified XRF technique compare favorably with inductively coupled plasma–mass spectrometry (ICP-MS) data (see table 2 of Fitton and Godard, 2004). In the present case, almost identical results were obtained for a duplicate analysis of one sample (see Table T1). As a result, the interpretations below are justified by the analytical precision and accuracy of the available XRF data.

To confirm and extend the results from the XRF analysis, seven of the samples were analyzed for major elements, trace elements, and rare earth elements (REEs) by ICP-MS using a whole-rock technique (Table T2). The analysis was done at ACME Analytical Laboratories Ltd., Vancouver, Canada. Crossplots of the data for individual element oxides or elements (not shown here) confirm that very similar values were obtained for both the XRF and ICP-MS methods. Of the elements that are most important for discrimination of tectonic settings of eruption, Nb values are slightly higher as analyzed by ICP-MS than by XRF, whereas Zr values are slightly lower. Such small differences, however, do not affect the interpretations given below.

Interpretation of the Chemical Analyses

Initial interpretation of the major element and trace element data was carried out using the XRF data. To help assess bulk chemical com-

position the samples were plotted on a Zr/Ti vs. Nb/Y diagram (Fig. F7). This allows rock classification using only immobile elements. All of the samples plot in the andesite/basalt field. One of the samples (AR130 in Table T1), however, was excluded from further consideration, as it contains numerous small carbonate veins based on visual inspection and was therefore considered to be more altered (although its inclusion would not change the interpretation).

Because all of the samples are altered to variable degrees, any interpretation of the tectonic setting of eruption must rely on the relative abundances of major and trace elements that are considered to be immobile under conditions of low-grade hydrothermal alteration typical at Site 1277 (Pearce and Cann, 1973). The large ion lithophile (LIL) elements Sr, K, Rb, and Ba are typically mobile compared to the high field–strength elements (HFS) Nb, Nd, Ti, Y, and Cr (Pearce, 1982). Recent work on the East Greenland margin (Leg 152) also has shown that K, Rb, and Ba are relatively mobile, whereas Si, Sc, Al, Fe, Zn, V, and Nb are less mobile (Larson et al., 1998). Yttrium, normally considered to be immobile in such seafloor settings, was found to be immobile at Site 917 but mobile at Site 918. The mobility was explained by the breakdown of clinopyroxene in these basalts (Larson et al., 1998). The Site 1277 basalts commonly contain clinopyroxene phenocrysts, most of which appear in thin section to be unaltered except in Flow 4.

Samples were also plotted on several geochemical diagrams that are known to be useful for discrimination of the tectonic settings of basaltic rocks. On a Ti/Zr vs. Y plot (Fig. F8A) the basalts mainly plot in the field of mid-ocean-ridge basalt (MORB), with one sample just into the field of within-plate basalt and one just within the island arc basalt field. On a V vs. Ti diagram (Fig. F8B) all of the samples plot in the field of ocean floor basalt. On a Ti/100 vs. Zr vs. 3Y diagram (Fig. F8C) all of the samples plot in the combined field of MORB, calc-alkaline basalt, and island arc tholeiites. On a 2Nb vs. Zr/4 vs. Y diagram (Fig. F8D) all of the basalts plot in the combined normal (N-)MORB-volcanic arc field (i.e., Field D).

Plotted on MORB-normalized spider plots (Fig. F9A), the immobile elements exhibit a MORB trend, with a slight relative depletion of Nb, which is characteristic of depleted MORB. The basalt from the uppermost Flow 4 (Core 210-1277A-1R) is slightly richer in the HFS element Cr compared to basalt from the underlying Flows 2 and 3 (Cores 210-1277A-3R through 5R), but the other HFS elements are slightly depleted compared to these flows. The relative enrichment of the LIL elements Sr, K, Rb, and Ba in all of the flows can be attributed to alteration because these elements are typically mobile as noted above, although a crustal influence on the melt cannot be excluded (see below).

When the three least-altered samples (<10 wt% CaO; see Table T1) from the two lower volcanic levels (Flows 2 and 3; Cores 210-1277A-3R through 5R) are plotted together they define a tight grouping (Fig. F9B). Nb shows a slight increase in enrichment relative to MORB but a decrease compared with the enrichment of higher molecular weight immobile trace elements (e.g., Ce). This "negative Nb anomaly" is unlikely to result from differential alteration because Nb is widely believed to be immobile under prevailing seafloor conditions (e.g., Pearce, 1982, 1983). Also, as noted above, the precision and accuracy of the analysis using the increased count time technique (Fitton et al., 1998) allows the negative Nb anomaly to be considered a real feature rather than an artifact of the analysis.

F7. Zr/Ti vs. Nb/Y, p. 56.

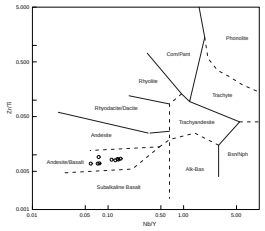

F8. Geochemical discriminations diagrams, p. 57.

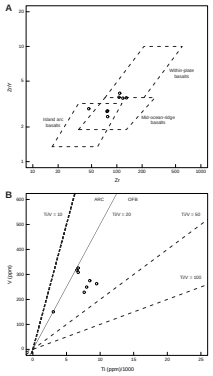

F9. XRF multielement plots, p. 59.

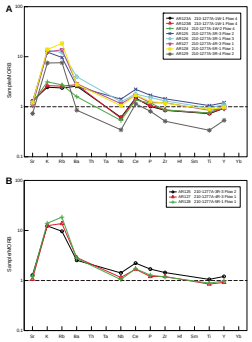

As noted above, seven samples were also analyzed by a whole-rock ICP-MS method (Table T2) to extend the results from the XRF analysis. The samples plot within or near the MORB field on most of the standard tectonic discrimination diagrams (e.g., Zr/Y vs. Zr [Fig. F10A], Ti vs. V [Fig. F10B], and Ti/100 vs. Zr vs. 3Y [Fig. F10C]). In a Hf/3 vs. Th vs. Ta plot (Wood, 1980) the samples plot in the enriched (E-)MORB/within-plate tholeiite, N-MORB, and island arc tholeiite fields (Fig. F10D). The spider plot of sample/MORB vs. element indicates near-MORB to slightly enriched patterns (Fig. F11A). The low normalized values of Nb relative to Th and Ce in particular, which are also relatively immobile elements, confirm that a negative Nb anomaly is present, as indicated by the XRF data. Finally, chondrite-normalized plots show N-MORB-like or slightly enriched patterns (Fig. F11B).

Comparisons of Basalt Composition

The analytical results from Site 1277 can be compared with the compositions of basalts from several representative areas, including the Iberia margin, Southwest Indian Ridge, East Pacific Rise, Goban Spur, Hatton Bank, Reykjanes Ridge, and the compositional array of Iceland basalts (Fig. F12). The Site 1277 basalts are chemically similar to basalts from the Goban Spur and lie within the field of East Pacific Rise basalts and some Southwest Indian Ridge basalts. However, they differ from the enriched basalts that characterize the Iceland array, as these exhibit higher degrees of mantle melting that is widely believed to relate to a North Atlantic mantle plume (Kempton et al., 2000).

As noted above, the Newfoundland margin basalts plot within or close to the field of basalts from Goban Spur (Deep Sea Drilling Project [DSDP] Leg 80), which is early formed oceanic crust located near the base of the continental shelf, southwest of the British Isles (de Graciansky, Poag, et al., 1985). In this area a narrow ocean–continent transition zone is characterized by faulted Hercynian basement cored at Site 549, passing laterally into "transitional" crust at Site 551, and then into early formed ocean crust at Site 550. Below Upper Cretaceous chalk at Site 551A, 58.9 m of basaltic flows and pillows with pink and white calcareous infillings was recovered. In addition, 33 m of basalts, pillow lavas, hyaloclastite, and minor limestones of inferred late Albian age was recovered at Site 550. Because the Newfoundland basalts plot within parts of the much wider compositional ranges of basalts from the East Pacific Rise and the Southwest Indian Ridge, they are compatible on chemical grounds alone with an origin related to seafloor spreading; however, their occurrence above exhumed mantle and being interbedded with serpentinite-rich mass flows at Site 1277 differs strongly from "normal" oceanic crust.

The Site 1277 basalts are generally more depleted than those from the Iberia margin, which range from MORB to transitional (T-)MORB and E-MORB. Published REE values of Iberia basalts analyzed by ICP-MS (Seifert et al. 1997; Cornen et al., 1999) are variable, ranging from 3.20 to 29.5 ppm. As a result, the compositional field on the Nb/Y vs. Zr/Y diagram (Fig. F12) is large and overlaps with some enriched plume-influenced basalts (e.g., Iceland) and is also similar to some continental flood basalts. Care should be taken when interpreting the Iberia analyses, as these were made on clasts within serpentinite breccias and they could have been derived from several different tectonic settings related to rifting and early seafloor spreading, as summarized in the following section.

F10. Geochemical plots, p. 60.

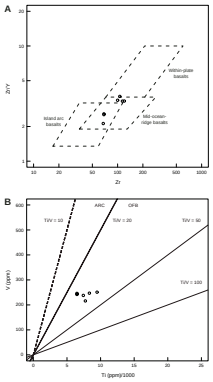

F11. ICP-MS multielement plots, p. 62.

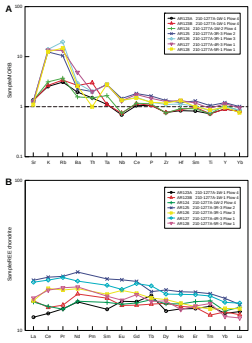

F12. Nb/Y vs. Zr/Y, p. 63.

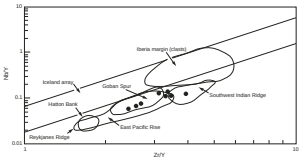

Volcanic rocks related to contemporaneous subduction (e.g., volcanic arc basalts) typically exhibit a well-defined negative Nb anomaly, as seen in modern lavas erupted above subduction zones (e.g., Pearce, 1982). However, the subduction component inferred from chemical analysis may not always relate to contemporaneous magmatism. Where subduction fluids interact with mantle, a subduction chemical signature may be incorporated into lithospheric mantle. This subduction component may be retained until it is released from the lithospheric mantle during some later tectonic event (e.g., an extensional event unrelated to the original subduction setting). A good example is the late Cenozoic basaltic magmatism of the western United States, which shows evidence of a lithosphere-hosted subduction component (e.g., Fitton et al., 1988). Previously, small negative Nb anomalies in basalts from Gorringe Bank on the south Iberia margin were interpreted as the effect of "contamination" of the melt by subcontinental mantle or by delaminated mantle lithosphere (Cornen et al., 1996), suggesting that the principle of an inherited subduction component may be widely applicable. As a cautionary note, however, small negative Nb anomalies may also occur and be unrelated to known subduction (e.g., in certain mid-ocean-ridge settings because of normal variations in partial melting). In principle, Nb may also be preferentially incorporated within certain Ti-rich minerals independent of subduction (e.g., rutile-bearing pyroxenites, as locally sampled from beneath the Iberia abyssal plain) (see Cornen et al., 1999).

It is likely that the negative Nb anomaly seen in the MORB-normalized plots of Site 1277 basalts represents a chemical signature that was inherited from subcontinental mantle that was affected by an earlier subduction event in the region. The probable origin of the subduction influence would be related to closure of the Iapetus or Rheic oceans. Similar conclusions are reached by Müntener and Manatschal (2006) based on the composition of the underlying peridotites.

The results from Site 1277 can also be compared with analytical data for two sills of alkaline diabase of Albian–Cenomanian age that were recovered from the lowest levels of the adjacent Site 1276 (Fig. F2). The resulting MORB-normalized patterns were interpreted to reflect alkaline "hotspot"-type magmatism >25 m.y. younger than the likely age of magmatism at Site 1277 (Hart and Blusztajn, 2006). Sr, Nd, and Pb isotopes and the relative depletion of Nb and Ta in the sills, as seen on normalized multielement plots, are suggestive of an additive component of crustal material. It is therefore possible that the composition of melts along the Newfoundland margin, including both Sites 1276 and 1277, was affected by the presence of continental crust and/or exhumed lithospheric mantle. Seismic refraction studies suggest that the ocean–continent transition zone of the Newfoundland margin is likely to include thinned continental crust that was emplaced during the later stages of continental breakup (Van Avendonk et al., 2006).

Assuming that the MORB at Site 1277 has incorporated a lithosphere-hosted subduction component, this has important implications for basalts that were erupted during continental breakup and are now preserved in orogenic belts exposed on land. The Site 1277 basalts represent one of the few known examples of basement emplaced during the very earliest stage of seafloor spreading (Fitton, in press). These settings are by their nature rarely available for study in modern submarine rifted margins, which are covered by thick deep-sea sediments. Instead, they are more commonly encountered in tectonically emplaced ancient rifted margins (e.g., Robertson, 2007).

In several orogenic belts (e.g., Tethys and Iapetus oceans) the tectonic setting of rifting is controversial. For example, the Triassic volcanic rocks of Greece, related to rifting of the Neotethys Ocean, have been explained in terms of either normal rifting unrelated to subduction (Dornsiepen and Manutsoglu, 1996) or as subduction-related (back-arc) rifting (Pe-Piper and Piper, 2002). The presence of a subduction signature, notably a negative Nb anomaly, has been taken as evidence that this rifting occurred in a contemporaneous subduction-related setting (Pe-Piper and Piper, 2002, and references therein). However, the field geological setting in the region is compatible with a continental rift setting unrelated to active subduction (Robertson et al., 1991; Robertson, 2006). Another example is rifting that opened the Iapetus Ocean, as preserved in Quebec, an area where a subduction-like chemistry has been explained by crustal assimilation during rifting and continental breakup (Camiré et al., 1995). The chemical analyses of the Site 1277 basalts show that distinctive negative Nb anomalies can occur in rifted margin settings, unrelated to contemporaneous subduction.

COMPARISONS WITH THE IBERIA-GALICIA MARGIN

Lithologies, structures, and geologic setting at Site 1277 are comparable to those drilled on the Iberia margin, including the Galicia Bank (ODP Leg 103) and the Iberia Abyssal Plain (ODP Legs 149 and 173), as well as Gorringe Bank farther south (Fig. **F13**). In particular, evidence of normal faulting that exhumed mantle lithosphere was previously documented on the Iberia margin at Sites 897, 899 (Sawyer, Whitmarsh, Klaus, et al., 1994), and 1070 (Whitmarsh, Beslier, Wallace, et al., 1998). These sites are located within the inferred ocean–continent transition zone (within the M-series magnetic anomalies). In addition, basalts from earliest formed oceanic crust have also been recovered farther north, on Goban Spur, in the United Kingdom southwestern approaches (Leg 80) (Kempton et al., 2000). Similarities and differences with the recovery on the Newfoundland margin are highlighted below.

F13. Tectonic and stratigraphic relations, p. 64.

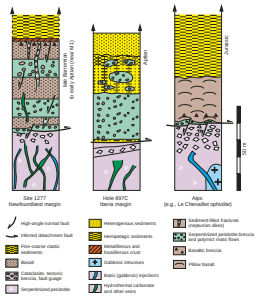

Exhumed Lithosphere

In contrast to the strongly depleted serpentinized harzburgite recovered from Site 1277, which indicates a highly depleted mantle source (Müntener and Manatschal, 2006), the Iberian examples include relatively enriched lherzolite, which implies a relatively undepleted mantle source (Cornen et al., 1999). This difference may reflect different types of basement beneath both margins, which could include much older ophiolitic rocks beneath the Newfoundland margin (Müntener and Manatschal, 2006).

The presence of spinel peridotites from the Iberia margin might be explained in three ways. First, they could record the products of melt extraction from juvenile (primary) mantle in an ocean ridge–like setting. This seems unlikely given their position within the ocean–continent transition zone. Second, they could represent inherited mantle that remained relatively undepleted, which would require major, but plausible, differences of basement type across the conjugate margins. Third, they could represent "refertilization" of previously depleted mantle that had a similar composition to mantle at Site 1277 (Mün-

tener and Manatschal, 2006). However, this would require regional differences in a process ("refertilization") that remains poorly understood.

Serpentinite Breccias Formed by Tectonic Processes

Serpentinite breccias were also drilled on the Iberia margin at Site 1070 during ODP Leg 173 (Whitmarsh, Beslier, Wallace, et al., 1998; Whitmarsh and Wallace, 2001). The "basement" recovered there begins with relatively massive, partially serpentinized peridotite that is intruded at the top by a relatively unaltered gabbro pegmatite dyke (Beard et al., 2002). This is overlain by calcite-cemented peridotite breccias, with clasts of serpentinized peridotite, variable amounts of pyroxene grains, and minor weakly deformed coarse-grained gabbro. The breccia shows a downward transition to noncohesive fault gouge and an interlocking jigsaw texture of clasts and was therefore interpreted as mainly, or entirely, of tectonic origin. In this case the fault gouge can be interpreted as the effect of deformation along an extensional detachment fault. The overlying breccias are likely to reflect brittle fracturing related to the inferred faulting, although some degree of local gravity reworking may also have taken place. Similarly, at Site 1277 the uppermost levels of the serpentinized ultramafic basement show evidence of intense tectonic brecciation along an inferred extensional detachment fault. Breccia clasts in the mass flows above also indicate intense brittle fragmentation of ultramafic and gabbroic rocks (Fig. **F3A, F3B**).

Deformation of Serpentinized Basement and Peridotite Breccias

Carbonate veins within serpentinized basement and individual serpentinite clasts at Sites 897 and 899 exhibit a complex history of fracturing and carbonate precipitation in an extensional setting (Morgan and Milliken, 1996). Some of the veins exhibit successive phases of filling of open fractures. These veins were interpreted as neptunian fractures that were filled with fine-grained carbonate, oxide grains, and serpentinite fragments. This material was possibly derived by brecciation of the wall rocks. The fractures were inferred to relate to stages in the exhumation of serpentinized peridotite to the seafloor. By contrast, later-stage fracturing and the formation of micrite-filled veins were interpreted to be the result of gravity collapse of uplifted basement, although they could also have resulted from continuing extension, as inferred at Site 1277. Stable isotopic and trace element analyses of the vein-filling carbonate at Site 897 and within serpentinite breccia at Site 899 suggest a low-temperature origin (<20°C) from seawater (Morgan and Milliken, 1996). Similar neptunian fissures and geopetal structures occur at Site 1277, as discussed earlier.

Fabric studies of the serpentinized peridotite breccias at Site 899 indicate an origin as cataclasite (Comas et al., 1996; Beslier et al., 1996). Calcite veining is most abundant in the upper part of the breccias and is most intense in clasts at the base of the reworked sequence. Fabric studies also indicate that two cataclastic events affected the breccias. Fabrics of the first event are associated with mylonitic textures, shear foliation, and calcite-free serpentinite veining. A later multiphase event involved serpentinization and penetrative cataclastic brecciation associated with abundant calcite and rare serpentinite veining.

These results are consistent with the existence of an extensional detachment separating an exhumed serpentinized ultramafic basement

from overlying mass flows. They also suggest a continuing history of faulting after mass flow emplacement, as inferred for Site 1277.

Sedimentology of Serpentinized Peridotite Breccias

Serpentinized peridotite breccias, comparable to those recovered at Site 1277, were cored in Holes 897C, 897D, and 899B (Comas et al., 1996) (Fig. F13). At Site 897, up to 143 m of basement rocks were recovered, composed of relatively undepleted peridotites. The peridotite basement in Hole 897C is covered by friable serpentinite breccia. Brecciated peridotite also occurs deeper in the peridotite basement in Hole 897D. The basement of both holes is overlain by heterogeneous deposits ("olistostromes"), including clasts and boulders of serpentinized peridotite and serpentinite breccia in sediments of early Aptian age.

At Site 899 (Hole 899B) no basement was encountered but a 188-m-thick lowermost sedimentary succession of early Aptian age includes heterogeneous serpentinite breccias, boulders, fault gouge, and fragments of weathered basalt, diabase, micrograbbo, and sheared amphibolite. During the Aptian, approximately coeval gravity deposits reached Sites 897 and 899 (located ~20 km apart), implying widespread sediment dispersal from highs to basinal areas (Comas et al., 1996).

On the Iberia-Galicia margin, the drilled intervals of serpentinized peridotite breccia, as thick as 5 m and separated by fine-grained sediment, were interpreted as relatively cohesive mass flows (olistostromes) (Comas et al., 1996). The clasts within the mass flows include reworked synrift sediments similar to those previously reported from Galicia Bank (Boillot et al., 1987; Kornprobst et al., 1988). Comas et al. (1996) proposed a relatively distal source for the serpentinite mass flows, from a remote transform-fault setting, although these authors also considered a more local origin related to normal faulting near or within the ocean–continent transition zone. Comas et al. (1996) also envisioned that the serpentinized peridotite breccias were deposited in a deep basinal setting, followed by block faulting, uplift, and covering by pelagic facies during latest Cretaceous–Paleogene time. In their view the peridotite ridges developed in response to normal faulting that followed continental breakup, possibly associated with a regional change in plate motion. On the other hand Gibson et al. (1996) interpreted the serpentinite breccias from Hole 899B as giant submarine landslips generated by slope failure on a large serpentinite fault scarp affected by extension, and they suggested that this fault was located within a few kilometers of Site 899.

In contrast to the above interpretations, the Site 1277 mass flows are interpreted as relatively proximal deposits that were derived from locally exhumed mantle and an inferred seafloor detachment fault. The writer believes a similar mechanism and tectonic setting of formation is also applicable to the Iberia-Galicia margin mass flows, although some of the material in these deposits is likely to have been transported farther and mixed from several different sources.

Mafic Magmatic Rocks

Only subordinate clasts or fragments of mafic rocks have been recovered from the Iberia-Galicia margin, consisting of basalts and microgabbros that are relatively undeformed (Cornen et al., 1996). The basalts exhibit porphyritic, intergranular, and variolitic textures. Most samples are strongly altered by low-temperature seafloor metamorphism. Petro-

graphic results, including the discovery of alkaline pyroxene, suggest that some of the basalts may be alkaline in composition, whereas porphyritic basalts containing pseudomorphed olivine phenocrysts and Ca-rich plagioclase are likely to be tholeiitic.

Chemical analysis of the basalt and diabase clasts from the Iberia Abyssal Plain (Holes 899B and 900A) and from Galicia Bank exhibit REE values and normalized spidergram patterns that indicate a wide range of E-MORB, T-MORB, and N-MORB (Kornprobst et al., 1988; Seifert and Brunotte, 1996; Seifert et al., 1997; Cornen et al., 1996) (see Fig. F12). Depleted tholeiites characterized by a marked negative Nb anomaly were recovered from Gorringe Bank, farther south (Cornen et al., 1999). Rare examples of metabasite clasts and boulders from the Iberia margin have been interpreted as Fe-Ti gabbros that were sheared and metamorphosed under greenschist-facies conditions (Schärer et al., 1995). Localized fragments of foliated amphibolites, compositionally similar to differentiated and chemically enriched flaser gabbro recovered at Site 900, may relate to alkaline synrift magmatism (Schärer et al., 1995; Gardien et al., 2001).

It can therefore be inferred that basic magmatic rocks of a wide compositional range were erupted on the Iberia-Galicia margin as a whole, potentially influenced by different magma sources (e.g., synrift vs. earliest seafloor spreading) and differences in the degree of partial melting. By contrast, only basalts of a narrow MORB-type composition are known from the Newfoundland margin.

Summary of Newfoundland-Iberia Comparisons

The serpentinized peridotite breccias recovered from holes drilled on the Iberia-Galicia and Newfoundland margins show many similarities. First, exhumed peridotites are present on both margins, although the composition of the Iberia-Galicia margin peridotite (Müntener and Herman, 2001; Abe, 2001) differs considerably from the peridotite recovered at Site 1277, as the latter is much more depleted (Müntener and Manatschal, 2006). Second, there is structural evidence of an extensional detachment on both margins separating exhumed serpentinized peridotite from mass flow deposits. Third, serpentinite breccias are interpreted as mass flows on both margins, although some of the Iberia mass flows may have traveled farther than those at Site 1277. Fourth, some of the clasts in the mass flows on both margins were derived from inferred extensional detachment surfaces. Fifth, several generations of extensional fracturing, neptunian dike infill, and low-temperature calcite veining followed initial high-temperature ductile deformation, cataclasis, and exhumation on both margins.

There are also several apparent differences between the two margins. First, the serpentinite mass flows of the Iberia margin are more heterogeneous and include clasts of margin-derived terrigenous sediment not seen at Site 1277. Second, MORB was recovered from intact flows at Site 1277, whereas only clasts of igneous rocks have been recovered from the Iberia-Galicia margin. Third, the Site 1277 basalts of MORB composition do not show the highly variable compositions (mainly N-MORB to E-MORB) of the basalt clasts on the Iberia-Galicia margin. These differences may, however, reflect the chance recovery of drilling in minute sections of complex terrain. All of the Iberia and Newfoundland sites can be interpreted to sample different parts of a wide zone (~150–200 km) of crustal exhumation within an ocean–continent transition.

COMPARISON WITH THE ALPS AND THE APENNINES

Interpretation of the North Atlantic rifted margins can benefit significantly from comparison with the rifting and early stages of opening of the Jurassic Tethys Ocean in the Alps and the Apennines where there is abundant evidence that mantle rocks were exposed and reworked during rifting. However, these are exposed within far-traveled thrust sheets, making palinspastic reconstruction difficult.

Much early evidence came from the Italian Apennines where Alpine ophiolites are well exposed (e.g., northern Apennines and Elba). These rocks experienced relatively little emplacement-related deformation and metamorphism during contractional orogenesis, making it relatively easy to recognize seafloor features (e.g., Abbate et al., 1980). Different sections expose a variety of mafic and ultramafic rocks depositionally overlain by lithologies that include carbonate-rich serpentinite breccia (i.e., ophicalcites; see below) intercalated with polymict breccia and basalts of MORB type (e.g., Barrett and Spooner, 1977; Abbate et al., 1980; Lagabrielle et al., 1984). During the 1970s and early 1980s the generally favored view was that exposure of plutonic rocks on the seafloor and the formation of related polymict sediments was largely along transform faults within the opening Jurassic ocean. Faulting of the oceanic basement was attributed to transcurrent faulting (e.g., Gianelli and Principi, 1977), transtension in a transcurrent rift (Weissert and Bernoulli, 1985; Ishiwatari, 1985), or rifting at a spreading center (Barrett and Spooner, 1977). Additional important evidence came from the French, Italian, and Swiss Alps; however, only a few relatively small ophiolitic remnants in these areas have escaped emplacement-related deformation and metamorphism sufficiently to allow primary ocean floor relationships to be restored. During the 1980s and 1990s individual ophiolitic "massifs" of the "internal" Alps were investigated. In all these areas the "ophiolite" association of mafic and ultramafic rocks overlain by polymict clastic sediments and basic volcanics differs strongly from the established concept of a Penrose-type ophiolite (Anonymous, 1972) that was modeled largely on the Jurassic Coast Range ophiolite in California, the Jurassic Vourinos ophiolite in Greece, and the Upper Cretaceous Troodos ophiolite in Cyprus. These ophiolites have since been shown to have formed in subduction-related settings based mainly on chemical evidence (e.g., Pearce et al., 1984; see also Robertson, 2002).

It was long assumed that ocean crust in the modern oceans should have a Penrose-type ophiolite structure. However, evidence from the Mid-Atlantic Ridge has shown that mantle can be exposed on the seafloor, especially in slow-spreading settings (e.g., Tucholke and Lin, 1994). The Apennine and Alpine Jurassic ophiolites were interpreted as a rifted slow-spreading ridge (Tricart and Lemoine, 1983; Lemoine et al., 1987; Lagabrielle and Cannat, 1990; Lagabrielle, 1994). However, the sediments overlying the exhumed plutonic basement locally include relatively coarse proximal terrigenous clastic sediments (e.g., with granite, mica schist, or dolomite), showing that the crust was in a proximal-margin position rather than in the setting of an open-ocean spreading ridge. Thus, some of the plutonic rocks could represent the exhumation of subcontinental mantle associated with the transition from a rifted continental margin to seafloor spreading. This interpretation was supported by geochemical investigations of both the plutonic ophiolitic

rocks (e.g., gabbro and serpentinite) (Pognante et al., 1986; Piccardo et al., 1990) and the overlying lavas of transitional or mid-ocean-ridge type (Beccaluva et al., 1984).

In recent years much progress has come from detailed comparisons of the results of ocean drilling on the Iberia and Newfoundland margins with several ophiolite sections in the Alps (Manatschal and Bernoulli, 1998; see Manatschal et al., in press, for a review) coupled with modeling studies (e.g., Lavier and Manatschal, 2006). Different sections document the exhumation of both middle crust and subcrustal mantle. For example, exhumed crust (e.g., gabbro or amphibolite) is preserved in several tectonic units, notably the Platta nappe (e.g., Piz d'Err-Piz Bial areas) (see Manatschal and Nievergelt, 1997, and references therein). This aspect is not discussed further here because similar crustal lithologies were not recovered at Site 1277.

Critical field relations similar to Site 1277, notably basaltic lavas covering detachment faults, are well exposed in eastern Switzerland (Manatschal and Nievergelt, 1997; Desmurs et al., 2001, 2002). Specific examples include the Totalp, the Err-Platta, and the Malenco units in the eastern Central Alps, in Graubünden (Switzerland), and also in northern Italy (Manatschal et al., 2001, 2003). Also, within the Lanzo metaophiolite of northern Italy, serpentinized peridotites document exhumed mantle that is overlain by basaltic rocks related to final continental breakup (Lagabrielle et al., 1989; Pelletier and Müntener, 2004).

One of the best-exposed examples, the Chenaillet ophiolite, straddles the French/Italian border and was examined on a field trip by members of the Leg 210 Scientific Party, who were impressed by the close similarities with the core recovery at Site 1277 (Fig. **F13**). At this location, serpentinized mantle peridotites and intrusive gabbros are topped by a prominent shear zone, interpreted as a large-scale oceanic detachment fault (Manatschal and Müntener, 2005). The detachment surface is directly overlain by dark tectonic-sedimentary breccias, interpreted as fault gouge and cataclasite reworked from within the zone of crustal extension. Basaltic pillow breccias and pillow lavas overlie the coarse clastic sediment or lie directly on the detachment. An important observation, demonstrated by detailed mapping, is that the detachment is cut and offset in a domino-like fashion by a number of high-angle normal faults. In places, these faults are covered and sealed by lava breccias and pillow basalts, showing that high-angle faulting was active at an early stage following basement exhumation (Manatschal and Müntener, 2005). These faults also cut the fault gouge and serpentinite-rich mass flows, confirming that the faulting took place after exhumation and mass wasting of the surface of the exhumed basement.

Other well-exposed reference sections are provided by the Platta nappes in southeast Switzerland, examined by participants in the interMARGINS workshop, 2004 (Manatschal and Müntener, 2004). Individual thrust sheets preserve remnants of the ocean–continent transition zone that is interpreted as part of the southern margin of the Jurassic Tethys (Froitzheim and Manatschal, 1996; Manatschal and Nievergelt, 1997). The Platta nappe records a zone of exhumed subcontinental mantle into which gabbros and basaltic dikes were locally intruded. Serpentinites of the exhumed mantle are directly overlain by tectonic-sedimentary breccias. Mid-ocean-ridge–composition pillow basalts and postrift sediments contain continentally derived material, indicating a proximal setting. Serpentinite-rich calcite-cemented breccias, known as ophicalcites, range from one type of lithology, in which the serpentinite is fissured and the fractures are infilled by fine-grained

red carbonate and calcite spar, to another type that is dominated by clast-supported fragmented breccia clasts (Bernoulli and Weissert, 1985). These lithologies, known as the Type 1 ophicalcite of Lemoine et al. (1987), are very similar to those drilled at Site 1277 and they include comparable geopetal infills that confirm that the ultramafic rocks were exposed on or near the seafloor. The clasts include foliated gabbro that was deformed under high-temperature conditions before being eroded and emplaced within the breccias. In places (e.g., in the Falotta area) the tectonic-sedimentary breccias are stratigraphically overlain by mid-ocean-ridge–type pillow basalts, which thicken oceanward in restored sections (Schaltegger et al., 2002). The basalts are interpreted to have been derived from a depleted mantle source in a setting of seafloor spreading immediately following continental breakup that opened the Jurassic Tethyan Ocean. The eruption of basalts appears to have been controlled by high-angle faults postdating the low-angle faulting that exhumed serpentinized peridotite; however, basaltic dikes are also locally cut by detachment faults. This implies that low-angle and high-angle faulting and basaltic volcanism were all closely associated in space and time (Manatschal et al., in press).

The field studies also confirm that different fault zones are present at different levels of the restored ocean–continent transition, and these can be interpreted as multiple detachments. The serpentinite breccias were formed by both tectonic processes (i.e., ductile shearing to brittle fragmentation) and sedimentary processes (i.e., as multiple mass flows) in different parts of individual sections. The breccias were deposited across the former detachment surface and were not restricted (e.g., to local fault scarps). The overlying bedded deep-sea sediments (e.g., radiolarite) are inclined at a low angle (<20°) relative to the underlying inferred detachment faults. This shows that these faults were active at a low angle at least during the later stages of their movement and that they were directly overlain and sealed by deep-sea sediments (Manatschal and Nievergelt, 1997).

POSSIBLE TECTONIC MODELS

Available evidence from Site 1277, as summarized in Figure **F14,** is limited, and thus several different tectonic models need to be considered. These models should also take account of evidence from the Iberia-Galicia margin and the Alps-Apennines. Debatable aspects include the source of the serpentinized peridotite and related gabbroic intrusive rocks; the setting of formation of the mylonitic fabrics and ductile-type deformation within both the basement serpentinized peridotite (Unit 2) and the clasts in the overlying sediments (Unit 1); the setting of basaltic volcanism and its magmatic source; and the later history of brittle deformation, fracturing, veining and hydrothermal alteration, and uplift of the peridotite ridge.

F14. Local seafloor relations, p. 65.

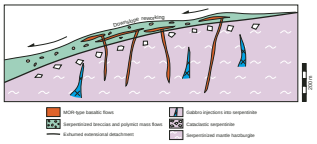

Setting of Serpentinized Harzburgite

The serpentinized spinel harzburgite is chemically highly depleted and can be considered to resemble depleted mantle-type sequences of suprasubduction-type ophiolites (Müntener and Manatschal, 2006). One possibility is that the harzburgite records the lower part of an ophiolite that was emplaced during Paleozoic closure of the Iapetus Ocean, similar to the Ordovician Bay of Islands ophiolite (Newfoundland), or

the Troodos ophiolite (Cyprus). In the southwest Pacific region, the Neogene–Holocene Woodlark Rift dissected a regionally emplaced meta-ophiolite, as confirmed by the presence of ophiolite-derived clastic debris on the footwall of the rift, drilled during ODP Leg 180 (Taylor, Huchon, Klaus, et al., 2000; Robertson et al., 2001). If the Site 1277 ultramafic rocks represent part of an unmetamorphosed ophiolite they would have been preserved at a high structural level, and thus no deep exhumation of mantle would be needed to exhume them during rifting of the Newfoundland margin. However, an origin solely as an emplaced ophiolite is unlikely in view of the width and length of the inferred zone of exhumed sub-continental mantle lithosphere on both sides of the Atlantic (as wide as 150–180 km wide) and the absence of recovery of any higher-level ophiolitic rocks (e.g., diabase).

A second possibility is that the serpentinized spinel harzburgite formed at an "unusual" seafloor spreading center. In such an interpretation it would, however, be necessary to explain why the ultramafic rocks at Site 1277 are so depleted and how these rocks were exhumed. One possibility to explain the depletion is that seawater gained access to the mantle from above, allowing hydrous melting and thus producing unusually depleted magmas. It is generally believed, however, that the chemical depletion of ophiolitic mantle harzburgite can only be explained by the introduction of water from below related to subduction (e.g., Pearce et al., 1984). In a seafloor spreading model the ultramafic rocks might have been exhumed as a result of slow spreading, creating exhumation structures similar to the megamullions of the Mid-Atlantic Ridge (Tucholke et al., 1998). In this interpretation, no crustal sequence (e.g., diabase/basalt) need have existed locally above the ultramafic rocks; however, large volumes of basalts would still be expected related to regional seafloor spreading, and these do not occur at Site 1277.

A third alternative, favored here, is that the recovered serpentinite represents mantle that is now chemically depleted because it experienced melt extraction in a subduction-related hydrous setting at some earlier time (i.e., prior to North Atlantic rifting) (Müntener and Manatschal, 2006). The likely setting would be subduction related to closure of the Iapetus or Rheic oceans during the Ordovician to Permian.

In this third interpretation, it is necessary to explain why the Iberia margin ultramafic rocks do not show a similar depletion. One possibility is simply that the Iberia source mantle was located far from the inferred subduction zone, for example mantle that was exhumed from beneath the edge of the African (Gondwana) craton. Another possibility is that the Iberia mantle was depleted like that at Site 1277, related to melt extraction in a subduction setting, and that the mantle was then "refertilized" at a later stage, either prior to or during Atlantic rifting. There is little evidence, however, to support this possibility at present.

In summary, an origin as subcrustal mantle that was affected by a prior subduction event is inferred. This implies that continental crust originally existed above the mantle at Site 1277 but was removed by extensional faulting. The mid-ocean-ridge–type basalts were presumably extracted from less depleted mantle that is in the vicinity of Site 1277 but has not been sampled.

Setting of Ductile Deformation Related to Extension

Several alternatives can be considered for the inferred high-temperature ductile deformation and cataclasis within the peridotite basement

(Unit 2) and also within many of the clasts in the overlying the mass flows (Unit 1).

A first possibility, favored here, is that the ductile deformation took place on one or more deep-seated extensional faults within a core-complex system and that any overlying continental crust was removed, allowing the exhumation of subcontinental mantle lithosphere. A second possibility is that the contact between Units 2 and 1 records detachment faulting between oceanic mantle and oceanic crust (e.g., related to "ultra-slow seafloor spreading"). It is difficult to distinguish between these two options based on the structural evidence alone because neither continental crust (e.g., schist and gneiss) nor normal oceanic crust detritus (e.g., lava and diabase) were observed within the debris flows at Site 1277. The implication is that the upper plate of whatever crustal type was detached from the area at a relatively early stage such that all the detritus at Site 1277 was derived from the exhumed lower plate.

A third possibility is that the observed deformation records normal faulting at a high structural level. This is unlikely in view of the high-temperature ductile deformation observed within the basement (Unit 2) and also in some clasts within the mass flows (e.g., serpentinite mylonite). Also, the cataclasis at the top of the basement (Unit 2) and the cataclastic fabrics in some clasts within the mass flows (Unit 1) resemble features related to the low-angle extensional faulting in the Alpine ophiolites, as summarized in the previous section.

Several factors are consistent with the presence of a regional-scale detachment at Site 1277, notably the absence of crustally derived (terrigenous) sediment and the fact that the mass flows (Unit 1) include clasts that appear to be have been eroded locally from the detachment, including fault gouge material. The primary mantle tectonite fabric in the basement cores is commonly steeply inclined and is itself cut by sub-vertical fractures and veins (Shipboard Scientific Party, 2004b) (e.g., Sample 210-1277A-9R-4, 26–46 cm). If it is assumed that the primary mantle fabric was originally gently inclined, as in many ophiolites (Nicolas, 1989), it is possible that the basement was rotated around a horizontal axis within an extensional fault system and then cut by later high-angle brittle fractures. However, the orientation of mantle fabrics in ophiolites is known to be variable. The fissures and veins in the mass flows are known to have developed subvertically (>80°) because they cut well-laminated, subhorizontal (<20°) sediments that preserve the paleohorizontal at the time of deformation. Similar subvertical fissures and veins cut the underlying serpentinized harzburgite, including the inferred high-temperature ductile shear zones. This suggests that any significant rotation was accomplished by exhumation before the serpentinite mass flows and basalts covered the seafloor.

Assuming that a regional-scale detachment was developed, two alternate end-member geometries can be considered. The first is an upward-concave fault (listric), as seismically imaged on the Galicia margin inboard of the locus of final breakup of continental crust (Reston et al., 1995; Krawczyk et al., 1996). The second is a downward-concave fault, which has not been directly observed in the Atlantic or elsewhere but which is inferred to be a geometric requirement of mantle exhumation (e.g., Tucholke and Lin, 1994; Lavier and Manatschal, 2006). A system of rolling hinge faults could involve near-simultaneous exhumation of both upper mantle and crust, potentially on both margins of the zone of continental breakup. A wide zone of thinned continental crust is now believed to be present along the Newfoundland margin, as sug-

gested by interpretations of the SCREECH 2 and SCREECH 3 seismic reflection data (Van Avendonk et al., 2006; Lau et al., 2006). Similar crustal thinning was previously suggested for the Iberia margin (Reston et al., 1995; Krawczyk et al., 1996), as noted above; however, the actual settings of exhumation of subcontinental mantle and continental crust may be complex and regionally variable, involving faulting of different scale, geometry, and timing that cannot yet be constrained by drilling or geophysical evidence.

Setting of Serpentinite Mass Flows

Two origins for these flows can be considered, taking account of evidence from the Iberia-Galicia margin and the Alps-Apennines. Both assume a relatively local origin for the mass flows.

First, the peridotite breccias may have been deposited during the exhumation of mantle in a continuous process (i.e., serpentinite mass flows are an inherent product of the process of exhumation). A possible problem here is that the exhuming mantle was not simultaneously covered by terrigenous sediment derived from the upper plate, whereas elsewhere topographic lows were flooded by terrigenous turbidites (e.g., Site 1276 and DSDP Site 398) (Tucholke, Sibuet, Klaus, et al., 2004) or accumulated a terrigenous component (Iberia margin Site 897) (Comas et al., 1996).

A second alternative is that the serpentinite breccias formed later than the exhumation of the mantle as a result of high-angle faulting that created discrete peridotite ridges. In this case the recovery at Site 1277 could represent mass wasting of material from such a serpentinite ridge into a local low (i.e., small basin) that was elevated well above the regional seafloor and therefore isolated from terrigenous sources. Mass wasting of an upfaulted serpentinite ridge might have resulted in a vertical sedimentary organization of the detritus (e.g., a fining-upward sequence as the ridge was denuded); however, this is not observed and, in fact, the largest known detached block (meter sized) is located toward the top of the recovery. Site 1277 serpentinite breccias also clearly originated as multiple debris flows rather than as massive slides from serpentinite fault scarps, as inferred for some of the Iberia breccias (Gibson et al., 1996).

The first (i.e., continuous) process is consistent with Alpine counterparts because serpentinite breccias seem to be a near-ubiquitous feature wherever exhumed mantle has been identified, rather than merely forming along discrete serpentinite ridges. The Alpine serpentinite breccias appear to have formed a laterally persistent blanket that was genetically linked with mantle exhumation along a gently inclined (<20°) master detachment. The most probable explanation for the absence of terrigenous sediment at Site 1277 is that the upper plate of detached continental crust was already far removed (several kilometers or more) before the serpentinite mass flows were deposited. The area of active mantle exhumation was possibly isolated from terrigenous input by topographic barriers (e.g., other mantle fault blocks) between Site 1277 and the rifted margin to the west. In continental core complexes (e.g., Aegean Turkey) detrital sediment overlying inferred low-angle extensional faults is similarly derived from the exhumed lower plate (i.e., high-grade metamorphics), with little or no material from the detached upper plate (i.e., lower grade or unmetamorphosed rocks) (e.g., Purvis and Robertson, 2004).

Setting of Basaltic Volcanism

Two main alternatives for the origin of the basaltic volcanism at Site 1277 are considered. The first is that the MORB from the Newfoundland margin formed in a setting of very slow seafloor spreading. However, the lava flows interbedded with serpentinite mass flows show that this basalt does not represent detritus from oceanic crust that was otherwise not recovered. The favored second alternative is that the MORB erupted following the completion of mantle exhumation and reflects the earliest basaltic volcanism related to the beginning of seafloor spreading. Assuming this is correct, sampling at Site 1277 was fortuitous; a drill location that reached basement farther west (continentward) would have sample only exhumed mantle lithosphere or continental crust, whereas a location farther east (oceanward) would have sampled "normal" oceanic crust.

The relatively depleted melt represented by the MORB volcanics is compatible with the extraction of melt from more fertile mantle than the depleted mantle harzburgite of the basement at Site 1277 (Müntener and Manatschal, 2006). One possible explanation is extreme mantle heterogeneity (i.e., highly depleted vs. undepleted upper mantle sources in a small area). Another possibility is that different slices of crust and mantle existed at different depths within a zone of rift-related extension along the Newfoundland margin. This possibly included ophiolitic mantle (i.e., the depleted ultramafic basement), continental crust (influencing the Th and Hf ICP-MS analysis), and deep "normal" upper mantle that is the source of the MORB. The Newfoundland margin is made of several tectonic terranes that were accreted at different times, notably the Avalon Terrane, which was emplaced during the Silurian–Devonian, and the Meguma Terrane, which was emplaced during the Carboniferous–Permian (Jansa and Wade, 1975; Williams et al., 1995). In addition, Hercynian-age (Carboniferous–Permian) lithosphere may be present in the vicinity of the Newfoundland margin, as suggested by the ages of detrital muscovites recovered at nearby Site 1276 (**Wilson and Hiscott,** this volume). In general, the presence of continental crust, mantle of different compositions, and small differences in the degree of partial melting could all have contributed to the observed chemical patterns of the Site 1277 basalts.

Setting of Late-Stage Brittle Deformation

The brittle deformation represented by subvertical fissures and veins in both the peridotite basement (Unit 2) and the mass flows (Unit 1) clearly postdated the ductile high-temperature deformation and exhumation. Several alternative scenarios are considered.

One possibility is that the brittle deformation represents the late stage of a single phase of extensional deformation (e.g., related to bending stresses that developed in the footwall during exhumation). Early high-temperature ductile deformation could have given way to brittle deformation during such progressive exhumation and cooling.

A second possibility is that the brittle fracturing reflects a separate phase of extension that followed initial mantle exhumation. This is favored for several reasons. First, faulting and veining in the serpentinite breccias could only have been preserved as brittle deformation structures after at least partial lithification of the serpentinite breccias and interbedded finer-grained sediments, which suggests the existence of a time gap between basement exhumation and high-angle brittle defor-

mation. Second, significant tilting would be expected during the brittle phase of progressive exhumation. However, the subtle primary lamination in the fine-grained sediments filling the fissures (i.e., geopetal fills) shows that relatively little tilting about a vertical axis (<20°) has taken place since the fissures opened and were filled with sediment. Third, evidence from the Iberia margin (Comas et al., 1996) and from the Alps (Manatschal et al., in press) suggests that a discrete phase of brittle deformation did indeed follow mantle exhumation in those areas. Such late-stage high-angle brittle deformation might reflect a continuation of the same tensional regime that controlled the exhumation. For example, in continental core complexes, early low-angle faults have been abandoned and replaced (i.e., cut through) by later high-angle faults when it became more energy efficient to generate new high-angle faults (Profett, 1986). On the other hand, the high-angle brittle structures might relate to a later, unrelated phase of crustal extension (see below).

A third possibility is that the high-angle structures might reflect gravity sliding or mass flow at the seafloor following exhumation. This interpretation would require the sliding and related internal deformation of a coherent mass of debris. However, gravity-driven structures in such debris might be variably oriented, listric, or low angle in geometry, in contrast to the consistent subvertical orientation observed at Site 1277.

The interpretation favored here is that the brittle fracturing and extension reflect the latest phase of extension related to mantle exhumation. This took place after exhumation of mantle along low-angle faults but possibly before the onset of "normal" seafloor spreading.

In-Plane Compression?

Several modeling studies have suggested that the initiation of "normal" mid-ocean-ridge spreading coincides with the release of in-plane tensile stress (i.e, relative compression) as large volumes of magma enter the rift zone (e.g., see Tucholke et al., 2007, for discussion). The modeling implies a long-wavelength lithosphere flexural response, which could be difficult or impossible to recognize using drilling data. Localized compression might also occur along weak zones in basement, resulting in local uplift, reverse faulting, or inversion of preexisting extensional faults. From this point of view, the Unit 2/1 boundary at Site 1277 represents an obvious weak zone located close to the locus of final breakup of subcontinental lithosphere, and it might possibly record a "relative compression event." The sediment infills of the high-angle fissures in fact record incremental widening related to progressive extension. Similar late-stage brittle extension was recorded on the Iberia margin (Beslier et al., 1996; Cornen at al., 1996; Morgan and Milliken, 1996). The proposed compression (late Aptian) postdates the normal faulting by as long as 14 m.y. and could therefore have postdated the end of extension documented by the veins (see Tucholke et al., in press). However, some the veins remain unfilled as open fractures and represent persistent zones of weakness. These open fractures could have collapsed if regional compression was locally expressed at Site 1277.

Faulting and Uplift of the Peridotite Ridge

Site 1277 was drilled close to the crest of the Mauzy Ridge (Fig. F2). It is uncertain when and how the ridge was uplifted. Deep seismic reflections lap against the Mauzy Ridge (see Fig. F2 in Shipboard Scientific Party, 2004a), showing that the ridge formed during or not long after

the final stages of continental breakup and that it is not likely to represent a geologically young feature. Two main possibilities can be considered.

One alternative is that the serpentinite ridge formed within the ocean–continent transition zone during exhumation of the mantle. Bending stresses associated with large-scale detachment faulting are thought to have broken the footwall and uplifted seafloor ridges to hundreds of meters high on the Mid-Atlantic Ridge (Tucholke et al., 1998). As noted earlier, continental core complexes are also known to undergo high-angle faulting following initial exhumation in areas such as the western United States (Profett, 1988) and western Turkey (Purvis and Robertson, 2004). This faulting is integral to progressive extension.

A second alternative is that the Mauzy Ridge was uplifted by normal faulting well after the mantle was first exhumed (i.e., during a later phase of extension), as proposed by Peron-Pindivic et al. (2007). The MORB lavas are on the crest of a long narrow ridge, elevated several hundred meters above the surrounding seafloor. This suggests that the ridge could have formed after clastic sedimentation and volcanism ended at Site 1277. The lavas were erupted on only gently inclined seafloor; eruption on a slope would have created pillow breccias or pillow lavas rather than the massive flows that dominate the core recovery. Extension is expected to have ended when the subcontinental mantle lithosphere finally separated and large volumes of magma entered the rift, initiating "normal" seafloor spreading. It has been proposed that this may have occurred as late as the late Aptian to early Albian (Tucholke et al., 2007). Thus, available evidence indicates the following progression of events:

1. Mantle exhumation,
2. Volcanism and mass wasting of exhumed mantle, and
3. Uplift of the ridge by high-angle normal faulting.

The time at which each of these events occurred and the question of their separation or overlap remains to be resolved by further drilling.

TECTONIC MODEL FOR CONTINENTAL BREAKUP

The inferred setting of rifting and final continental breakup at Site 1277 is summarized here (Fig. F15), building on comparisons with the Iberia-Galicia margin and the Alps-Apennines and adopting the preferred interpretations.

Rifting of the future Newfoundland continental margin and the conjugate Iberia margin (Sawyer, Whitmarsh, Klaus, et al., 1994; Beslier, Whitmarsh, Wallace, and Girardeau, 2001) took place during a prolonged period of pulsed crustal extension (e.g., Jansa and Wade, 1975; Tucholke, Sibuet, Klaus, et al., 2004), which culminated in the exhumation of subcontinental mantle lithosphere to create new seafloor at Site 1277 by late Barremian time. Upper-plate crustal rocks were removed from the immediate area, leaving an extensional detachment exposed on the seafloor. This detachment zone and underlying mantle peridotite together with minor gabbroic intrusives then underwent submarine erosion on a gently sloping seafloor (possibly <20°), giving rise to mainly coarse grained clastic sediments. Individual debris flows include up to meter-sized blocks of gabbro and serpentinized peridotite, together with derived clasts of serpentinite mylonite and cataclasite.

F15. Tectonic model, p. 66.

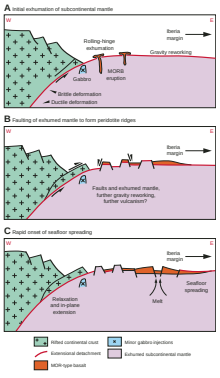

Three basaltic lavas flows were erupted locally, interspersed with the mass flows (Fig. F14). Chemical analysis showed that the basaltic rocks are of MORB composition, with a marked relative depletion of Nb. The negative Nb anomaly is suggestive of an inherited subduction influence on mantle composition. Eruptions were episodic and of low volume at Site 1277.

The basaltic lavas and interbedded clastic sediments later experienced extensional fracturing. Subvertical cracks opened, allowing carbonate silt to filter downward, together with hyaloclastite and basalt fragments. After cementation, refracturing took place, allowing further sediment infill and a later phase of precipitation of hydrothermal spar, as extension continued. These features may have developed during late-stage, high-angle normal faulting that uplifted the Mauzy Ridge.

Many lithologies are extensively altered and replaced, mainly by calcite. Some individual clasts in the polymict sediments have a wide variety of degrees of alteration within a single sample, showing that the alteration was variable and began at a relatively early stage before the rocks were exposed at the seafloor. On the other hand, the alteration (e.g., carbonate veining) that affects sediment infill of the neptunian fissures occurred later. Extension coupled with alteration, therefore, persisted for an extended period at Site 1277. The sedimentary-volcanic succession at Site 1277 was finally covered by a ferromanganiferous and fossiliferous crust that capped the Mauzy Ridge, above which terrigenous deep-sea sediment eventually accumulated.

CONCLUSIONS

1. Site 1277, near the crest of the Mauzy Ridge (near magnetic Anomaly M1), documents the formation of new seafloor by exhumation of subcontinental mantle lithosphere. It records part of the transition between exhumation of subcontinental mantle lithosphere and the initiation of "normal" seafloor spreading, and it is associated with minor MORB volcanism.
2. Serpentinized spinel harzburgite and minor intrusive gabbro were exhumed to the seafloor by means of a system of one or more extensional detachment faults. The brittle continental crust was completely removed, allowing mylonitic and cataclastic serpentinite (fault gouge) to be directly exposed on the seafloor above serpentinized ultramafic mantle.
3. The inferred detachment fault underwent submarine erosion to produce multiple debris flows dominated by lithoclasts of altered serpentinite and gabbro, occasionally larger than one meter. The mass flows ranged from cohesive matrix-supported debris flows with outsize blocks lower in the section to less cohesive pebbly debris flows including well-rounded clasts, generally higher in the section. A ferromanganiferous crust containing planktonic foraminifers then accumulated on the Mauzy Ridge. The ridge was much later covered by a relatively thin terrigenous deep-sea sedimentary succession.
4. Three intervals of basaltic lavas were erupted, interspersed with minor hyaloclastite (glassy chilled basalt). The middle lava interval consists of two sheet flows, whereas the upper flow includes lava breccia and possible pillow lavas. These flows, however, are small and basement at Site 1277 is dissimilar to "normal" oceanic crust.

5. Following eruption, high-angle fissures and fractures opened in the volcanic-sedimentary succession and were repeatedly infilled with calc-siltite, together with detrital grains of basalt and hyaloclastite, to form neptunian dykes. Hydrothermal calcite cementation and replacement of both clasts and matrix took place repeatedly, interrupted by fracturing and reopening of fissures in a setting of continuing extension. The fracturing may have resulted from continuing extension of the exhumed subcontinental mantle lithosphere until in-plane tensile stress was finally relaxed when subcontinental mantle lithosphere separated and "normal" seafloor spreading began; this may have taken place near the Aptian/Albian boundary.
6. The serpentinized harzburgite basement shows evidence of brittle high-angle fracturing and hydrothermal cementation like that of the overlying volcanic-sedimentary unit, suggesting that both the basement and its volcanic-sedimentary cover were deformed together in response to in-plane extension.
7. It is probable that the basement ridge (Mauzy Ridge) was uplifted by high-angle normal faulting in response to crustal extension after the initial exhumation of the subcontinental mantle lithosphere but prior to the onset of "normal" seafloor spreading.
8. The absence of terrigenous components in the volcanic-sedimentary sequence indicates that Site 1277 was isolated from margin-derived turbidites at the time the basement was exhumed. The most likely reason is the presence of a complex fault topography between the site and the adjacent rifted margin.
9. The basalts are similar to, or slightly enriched, relative to N-MORB composition. This suggests the existence of a relatively fertile mantle source at some depth below the highly depleted serpentinized spinel harzburgites that were cored at Site 1277.
10. An analytically significant negative Nb anomaly is present in MORB-normalized plots of the basalts from Site 1277. This anomaly is interpreted to be a subduction signature inherited from subcontinental mantle lithosphere that was involved in a preexisting subduction event, possibly related to Paleozoic closure of the Iapetus or Rheic oceans. Thus, care should be taken when interpreting similar negative Nb anomalies in ancient rift basalts exposed in orogenic belts (e.g., Tethys) as indicative of contemporaneous subduction, or arc volcanism, especially when the field relations are consistent with a rift setting that is unrelated to subduction.

ACKNOWLEDGMENTS

I thank my shipboard colleagues for ongoing discussions, in particular Gianreto Manatschal and Brian Tucholke for insights into the significance of the results from Site 1277. I also thank Othmar Müntener and Brian Tucholke for discussion of results after the cruise. Gianreto Manatschal and Othmar Müntener are also thanked for leading field trips to the Alpine ophiolites, which illustrated similarities with Site 1277. The manuscript benefited considerably from comments by O. Müntener, B. Tucholke, and an anonymous reviewer; discussions with G. Fitton and T. Ustaömer also assisted. G. White assisted with drafting of figures. I also thank Brian Tucholke for his help with editing the paper.

This research used samples and/or data provided by the Ocean Drilling Program (ODP). ODP is sponsored by the U.S. National Science Foundation (NSF) and participating countries under management of Joint Oceanographic Institutions (JOI), Inc. The research was funded by a Rapid Response Grant (RRG) from the United Kingdom Natural Environmental Research Council (NERC).

REFERENCES

Abbate, E., Bortolotti, V., and Principi, G., 1980. Apennine ophiolites: a peculiar oceanic crust. *Ofioliti,* 1:59–96.

Abe, N., 2001. Petrochemistry of serpentinized peridotite from the Iberia Abyssal Plain (ODP Leg 173): its character intermediate between suboceanic and subcontinental upper mantle. *In* Wilson, R.C.L., Whitmarsh, R.B., Taylor, B., and Froitzheim, N. (Eds.), *Non-volcanic Rifting of Continental Margins: Evidence from Land and Sea.* Geol. Soc. Spec. Publ., 187:143–159.

Anonymous, 1972. Penrose field conference on ophiolites. *Geotimes,* 17:24–25.

Barrett, T.J., and Spooner, E.T.C., 1977. Ophiolitic breccias associated with allochthonous oceanic crustal rocks in the east Ligurian Apennines, Italy—a comparison with observations from rifted ocean ridges. *Earth Planet. Sci. Lett.,* 35(1):79–91. **doi:10.1016/0012-821X(77)90031-0**

Bathurst, R.G.C., 1971. *Developments in Sedimentology* (Vol. 12): *Carbonate Sediments and Their Diagenesis:* Amsterdam (Elsevier).

Beard, J.S., Fullagar, P.D., and Sinha, A.K., 2002. Gabbroic pegmatite intrusions, Iberia Abyssal Plain, ODP Leg 173, Site 1070: magmatism during a transition from nonvolcanic rifting to sea-floor spreading. *J. Petrol.,* 43(5):885–905. **doi:10.1093/petrology/43.5.885**

Beccaluva, L., Dal Paiz, G.V., and Macciotta, G., 1984. Transitional to MORB affinities in ophiolitic metabasites from the Zermatt-Saas, Combin and Antrona units, western Alps: implications for the palaeogeographic evolution of the western Tethyan Basin. *In* Zwart, H.J., Hartman, P., and Tobi, A.C., (Eds.), *Ophiolites and Ultramafic Rocks: a Tribute to Emile den Tex*. Geol. Mijnbouw, 63:165–177.

Beslier, M.-O., Cornen, G., and Girardeau, J., 1996. Tectono-metamorphic evolution of peridotites from the ocean/continent transition of the Iberia Abyssal Plain margin. *In* Whitmarsh, R.B., Sawyer, D.S., Klaus, A., and Masson, D.G. (Eds.), *Proc. ODP, Sci. Results,* 149: College Station, TX (Ocean Drilling Program), 397–412. **doi:10.2973/odp.proc.sr.149.218.1996**

Beslier, M.-O., Whitmarsh, R.B., Wallace, P.J., and Girardeau, J. (Eds.), 2001. *Proc. ODP, Sci. Results,* 173: College Station, TX (Ocean Drilling Program). **doi:10.2973/odp.proc.sr.173.2001**

Bernoulli, D., and Weissert, H., 1985. Sedimentary fabrics in Alpine ophicalcites, South Pennine Arosa zone, Switzerland. *Geology,* 13(11):755–758. **doi:10.1130/0091-7613(1985)13<755:SFIAOS>2.0.CO;2**

Boillot, G., Grimaud, S., Mauffret, A., Mougenot, D., Kornprobst, J., Mergoil-Daniel, J., and Torrent, G., 1980. Ocean-continent boundary off the Iberian margin: a serpentinite diapir west of the Galicia Bank. *Earth Planet. Sci. Lett.,* 48(1):23–34. **doi:10.1016/0012-821X(80)90166-1**

Boillot, G., Winterer, E.L., Meyer, A.W., et al., 1987. *Proc ODP, Init. Repts.,* 103: College Station, TX (Ocean Drilling Program). **doi:10.2973/odp.proc.ir.103.1987**

Boynton, W.V., 1984. Cosmochemistry of the rare earth elements: meteorite studies. *In* Henderson, P. (Ed.), *Developments in Geochemistry* (Vol. 2): *Rare Earth Element Geochemistry:* New York (Elsevier), 63–114.

Camiré, G., La Flèche, M.R., and Jenner, G.A., 1995. Geochemistry of pre-Taconian mafic volcanism in the Humber zone of the northern Appalachians, Québec, Canada. *Chem. Geol.,* 119(1–4):55–77. **doi:10.1016/0009-2541(94)00104-G**

Comas, M.C., Sánchez-Gómez, M., Cornen, G., and de Kaenel, E., 1996. Serpentized peridotite breccia and olistostrome on basement highs of the Iberia Abyssal Plain: implications for tectonic margin evolution. *In* Whitmarsh, R.B., Sawyer, D.S., Klaus, A., and Masson, D.G. (Eds.), *Proc. ODP, Sci. Results,* 149: College Station, TX (Ocean Drilling Program), 577–591. **doi:10.2973/odp.proc.sr.149.228.1996**

Cornen, G., Beslier, M.-O., and Girardeau, J., 1996. Petrology of the mafic rocks cored in the Iberia Abyssal Plain. *In* Whitmarsh, R.B., Sawyer, D.S., Klaus, A., and Mas-

son, D.G. (Eds.), *Proc. ODP, Sci. Results,* 149: College Station, TX (Ocean Drilling Program), 449–469. **doi:10.2973/odp.proc.sr.149.220.1996**

Cornen, G., Girardeau, J., and Monnier, C., 1999. Basalts, underplated gabbros and pyroxenites record the rifting process of the West Iberian margin. *Contrib. Mineral. Petrol.,* 67:111–142.

de Graciansky, P.C., Poag, C.W., et al., 1985. *Init. Repts. DSDP,* 80: Washington, DC (U.S. Govt. Printing Office). **doi:10.2973/dsdp.proc.80.1985**

Desmurs, L., Manatschal, G., and Bernoulli, D., 2001. The Steinmann Trinity revisited: mantle exhumation and magmatism along an ocean-continent transition: the Platta nappe, eastern Switzerland. *In* Wilson, R.C.L., Whitmarsh, R.B., Taylor, B., and Froitzheim, N. (Eds.), *Non-volcanic Rifting of Continental Margins: a Comparison of Evidence from Land and Sea.* Geol. Soc. Spec. Publ., 187:235–266.

Desmurs, L., Müntener, O., and Manatschal, G., 2002. Onset of magmatic accretion within a magma-poor rifted margin: a case study from the Platta ocean-continent transition, eastern Switzerland. *Contrib. Mineral. Petrol.,* 144(3):365–382.

Dornsiepen, U.F., and Manutsoglu, E., 1996. Die vulkanite oder anorogene Trapp-Basalte? *Z. Dtsch. Geol. Ges.,* 147:101–123.

Fisher, R.V., and Schmincke, H.-U., 1984. *Pyroclastic Rocks:* New York (Springer-Verlag).

Fitton, J.G., in press. The OIB paradox. *In* Foulger, G.R., and Jurdy, D.M. (Eds.), *Plates, Plumes, and Planetary Processes*. Spec. Pap.—Geol. Soc. Am.

Fitton, J.G., and Godard, M., 2004. Origin and evolution of magmas on the Ontong Java Plateau. *In* Fitton, J.G., Mahoney, J.J., Wallace, P.J., and Saunders, A.D. (Eds.), *Origin and Evolution of the Ontong Java Plateau*. Geol. Soc. Spec. Publ., 229:151–178.

Fitton, J.G., James, D., Kempton, P.D., and Leeman, W.P., 1988. The role of lithospheric mantle in the generation of late Cenozoic basic magmas in the western United States. *In* Menzies-Martin, A., and Cox, K.G. (Eds.), *Oceanic and Continental Lithosphere: Similarities and Differences*. J. Petrol., 1988:331–349.

Fitton, J.G., Saunders, A.D., Larsen, L.M., Hardarson, B.S., and Norry, M.J., 1998. Volcanic rocks from the southeast Greenland margin at 63°N: composition, petrogenesis, and mantle sources. *In* Saunders, A.D., Larsen, H.C., and Wise, S.W., Jr. (Eds.), *Proc. ODP, Sci. Results,* 152: College Station, TX (Ocean Drilling Program), 331–350. **doi:10.2973/odp.proc.sr.152.233.1998**

Floyd, P.A., and Winchester, J.A., 1975. Magma type and tectonic setting discrimination using immobile elements. *Earth Planet. Sci. Lett.,* 27(2):211–218. **doi:10.1016/0012-821X(75)90031-X**

Froitzheim, N., and Manatschal, G., 1996. Kinematics of Jurassic rifting, mantle exhumation, and passive-margin formation in the Austroalpine and Penninic nappes (eastern Switzerland). *Geol. Soc. Am. Bull.,* 108(9):1120–1133. **doi:10.1130/0016-7606(1996)108<1120:KOJRME>2.3.CO;2**

Gardien, V., Poupeau, G., Muceku, B., Hébert, R., Beaudoin, G., and Labrin, E., 2001. The evolution of amphibolites from Site 1067, ODP Leg 173 (Iberia Abyssal Plain): Jurassic rifting to the Pyrenean compression. *In* Wilson, R.C.L., Whitmarsh, R.B., Taylor, B., and Froitzheim, N. (Eds.), *Non-volcanic Rifting of Continental Margins: a Comparison of Evidence from Land and Sea*. Geol. Soc. Spec. Publ., 187:191–208.

Gianelli, G., and Principi, G., 1977. Northern Apennine ophiolite: an ancient transcurrent fault zone. *Boll. Soc. Geol. Ital.,* 96:53–58.

Gibson, I.L., Milliken, K.L., and Morgan, J.K., 1996. Serpentinite-breccia landslide deposits generated during crustal extension at the Iberia margin. *In* Whitmarsh, R.B., Sawyer, D.S., Klaus, A., and Masson, D.G. (Eds.), *Proc. ODP, Sci. Results,* 149: College Station, TX (Ocean Drilling Program), 571–575. **doi:10.2973/odp.proc.sr.149.226.1996**

Gradstein, F.M., Ogg, J.G., and Smith, A. (Eds.), 2004. *A Geologic Time Scale 2004:* Cambridge (Cambridge Univ. Press). Available from the World Wide Web: <**http://www.stratigraphy.org/cheu.pdf**>.

Hart, S.R., and Blusztajn, J., 2006. Age and geochemistry of the mafic sills, ODP Site 1276, Newfoundland margin. *Chem. Geol.,* 235(3–4):222–237. **doi:10.1016/j.chemgeo.2006.07.001**

Ishiwatari, A., 1985. Igneous petrogenesis of the Yakuno ophiolite (Japan) in the context of the diversity of ophiolites. *Contrib. Mineral. Petrol.,* 89(2–3):155–167. **doi:10.1007/BF00379450**

Jansa, L.F., and Wade, J.A., 1975. Geology of the continental margin off Nova Scotia and Newfoundland. *In* Linden, W.J.M., and Wade, J.A. (Eds.), *Offshore Geology of Eastern Canada* (Vol. 2): *Regional Geology.* Pap.—Geol. Surv. Can., 51–105.

Kempton, P.D., Fitton, J.G., Saunders, A.D., Nowell, G.M., Taylor, R.N., Hardarson, B.S., and Pearson, G., 2000. The Iceland plume in space and time: a Sr–Nd–Pb–Hf study of the North Atlantic rifted margin. *Earth Planet. Sci. Lett.,* 177(3–4):255–271. **doi:10.1016/S0012-821X(00)00047-9**

Kornprobst, J., Vidal, P., and Malod, J., 1988. Les basaltes de la Marge de Galice (Nord de la Péninsule Ibérique): hétérogénéité des spectres de terres rares à la transition continent/océan. Données géochimiques préliminaires. *C. R. Acad. Sci., Ser. II: Mec., Phys., Chim., Sci. Terre Univers.,* 306:1359–1364.

Krawczyk, C.M., Reston, T.J., Beslier, M.-O., and Boillot, G., 1996. Evidence for detachment tectonics on the Iberia Abyssal Plain rifted margin. *In* Whitmarsh, R.B., Sawyer, D.S., Klaus, A., and Masson, D.G. (Eds.), *Proc. ODP, Sci. Results,* 149: College Station, TX (Ocean Drilling Program), 603–615. **doi:10.2973/odp.proc.sr.149.244.1996**

Lagabrielle, Y., 1994. Ophiolites of the southwestern Alps and the structure of the Tethyan oceanic lithosphere. *Ofioliti,* 19:413–434.

Lagabrielle, Y., and Cannat, M., 1990. Alpine Jurassic ophiolites resemble the modern central Atlantic basement. *Geology,* 18(4):319–322. **doi:10.1130/0091-7613(1990)018<0319:AJORTM>2.3.CO;2**

Lagabrielle, Y., Fudral, S., and Kienast, J.-R., 1989. The oceanic cover of the Lanzo peridotite body (western Italian Alps): lithostratigraphic and petrological evidence. *Geodin. Acta (Paris),* 3:43–55.

Lagabrielle, Y., Polino, R., Auzende, J.M., Blanchet, R., Caby, R., Fudral, F., Lemoine, M., Mevel, C., Ohnenstetter, M., Robert, D., and Tricart, P., 1984. Le témoins d'une tectonique intraocéanique dans le domaine téthysien: analyse des rapports entre les ophiolites et leurs couvertures métasédimentaires dans la zone piédmontaise des Alpes franco-italiennes. *Ofioliti,* 9:67–88.

Larson, L.M., Fitton, J.G., Bailey, J.C., and Kystol, J., 1998. XRF analyses of volcanic rocks from Leg 152 by laboratories in Edinburgh and Copenhagen: implications for the mobility of yttrium and other elements during alteration. *In* Saunders, A.D., Larsen, H.C., and Wise, S.W., Jr. (Eds.), *Proc. ODP, Sci. Results,* 152: College Station, TX (Ocean Drilling Program), 425–429. **doi:10.2973/odp.proc.sr.152.246.1998**

Lau, K.W.H., Louden, K.E., Funck, T., Tucholke, B.E., Holbrook, W.S., Hopper, J.R., and Larsen, H.C., 2006. Crustal structure across the Grand Banks-Newfoundland Basin continental Margin - I. Results from a seismic refraction profile. *Geophys. J. Int.,* 167(1):127–156. **doi:10.1111/j.1365-246X.2006.02988.x**

Lavier, L.L., and Manatschal, G., 2006. A mechanism to thin the continental lithosphere at magma-poor margins. *Nature (London, U. K.),* 440(7082):324–328. **doi:10.1038/nature04608**

Lemoine, M., Tricart, P., and Boillot, G., 1987. Ultramafic and gabbroic ocean floor of the Ligurian Tethys (Alps, Corsica, Apennines): in search of a genetic imodel. *Geology,* 15(7):622–625. **doi:10.1130/0091-7613(1987)15<622:UAGOFO>2.0.CO;2**

Manatschal, G., and Bernoulli, D., 1998. Rifting and early evolution of ancient ocean basins: the record of the Mesozoic Tethys and of the Galicia-Newfoundland margins. *Mar. Geophys. Res.,* 20(4):371–381. **doi:10.1023/A:1004459106686**

Manatschal, G., Froitzheim, N., Rubenach, M., and Turrin, B., 2001. The role of detachment faulting in the formation of an ocean–continent transition: insights

from the Iberia Abyssal Plain. *In* Wilson, R.C.L., Whitmarsh, R.B., Taylor, B., and Froitzheim, N. (Eds.), *Non-volcanic Rifting of Continental Margins: a Comparison of Evidence from Land and Sea*. Geol. Soc. Spec. Publ., 187:405–428.

Manatschal, G., and Müntener, O., 2004. Remnants of the ancient Tethys margin preserved in the Ortler, Err-Platta, and Tasna units in SE-Switzerland and N-Italy (Central Alps) [Modeling the Extensional Deformation of the Lithosphere (IMEDL 2004), Pontresina, 10–16 July 2004].

Manatschal, G., and Müntener, O., 2005. *Remnant of the Ancient European Margin and Alpine Tethys Ocean Preserved in SE France and NW Italy:* ODP Leg 210 Postcruise Meeting Field Guide.

Manatschal, G., Müntener, O., Desmurs, L., and Bernoulli, D., 2003. An ancient ocean–continent transition in the Alps: the Totalp, Err-Platta, and Malenco units in the eastern Central Alps (Graubünden and northern Italy). *Eclogae Geol. Helv.,* 96:131–146.

Manatschal, G., Müntener, O., Lavier, L.L., Minshull, T.A., and Peron-Pinvidic, G., in press. Observations from the Alpine Tethys and Iberia/Newfoundland margins pertinent to the interpretation of continental break-up. *In* Karner, G., Manatschal, G., and Pinheiro, L. (Eds.), *MARGINS Theoretical and Experimental Earth Science Series*. Geol. Soc. Spec. Publ., 282.

Manatschal, G., and Nievergelt, P., 1997. A continent-ocean transition recorded in the Err and Platta nappes (eastern Switzerland). *Eclogae Geol. Helv.,* 90:3–27.

Morgan, J.K., and Milliken, K.L., 1996. Petrography of calcite veins in serpentinized peridotite basement rocks from the Iberia Abyssal Plain, Sites 897 and 899: kinematic and environmental implications. *In* Whitmarsh, R.B., Sawyer, D.S., Klaus, A., and Masson, D.G. (Eds.), *Proc. ODP, Sci. Results,* 149: College Station, TX (Ocean Drilling Program), 559–569. **doi:10.2973/odp.proc.sr.149.230.1996**

Müntener, O., and Herman, J., 2001. The role of lower crust and continental upper mantle during formation of non-volcanic passive margins: evidence from the Alps. *In* Wilson, R.C.L., Whitmarsh, R.B., Taylor, B., and Froitzheim, N. (Eds.), *Non-volcanic Rifting of Continental Margins: a Comparison of Evidence from Land and Sea*. Geol. Soc. Spec. Publ., 187:267–288.

Müntener, O., and Manatschal, G., 2006. High degrees of melt extraction recorded by spinel harzburgite of the Newfoundland margin: the role of inheritance and consequences for the evolution of the southern North Atlantic. *Earth Planet. Sci. Lett.,* 252(3–4):437–452. **doi:10.1016/j.epsl.2006.10.009**

Nicolas, A., 1989. *Structure of Ophiolites and Dynamics of the Oceanic Lithosphere:* Dordrecht (Kluwer).

Pearce, J.A., 1982. Trace element characteristics of lavas from destructive plate boundaries. *In* Thorpe, R.S. (Ed.), *Andesites: Orogenic Andesites and Related Rocks:* New York (Wiley), 525–548.

Pearce, J.A., 1983. The role of sub-continental lithosphere in magma genesis at active continental margins. *In* Hawkesworth, C.J., and Norry, M.J. (Eds.), *Continental Basalts and Mantle Xenoliths:* Nantwich (Shiva Publ.), 230–249.

Pearce, J.A., and Cann, J.R., 1973. Tectonic setting of basic volcanic rocks determined using trace element analyses. *Earth Planet. Sci. Lett.,* 19(2):290–300. **doi:10.1016/0012-821X(73)90129-5**

Pearce, J.A., Lippard, S.J., and Roberts, S., 1984. Characteristics and tectonic significance of supra-subduction zone ophiolites. *In* Kokelaar, B.P., and Howells, M.F. (Eds.), *Marginal Basin Geology.* Geol. Soc. Spec. Publ., 16:74–94.

Pearce, J.A., and Norry, M.J., 1979. Petrogenetic implications of Ti, Zr, Y, and Nb variations in volcanic rocks. *Contrib. Mineral. Petrol.,* 69(1):33–47. **doi:10.1007/BF00375192**

Pelletier, T., and Müntener, O., 2004. High pressure metamorphic evolution of oceanic crust: the example of the Lanzo Massif and its sedimentary cover (western Alps). *Geophys. Res. Abstr.,* 6:01550.

Pe-Piper, G., and Piper, D.W.J., 2002. *Beitrage zur Regionalen Geologie der Erde* (Vol. 30): *the Igneous Rocks of Greece: the Anatomy of an Orogen:* Berlin (Gebrüder Borntaeger).

Péron-Pinvidic, G., Manatschal, G., Minshull, T.A., and Sawyer, D.S., 2007. Tectonosedimentary evolution of the deep Iberia-Newfoundland margins: evidence for a complex breakup history. *Tectonics,* 26:TC2011. **doi:10.1029/2006TC001970**

Piccardo, G.B., Rampone, E., and Vannucci, R., 1990. Upper mantle evolution during continental rifting and oceanic formation: evidences from peridotite bodies of the western Alpine-northern Apennine system. *Mem. Soc. Geol. Fr.,* 156:323–333.

Pognante, U., Perotto, A., Salino, C., and Toscani, L., 1986. The ophiolitic peridotite of the western Alps: record of the evolution of a small oceanic-type basin in the Mesozoic Tethys. *TMPM, Tschermaks Mineral. Petrogr. Mitt.,* 35:47–65.

Profett, J.M., 1986. Ceonozoic geology of the Yerrington district, Nevada and implications for the nature and origin of basin and range faulting. *Geol. Soc. Am. Bull.,* 88:247–266.

Purvis, M., and Robertson, A., 2004. A pulsed extension model for the Neogene–Recent E–W-trending Alasehir Graben and the NE–SW-trending Selendi and Gördes Basins, western Turkey. *Tectonophysics,* 391(1–4):171–201. **doi:10.1016/j.tecto.2004.07.011**

Reston, T.J., Krawczyk, C.M., and Hoffmann, H.J., 1995. Detachment tectonics during Atlantic rifting: analysis and interpretation of the S reflection, the west Galicia margin. *In* Scrutton, R.A., Stoker, M.S., Shimmield, G.B., and Tudhope, A.W. (Eds.), *The Tectonics, Sedimentation, and Palaeoceanography of the North Atlantic Region.* Geol. Soc. Spec. Publ, 90:93–109.

Robertson, A.H.F., 2002. Overview of the genesis and emplacement of Mesozoic ophiolites in the eastern Mediterranean Tethyan region. *Lithos,* 65(1–2):1–67. **doi:10.1016/S0024-4937(02)00160-3**

Robertson, A.H.F., 2006. Field-based evidence from the south Mediterranean region (Crete, Peloponnese, Evia, Sicily) used to test alternative models for the regional tectonic setting of Tethys during late Palaeozoic–early Mesozoic time. *In* Robertson, A.H.F., and Mountrakis, S. (Eds.), *Tectonic Development of the Eastern Mediterranean Region.* Geol. Soc. Spec. Publ., 210:91–154.

Robertson, A.H.F., 2007. Overview of tectonic settings related to the rifting and opening of Mesozoic ocean basins in the eastern Tethys: Oman, Himalayas and eastern Mediterranean regions. *In* Karner, G.D., Manatschal, G., and Pinheiro, L.M. (Eds.), *Imaging, Mapping, and Modelling Continental Lithosphere Extension and Breakup*, Geol. Soc., Spec. Publ., 282:9–46.

Robertson, A.H.F., Awadallah, S.A.M., Gerbaudo, S., Lackschewitz, K.S., Montelone, B.D., Sharp, T.R., and other members of the Shipboard Scientific Party, 2001. Evolution of the Miocene–Recent Woodlark rift basin, SW Pacific, inferred from sediments drilled during Ocean Drilling Program Leg 180. *In* Wilson, R.C.L., Whitmarsh, R.B., Taylor, B., and Froitzheim, N. (Eds.), *Non-Volcanic Rifting of Continental Margins: a Comparison of Evidence from Land and Sea.* Geol. Soc. Spec. Publ., 187:335–372.

Robertson, A.H.F., Clift, P.D., Degnan, P.J., and Jones, G., 1991. Palaeogeographic and palaeotectonic evolution of the eastern Mediterranean Neotethys. *Palaeogeogr., Palaeoclimatol., Palaeoecol.,* 87(1–4):289–343. **doi:10.1016/0031-0182(91)90140-M**

Sawyer, D.S., Whitmarsh, R.B., Klaus, A., et al., 1994. *Proc. ODP, Init. Repts.,* 149: College Station, TX (Ocean Drilling Program). **doi:10.2973/odp.proc.ir.149.1994**

Schärer, U., Kornprobst, J., Beslier, M.-O., Boillot, G., and Girardeau, J., 1995. Gabbro and related rock emplacement beneath rifting continental crust: U–Pb geochronological and geochemical constraints for the Galicia passive margin (Spain). *Earth Planet. Sci. Lett.,* 130(1–4):187–200. **doi:10.1016/0012-821X(94)00261-V**

Schaltegger, U., Desmurs, L., Manatschal, G., Müntener, O., Meier, M., Frank, M., and Bernoulli, D., 2002. The transition from rifting to sea-floor spreading within a magma-poor rifted margin: field and isotopic constraints. *Terra Nova,* 14(3):156–162. **doi:10.1046/j.1365-3121.2002.00406.x**

Seifert, K., and Brunotte, D., 1996. Geochemistry of weathered mid-ocean ridge basalt and diabase clasts from Hole 899B in the Iberia Abyssal Plain. *In* Whitmarsh, R.B., Sawyer, D.S., Klaus, A., and Masson, D.G. (Eds.), *Proc. ODP, Sci. Results,* 149: College Station, TX (Ocean Drilling Program), 497–515. **doi:10.2973/odp.proc.sr.149.225.1996**

Seifert, K.E., Chang, C.-W., and Brunotte, D.A., 1997. Evidence from the Ocean Drilling Program Leg 149 mafic igneous rocks for oceanic crust in the Iberia Abyssal Plain ocean-continent transition zone. *J. Geophys. Res.,* 102(B4):7915–7928. **doi:10.1029/96JB03912**

Shervais, J.W., 1982. Ti-V plots and the petrogenesis of modern and ophiolitic lavas. *Earth Planet. Sci. Lett.,* 59(1):101–118. **doi:10.1016/0012-821X(82)90120-0**

Shillington, D.J., Holbrook, W.S., Van Avendonk, H.J.A., Tucholke, B.E., Hopper, J.R., Louden, K.E., Larsen, H.C., and Nunes, G.T., 2006. Evidence for asymmetric nonvolcanic rifting and slow incipient oceanic accretion from seismic reflection data on the Newfoundland margin. *J. Geophys. Res.,* 111(B9):B09402. **doi:10.1029/2005JB003981**

Shipboard Scientific Party, 2004a. Leg 210 summary. *In* Tucholke, B.E., Sibuet, J.-C., Klaus, A., et al., *Proc. ODP, Init. Repts.,* 210: College Station, TX (Ocean Drilling Program), 1–78. **doi:10.2973/odp.proc.ir.210.101.2004**

Shipboard Scientific Party, 2004b. Site 1277. *In* Tucholke, B.E., Sibuet, J.-C., Klaus, A., et al., *Proc. ODP, Init. Repts.,* 210: College Station, TX (Ocean Drilling Program), 1–358. **doi:10.2973/odp.proc.ir.210.104.2004**

Taylor, B., Huchon, P., Klaus, A., et al., 2000. *Proc. ODP, Init. Repts.,* 180: College Station, TX (Ocean Drilling Program). **doi:10.2973/odp.proc.ir.180.2000**

Tricart, P., and Lemoine, M., 1983. Serpentinite oceanic bottom in south Queyras ophiolites (French western Alps): record of the incipient oceanic opening of the Mesozoic Ligurian Tethys. *Eclogae Geol. Helv.,* 76:611–629.

Tucholke, B.E., and Lin, J., 1994. A geological model for structure of ridge segments in slow spreading ocean crust. *J. Geophys. Res.,* 99(B6):11937–11958. **doi:10.1029/94JB00338**

Tucholke, B.E., Lin, J., and Kleinrock, M.C., 1998. Megamullions and mullion structure defining oceanic metamorphic core complexes on the Mid-Atlantic Ridge. *J. Geophys. Res.,* 103(B5):9857–9866. **doi:10.1029/98JB00167**

Tucholke, B.E., Sawyer, D.S., and Sibuet, J.-C., 2007. Breakup of the Newfoundland-Iberia Rift. *In* Karner, G.D., Manatschal, G., and Pinheiro, L.M. (Eds.), *Imaging, Mapping, and Modelling Continental Lithosphere Extension and Breakup*, Geol. Soc., Spec. Publ., 282:9–46.

Tucholke, B.E., Sibuet, J.-C., Klaus, A., et al., 2004. *Proc. ODP, Init. Repts.,* 210: College Station, TX (Ocean Drilling Program). **doi:10.2973/odp.proc.ir.210.2004**

Van Avendonk, H.J.A., Holbrook, W.S., Nunes, G.T., Shillington, D.J., Tucholke, B.E., Louden, K.E., Larsen, H.C., and Hopper, J.R., 2006. Seismic velocity structure of the rifted margin of the eastern Grand Banks of Newfoundland, Canada. *J. Geophys. Res.,* 111(B11):B11404. **doi:10.1029/2005JB004156**

Weissert, H.J., and Bernoulli, D., 1985. A transform margin in the Mesozoic Tethys: evidence from the Swiss Alps. *Geol. Rundsch.,* 74(3):665–679. **doi:10.1007/BF01821220**

Whitmarsh, R.B., Beslier, M.-O., Wallace, P.J., et al., 1998. *Proc. ODP, Init. Repts.,* 173: College Station, TX (Ocean Drilling Program). **doi:10.2973/odp.proc.ir.173.1998**

Whitmarsh, R.B., Manatschal, G., and Minshull, T.A., 2001. Evolution of magma-poor continental margins from rifting to seafloor spreading. *Nature (London, U. K.),* 413(6852):150–154. **doi:10.1038/35093085**

Whitmarsh, R.B., and Wallace, P.J., 2001. The rift-to-drift development of the west Iberia nonvolcanic continental margin: a summary and review of the contribution of Ocean Drilling Program Leg 173. *In* Beslier, M.-O., Whitmarsh, R.B., Wallace, P.J., and Girardeau, J. (Eds.), *Proc. ODP, Sci. Results,* 173: College Station, TX (Ocean Drilling Program), 1–36. **doi:10.2973/odp.proc.sr.173.017.2001**

Williams, H., O'Brien, S.J., King, A.F., and Anderson, M.M., 1995. Avalon Zone—Newfoundland. *In* Keen, M.J., and Williams, G.L. (Eds.), *The Geology of North America* (Vol. 2): *Geology of the Continental Margin of Eastern Canada:* Boulder (Geol. Soc. Am.), 226–237.

Wood, D.A., 1980. The application of a Th-Hf-Ta diagram to problems of tectonomagmatic classification and to establishing the nature of crustal contamination of basaltic lavas of the British Tertiary volcanic province. *Earth Planet. Sci. Lett.,* 50(1):11–30. **doi:10.1016/0012-821X(80)90116-8**

Figure F1. Bathymetric map showing the locations of Sites 1276 and 1277 along the rifted margin of Newfoundland. Modified from Tucholke, Sibuet, Klaus, et al. (2004).

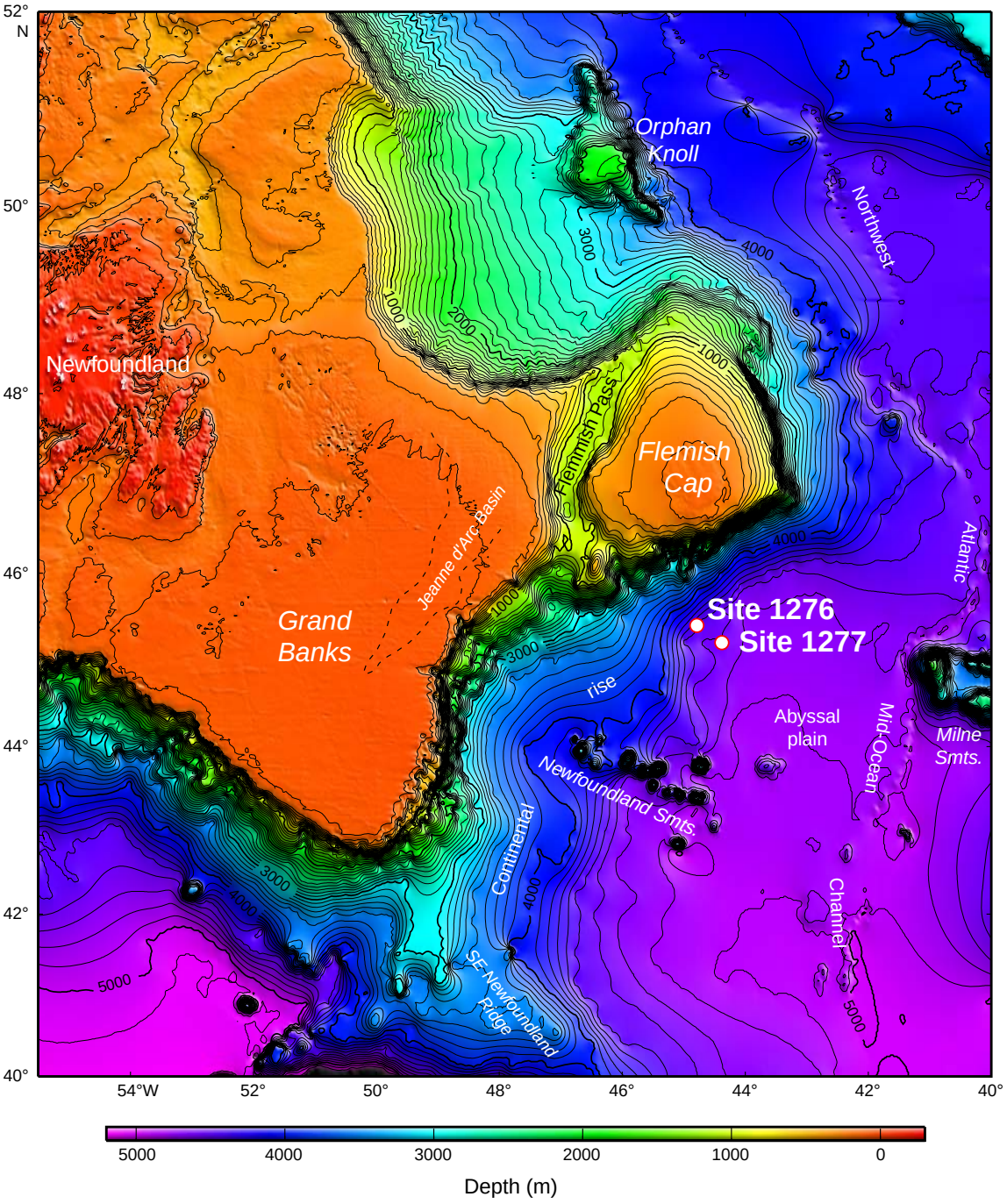

Figure F2. Seismic profile across the continental slope–rise of the Newfoundland rifted margin showing the location of Site 1277 on the Mauzy Ridge, a high located directly oceanward of magnetic Anomaly M1, inferred to be Early Cretaceous (late Barremian) in age (from **Tucholke and Sibuet** this volume).

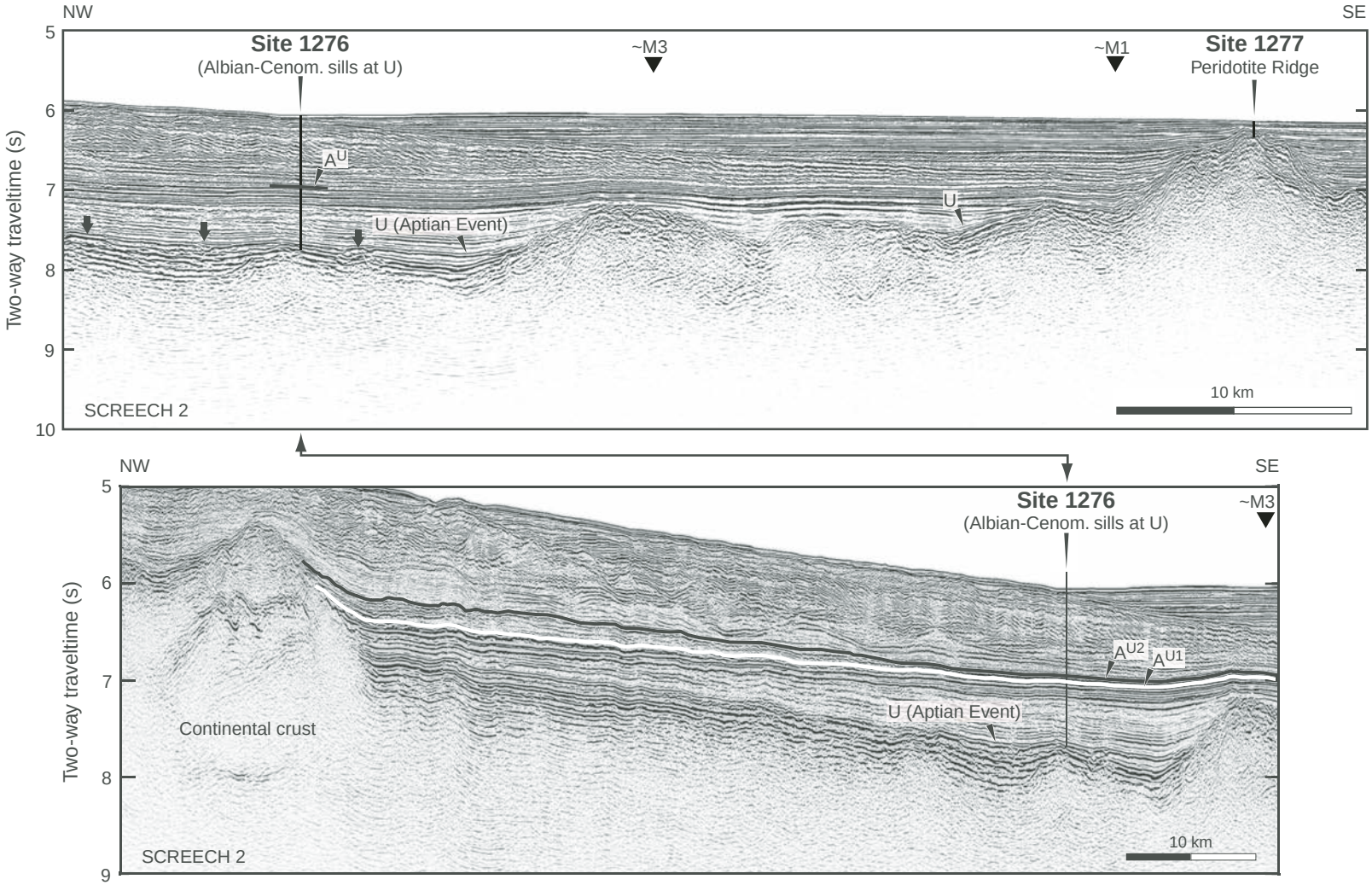

Figure F3. Summary of lithology at Site 1277. Generalized locations of core photographs and photomicrographs shown in other figures are indicated by figure numbers (e.g., F5N). Modified from Tucholke, Sibuet, Klaus, et al. (2004). **A.** Recovered section in Unit 1 above an inferred extensional detachment is shown in the two outside columns. Intervals discussed in the text are marked by the vertical numbered bars. Four basalt flows are identified and their limits within the cores are shown. The overall core recovery (i.e., Unit 1; Core 210-1277A-1W through 5R; Unit 2; Cores 6R through 9R) is indicated in the middle column. (Continued on next page.)

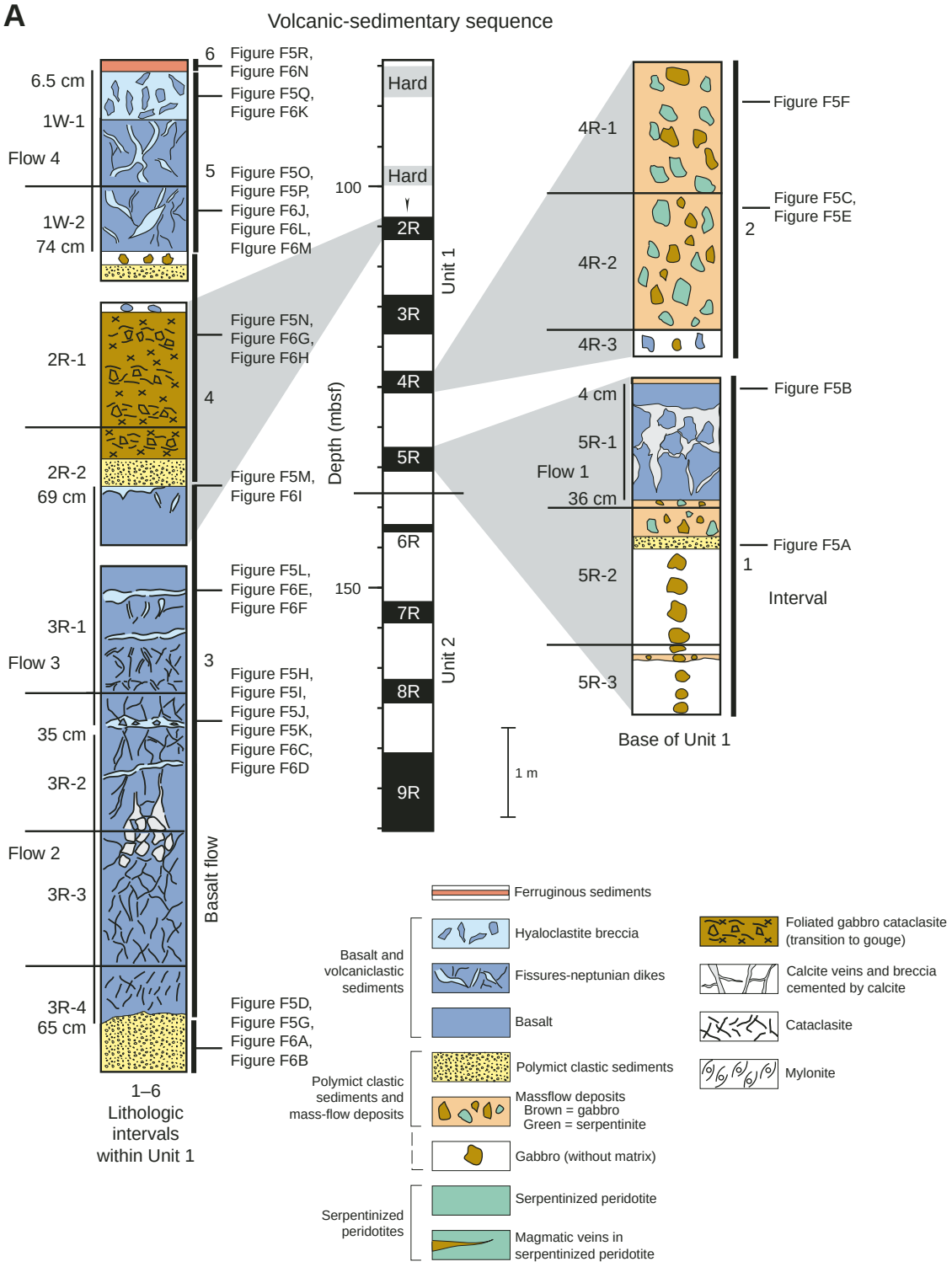

Figure F3 (continued). B. Recovered section in Unit 2 ("basement") below the inferred extensional detachment is shown in the two outside columns, with the overall recovery in the middle column.

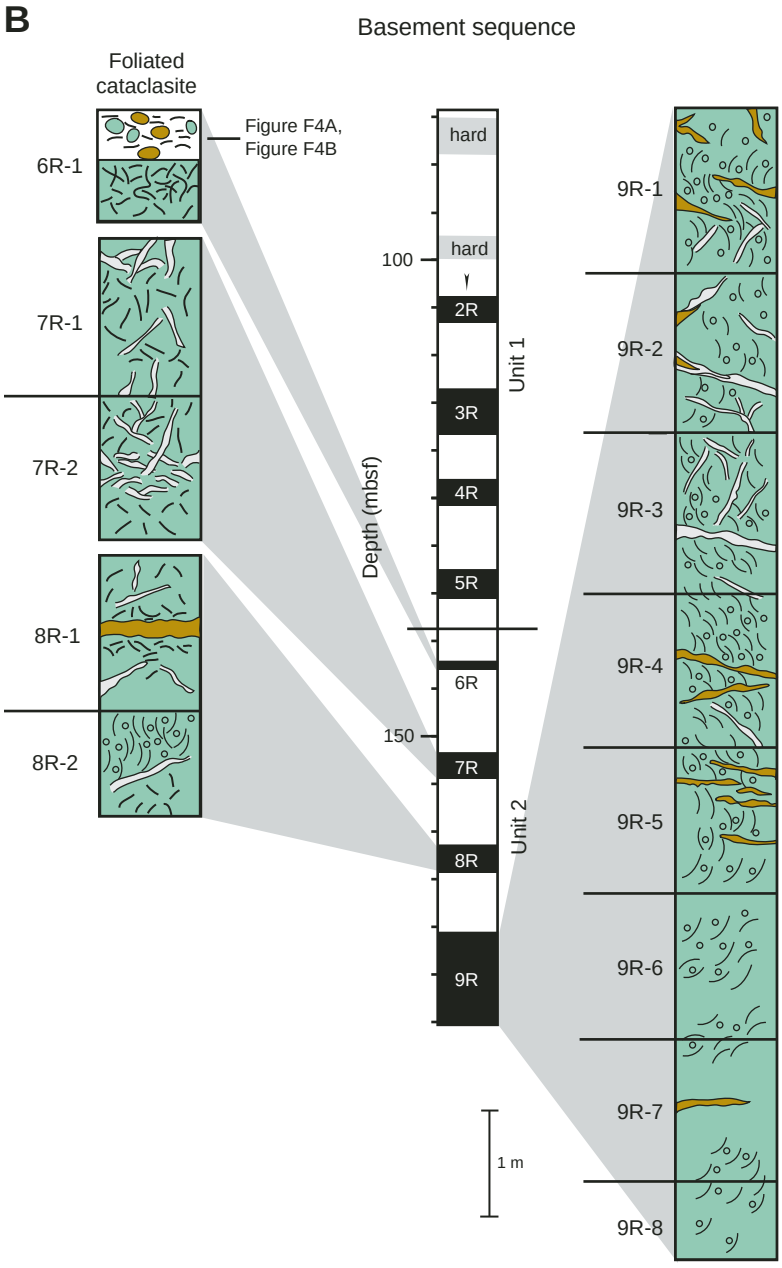

Figure F4. Core photographs from beneath the inferred extensional detachment (Unit 2). The approximate stratigraphic positions are shown on Figure F3B, p. 45. **A.** Strongly brecciated and altered gabbro with large angular clasts set in a matrix of finely comminuted gabbro, upper part of Unit 2 below the extensional detachment (interval 210-1277A-6R-1, 9–32 cm). **B.** Tectonically brecciated serpentinized harzburgite with calcite spar veining and cement. The clasts exhibit a characteristic fabric of angular clasts set in a finer grained matrix, cut by minor later-stage calcite spar veins, upper part of Unit 2 below the extensional detachment (interval 210-1277A-6R-1, 53–67.5 cm).

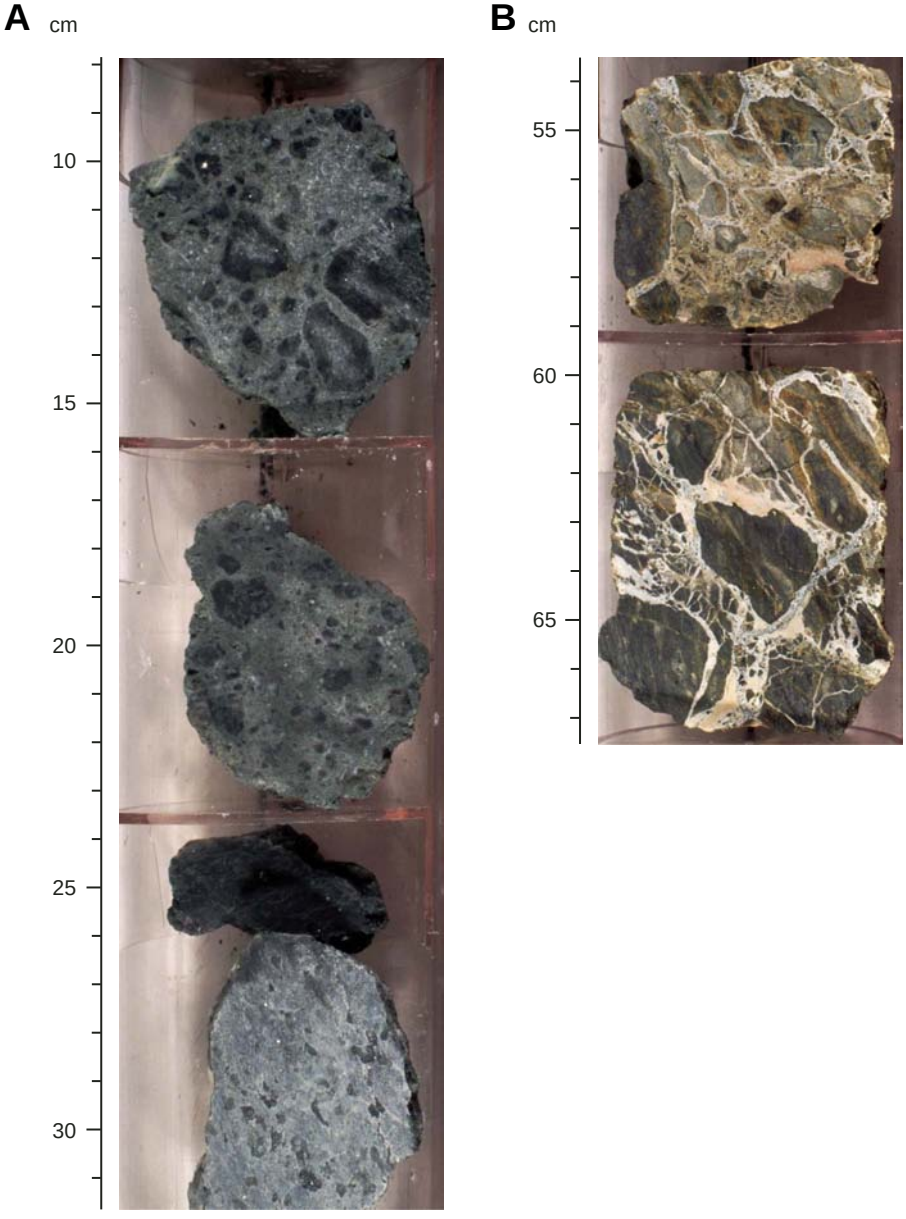

Figure F5. Core photographs of lithologies of volcanic-sedimentary Unit 1. Generalized stratigraphic positions are shown on Figure F3A, p. 44. **A.** Unique sample of a graded, laminated, medium- to fine-grained ferruginous clastic sediment, possibly deposited by a turbidity current, from a setting some distance from Site 1277 (interval 210-1277A-5R-2, 33–43 cm). **B.** Piece of the lowermost basalt (inferred Flow 1) showing tectonic brecciation and infill of calcite-cemented volcaniclastic sand and silt. Unfilled subvertical cracks are lined with calcite spar. Note the thin later-stage calcite veins that cut both the basalt and the calcite-cemented infilling sediment (interval 210-1277A-5R-1, 24–57 cm). **C.** Large clast of serpentinized harzburgite within mass flow, cut by subvertical calcite-filled fractures (interval 210-1277A-4R-2, 107.5–130.5 cm). (Continued on next five pages.)

Figure F5 (continued). D. Angular clasts of altered sheared serpentinized harzburgite (serpentinite mylonite) set in a calcareous matrix and cut by small irregular calcite veins (interval 210-1277A-3R-4, 118.5–132.5 cm). **E.** Pale gabbroic clast within serpentinite-bearing debris flow (interval 210-1277A-4R-2, 30–53 cm). **F.** Altered rounded serpentinized harzburgite clast set in a poorly sorted matrix including smaller clasts of serpentinite, later cut by calcite veins (interval 210-1277A-4R-1, 51–74.1 cm). (Continued on next page.)

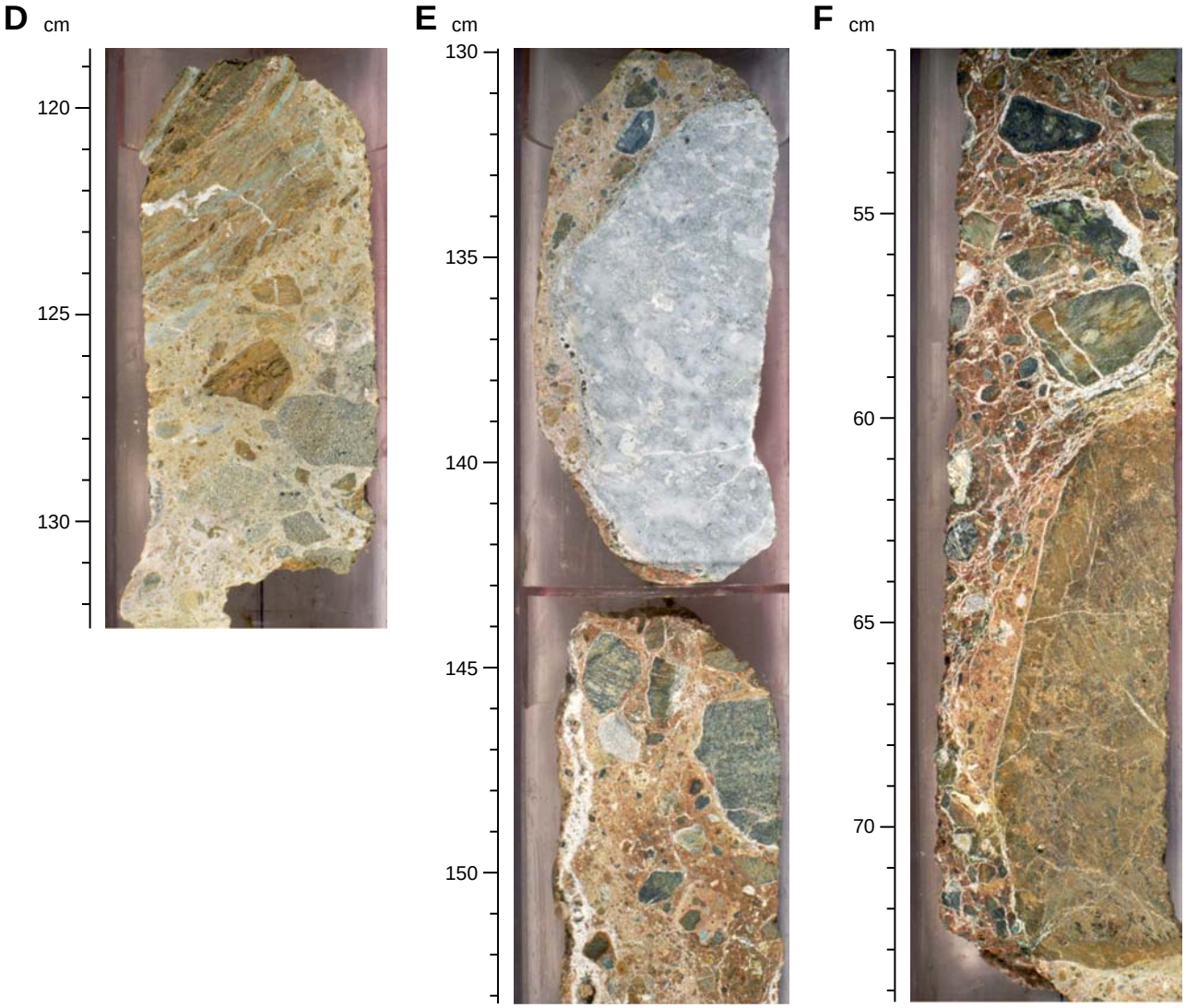

Figure F5 (continued). G. Poorly sorted granulestone cemented by calcite spar overlain in a primary contact with basaltic Flow 2 (interval 210-1277A-3R-4, 60–80 cm). **H.** Fractured massive basalt in which the internal cavity was sufficiently large to allow an infill of layered calc-siltite and basalt detritus to form (Flow 2) (interval 210-1277A-3R-2, 102–122 cm). **I.** Fractured massive basalt. The fracture is infilled with calcite spar and detrital material, with little relative movement of the opposing walls of the fracture (Flows 2 and 3) (interval 210-1277A-3R-2, 31–54 cm). (Continued on next page.)

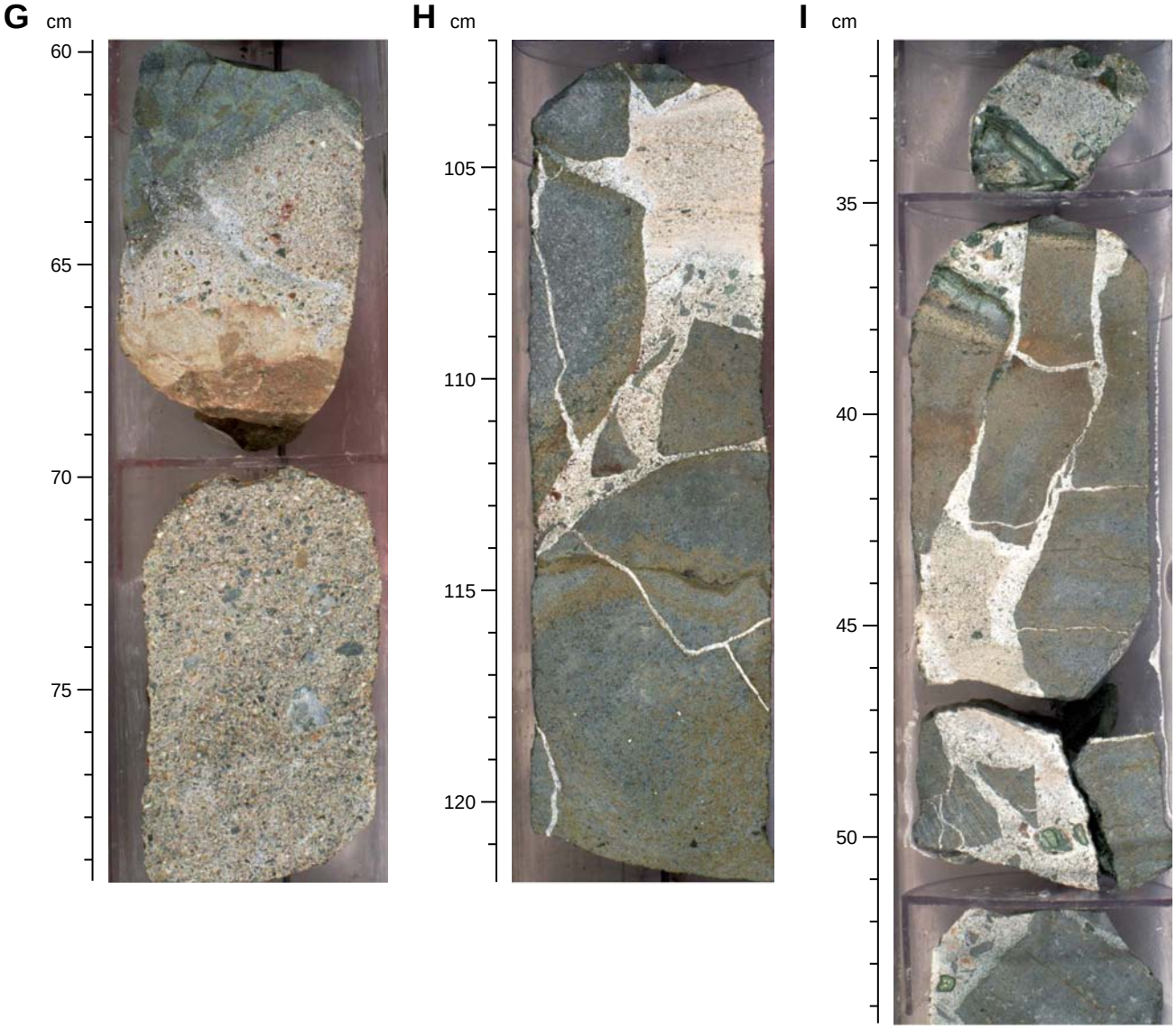

Figure F5 (continued). J. Brecciated massive basalt with spalled fragments of green hyaloclastite and calcite spar cement. Unusually, the upper part of the interval is reddened as a result of apparent seafloor oxidation (Flow 2) (interval 210-1277A-3R-2, 126–149 cm). **K.** Fractured massive basalt with hyaloclastite clast and calcite spar cement (Flow 2) (interval 210-1277A-3R-2, 81–101 cm). **L.** Spalled interlava hyaloclastite cemented by calcite spar. Little compaction took place prior to cementation (Flow 3) (interval 210-1277A-3R-1, 8.5–32 cm). (Continued on next page.)

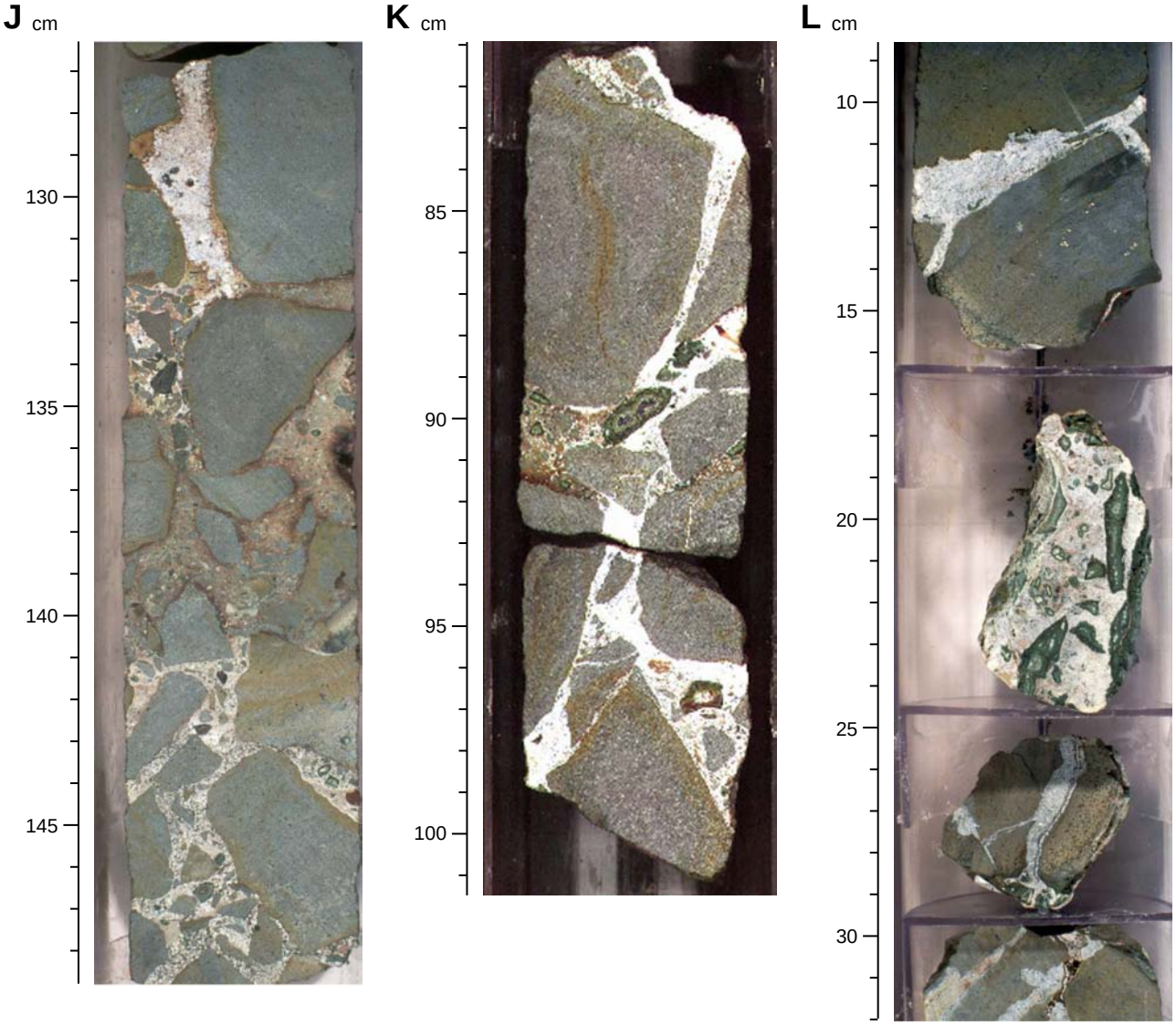

Figure F5 (continued). M. Basalt showing fracturing and infill with hyaloclastite and basalt detritus (Flow 3) (interval 210-1277A-2R-2, 69–73 cm). **N.** Sheared and brecciated gabbro (interval 210-1277A-2R-1, 96–107 cm). **O.** Graded conglomerate-breccia cemented by calcite spar (interval 210-1277A-1W-2, 91–105 cm). (Continued on next page.)

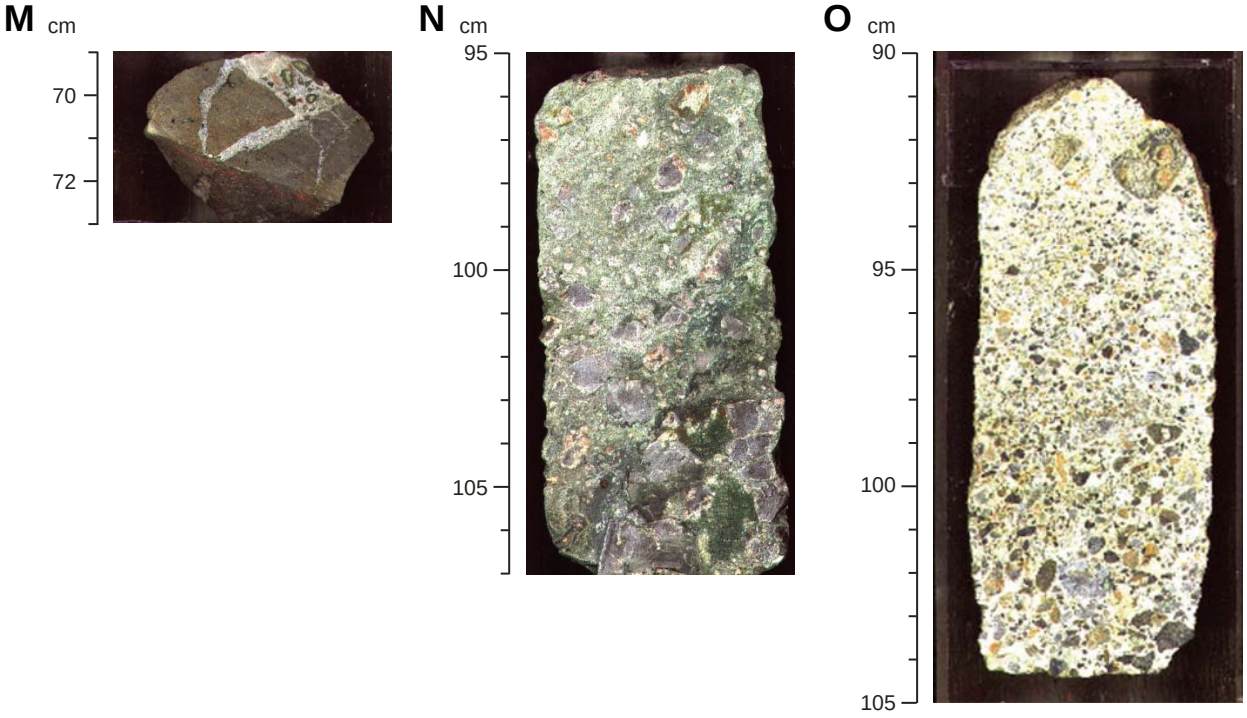

Figure F5 (continued). P. Basalt (possibly pillow lava) with pocket of spalled hyaloclastite cemented by calcite spar (Flow 1) (interval 210-1277A-1W-2, 20–40 cm). **Q.** Basalt and green hyaloclastite breccia cut by extensional fracture infilled with two generations of calcareous internal sediment (interval 210-1277A-1W-1, 40–60 cm). **R.** Red-brown ferruginous crust above basalt clasts that are set within green hyaloclastite; from the highest recovered levels of the succession at Site 1277 (interval 210-1277A-1W-1, 1–28 cm).

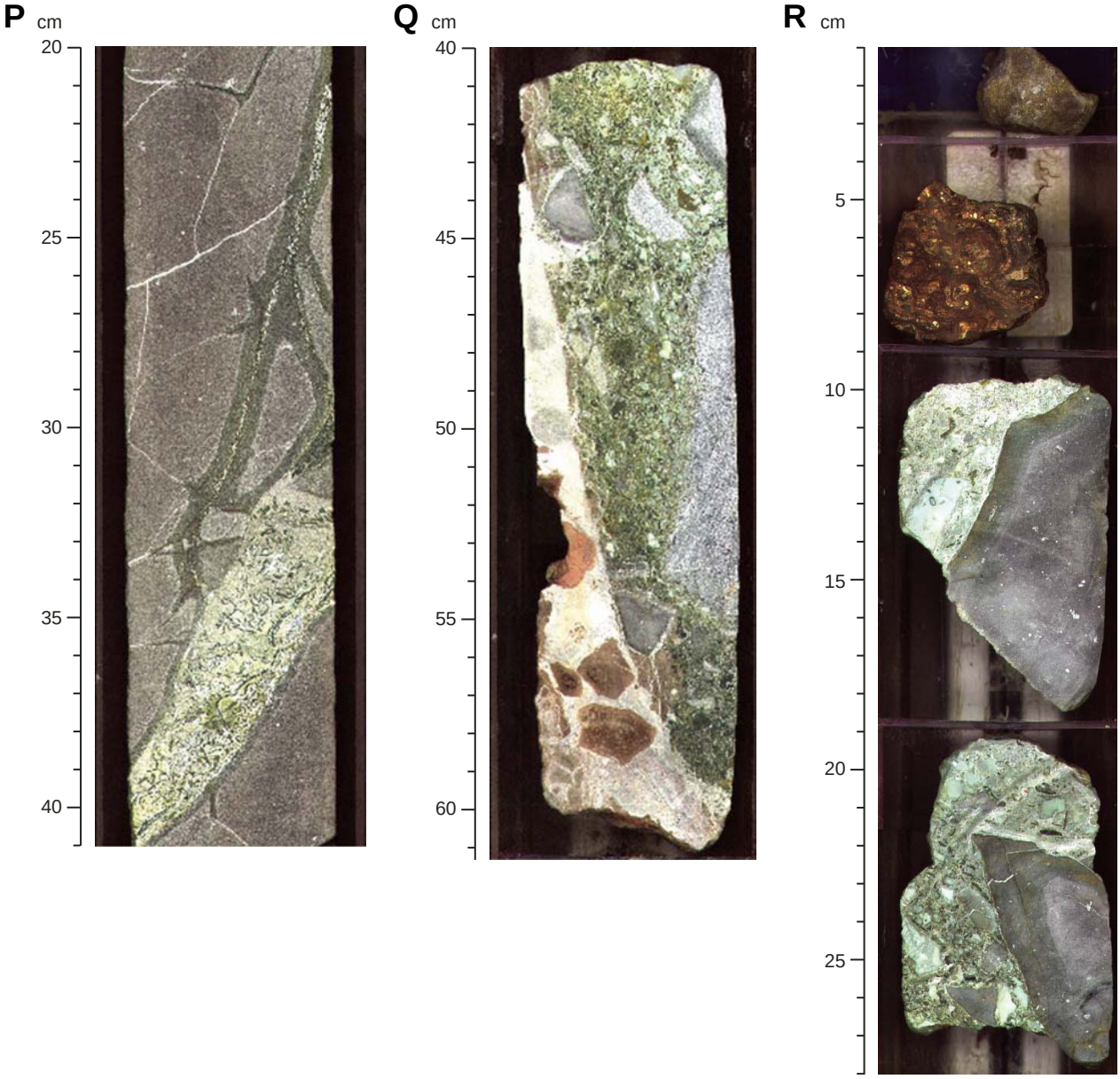

Figure F6. Photomicrographs of thin sections from the volcanic–sedimentary succession (Unit 1). Generalized stratigraphic positions are shown on Figure F3A, p. 44. **A.** Breccia-conglomerate. Detrital grains of variably altered serpentinite (sp) within a matrix of ferruginous calc-siltite (s). The matrix was later cut by fractures that were infilled by calcite spar (c). The veins tend to avoid the detrital grains and are concentrated in the fine-grained matrix (Sample 210-1277A-3R-4, 86–89 cm; same thin section as in B). Cross-polarized light. **B.** Breccia-conglomerate. Detrital serpentinite grains (sp) within a calc-siltite matrix (s), partly replaced by calcite with altered volcanic glass (ga). m = micritic carbonate. Cross-polarized light. **C.** Calc-siltite fill of neptunian fissure showing subparallel lamination (l) and compaction (c) into small depressions between detrital grains. This sample is within coarse basalt-derived volcaniclastic sediment (see Fig. F5H, p. 49). Note the relatively low angle of the primary laminations (<20°). The downward curvature of the laminations near the bottom is the result of differential compaction (Sample 210-1277A-3R-2, 105–108 cm). Plane-polarized light. **D.** Devitrified glass texture (d) within chilled selvage at the top of massive basalt Flow 2. Some calcite spar (c) is present (Sample 210-1277A-3R-2, 36–39 cm). (Continued on next two pages.)

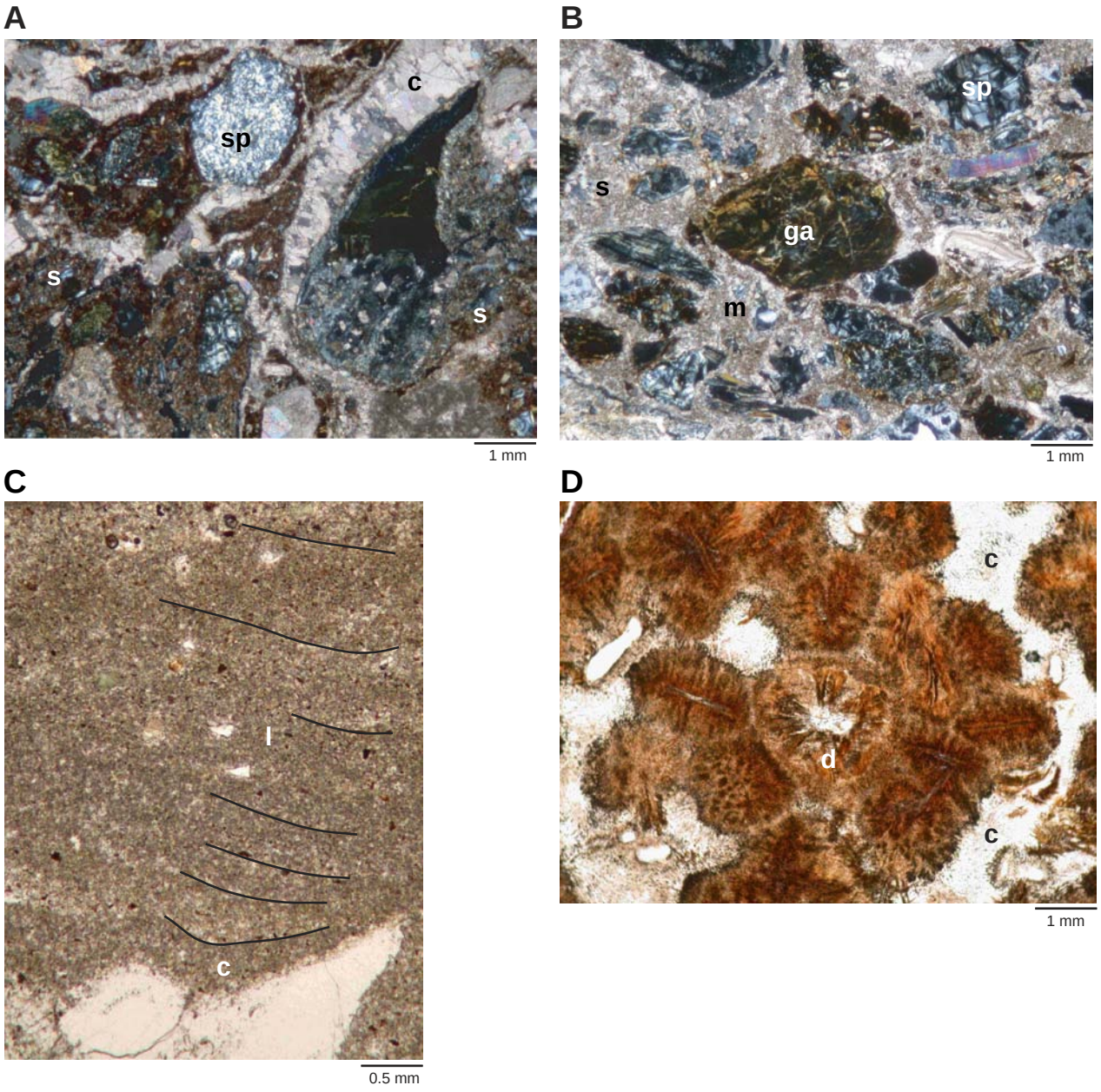

Figure F6 (continued). **E.** Hyaloclastite surrounded by calcite spar within basaltic Flow 3 (Sample 210-1277A-3R-1, 7–9 cm; same thin section as F). Cross-polarized light. **F.** Hyaloclastite (h) within calcite spar (c) within basaltic Flow 3. The spar originated as a calc-siltite that was later partially recrystallized to calcite spar. Plane-polarized light. **G.** Sheared gabbro cataclasite. Very altered feldspar porphyroblast (f) within a sheared fine-grained chloritic matrix (m) that is partly replaced by calcite (Sample 210-1277A-2R-1, 91–94 cm). Cross-polarized light. **H.** Sheared gabbro cataclasite. Plagioclase porphyroblast (pl) within a sheared matrix (m) that is partly recrystallized to calcite spar (c) (Sample 210-1277A-2R-1, 91–94 cm. Cross-polarized light. Same thin section as G. (Continued on next page.)

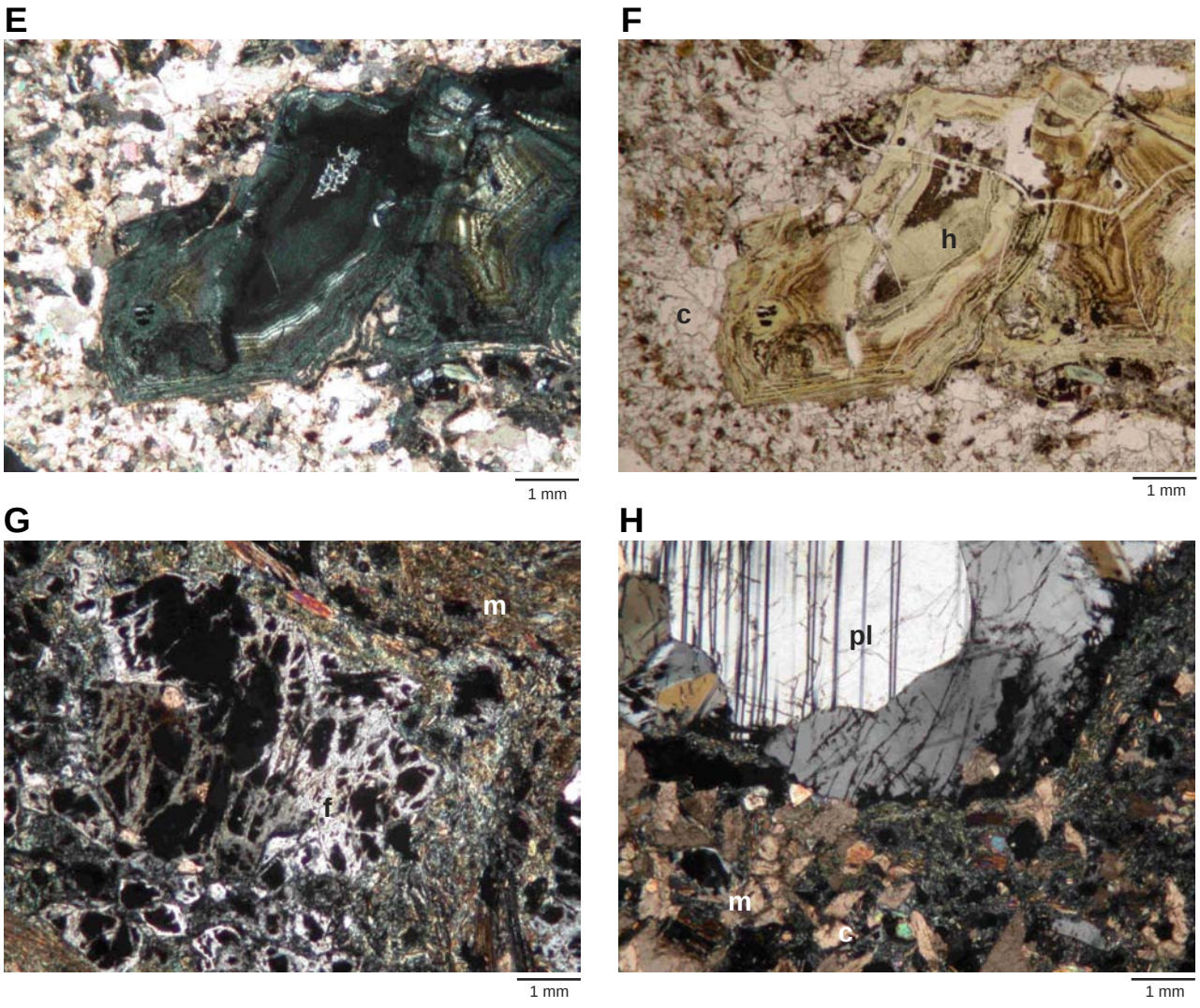

Figure F6 (continued). **I.** Detrital serpentinite grains (sp) within calc-siltite (s) (Sample 210-1277A-2R-2, 59–62 cm). Cross-polarized light. **J.** Calcite spar (c) filling vein within calc-siltite (s). The calcite contains numerous grains of serpentinite (sp), mainly replaced by calcite spar (Sample 210-1277A-1W-2, 87–90 cm). Plane-polarized light. **K.** Internal carbonate silt (calc-siltite) (s) within hyaloclastites (h) that has undergone partial dissolution to create elongate cavities that were later infilled by prismatic carbonate spar (p) (Sample 210-1277A-1W-1, 101–104 cm). Plane-polarized light. **L.** Spalled hyaloclastite (h) and calc-siltite (s) (Sample 210-1277A-1W-2, 38–41 cm). Plane-polarized light. **M.** Calc-siltite (s) and hyaloclastites (h) within the uppermost basaltic Flow 4. The calc-siltite was partly dissolved and cemented by vug-filling calcite spar (c) (Sample 210-1277A-1W-2, 38–41 cm). **N.** Vein (fracture) in altered basalt clast, infilled with pink calc-siltite (s) (Sample 210-1277A-1W-1, 36–39 cm). Gently inclined lamination is visible. Cross-polarized light.

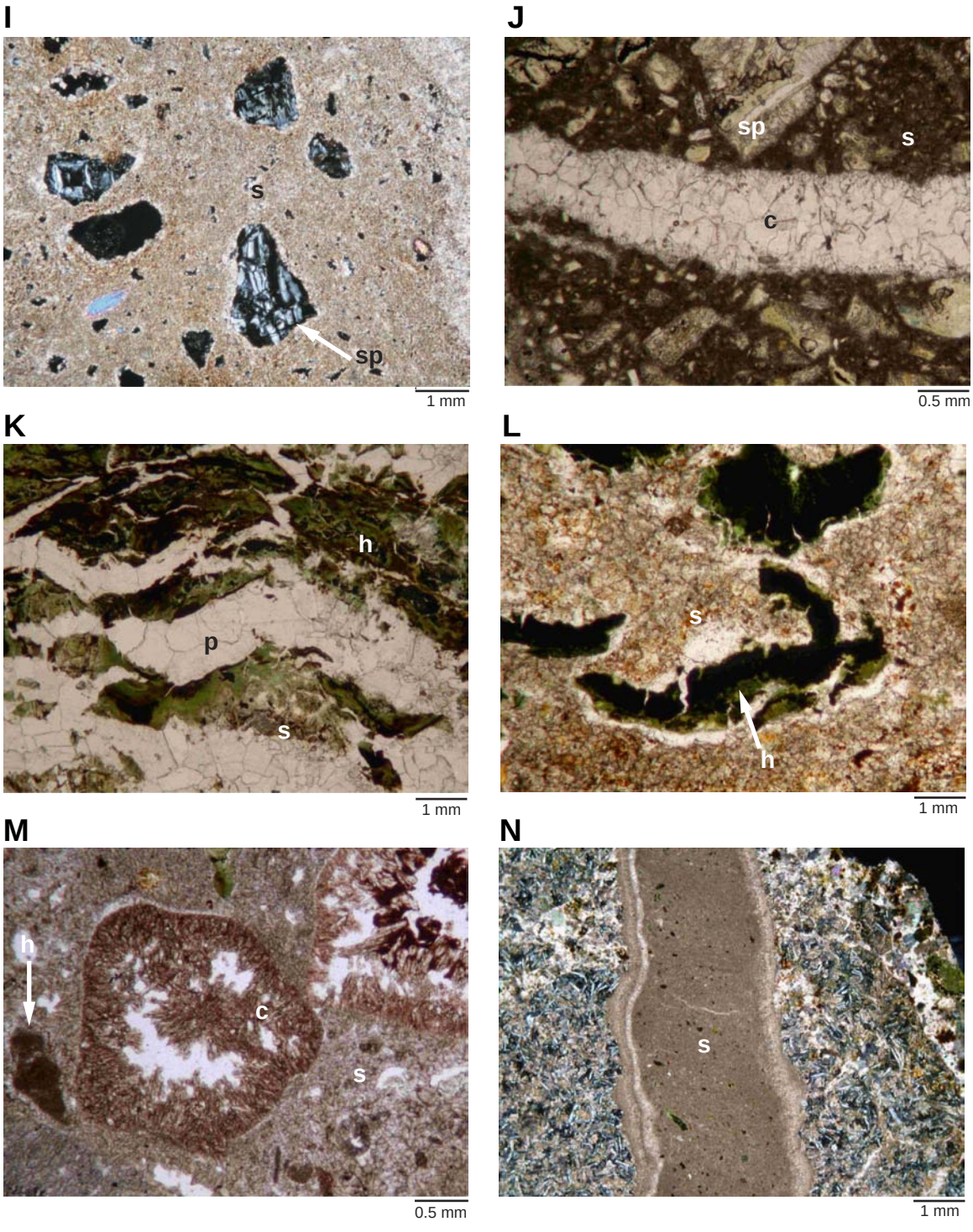

Figure F7. Zr/Ti vs. Nb/Y plot using XRF data, showing that Site 1277 basalts (solid circles) have affinities with andesite/basalt. Ti ppm is recalculated from TiO_2. Plot after Floyd and Winchester (1975). Alk-Bas = alkali basalt, Bsn/Nph = basanite/nephelenite, Com/Pant = comendite/pantellite.

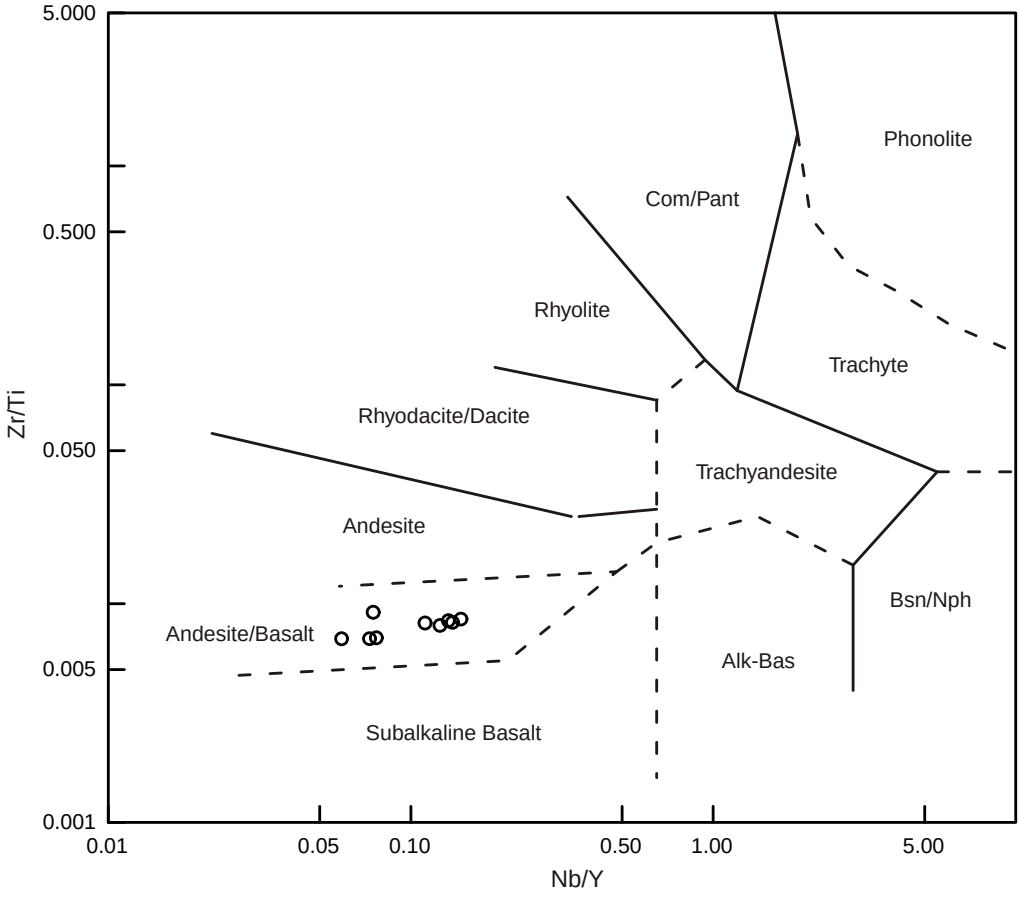

Figure F8. Geochemical discrimination diagrams for Site 1277 basalts using XRF data. TiO_2 is recalculated as Ti ppm. **A.** Zr/Y vs. Zr plot from Pearce and Norry (1979). **B.** V vs. Ti plot from Shervais (1982). ARC = volcanic arcs, OFB = ocean floor basalt. (Continued on next page.)

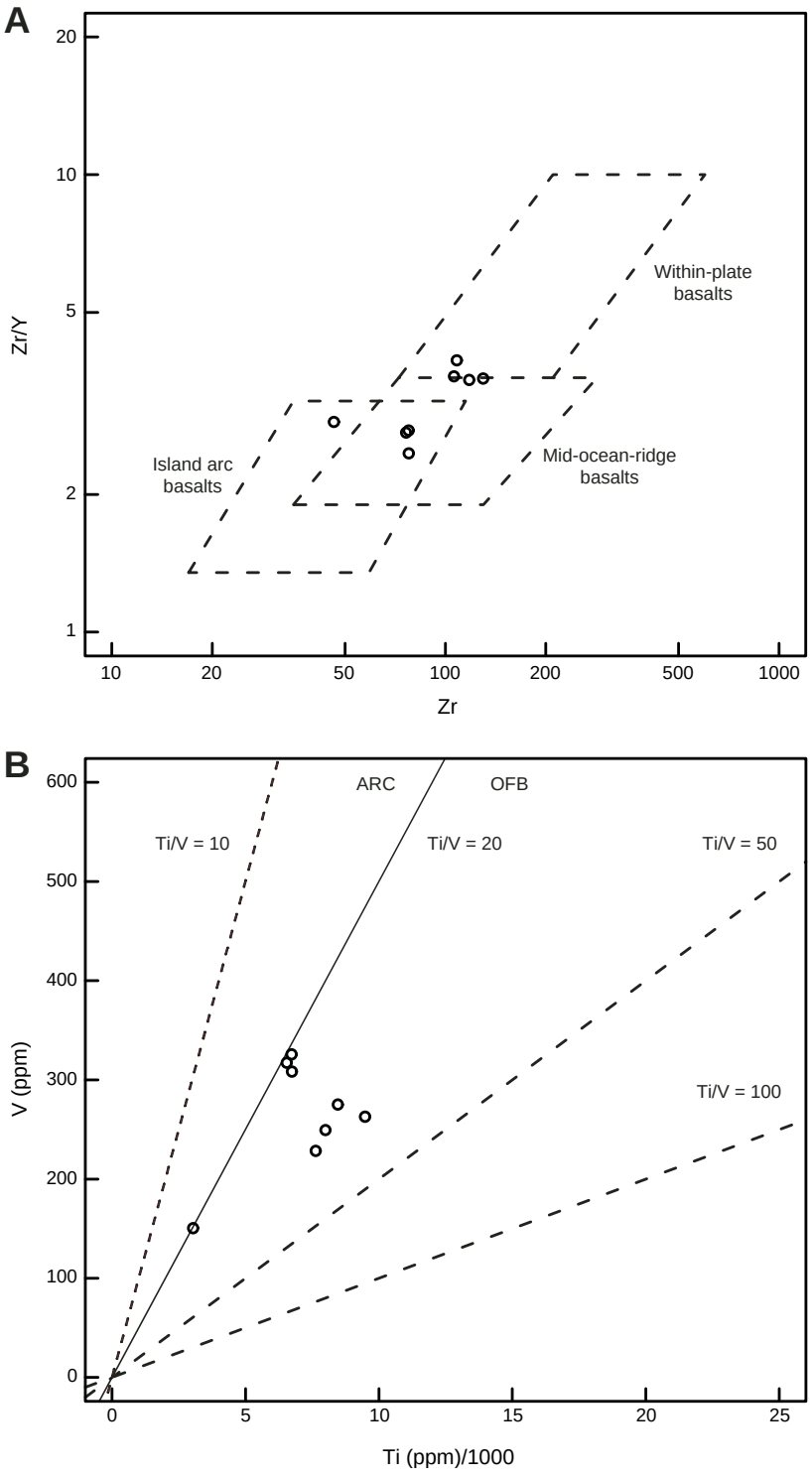

Figure F8 (continued). C. Ti/100 vs. Zr vs. 3Y. Plot from Pearce and Cann (1973). IAT = island arc tholeiite, MORB = mid-ocean-ridge basalt, CAB = calc-alkali basalt, WPB = within-plate basalt. **D.** 2Nb vs. Zr/4 vs. Y (Wood, 1980). Al and All = within-plate basalt, B = enriched mid-ocean-ridge basalt, C = within-plate basalt/calc-alkali basalt, D = normal mid-ocean-ridge basalt/calc-alkali basalt.

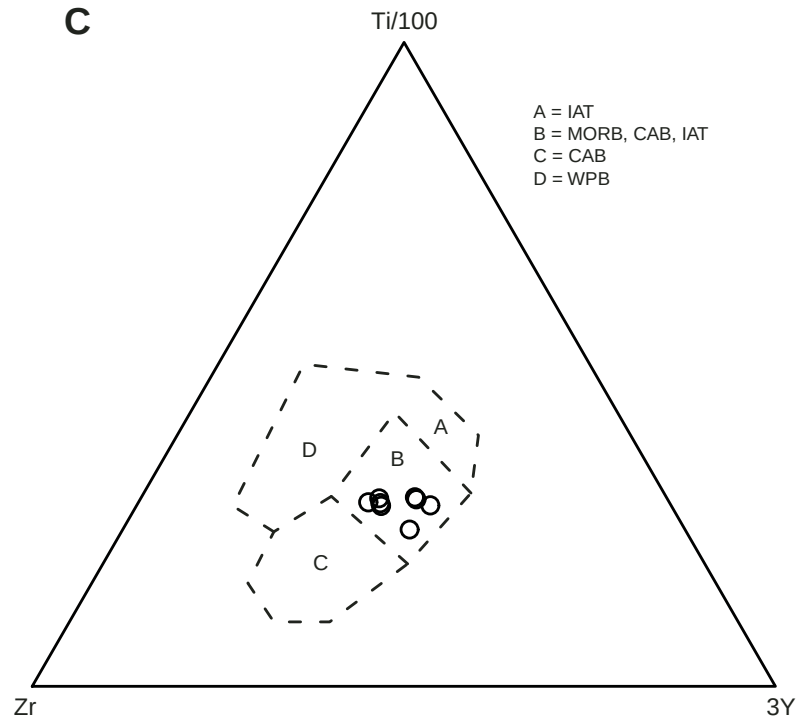

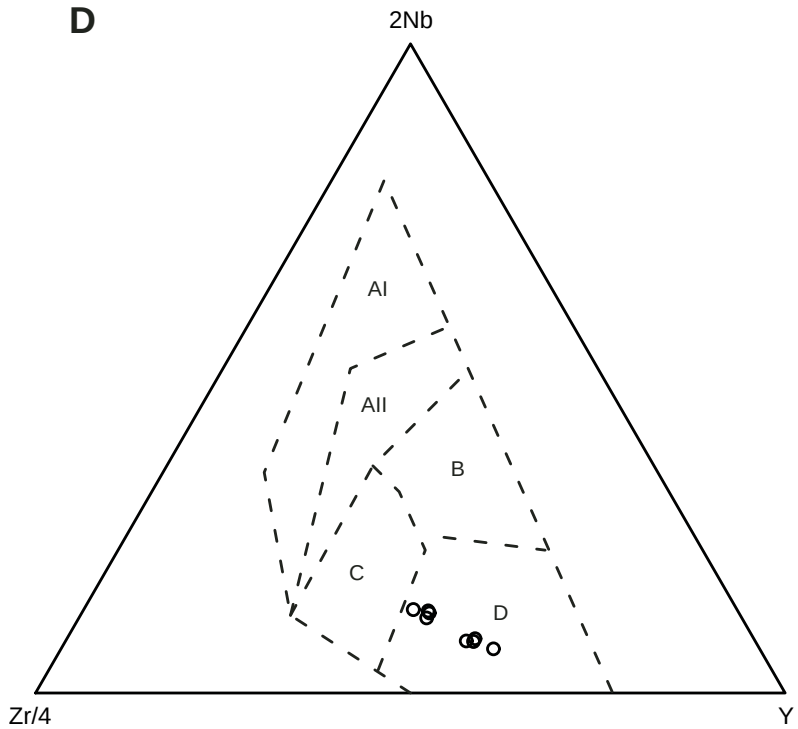

Figure F9. Normal-mid-ocean-ridge basalt (MORB) normalized multielement plots. Normalizing values in parts per million: Sr = 120, K = 1245, Rb = 2, Ba = 20, Th = 0.2, Ta = 0.18, Nb = 3.5, Ce = 10, P = 534, Zr = 90, Hf = 2.4, Sm = 3.3, Ti = 8992, Y = 30, Yb = 3.4 (Pearce, 1982). **A.** XRF data. **B.** Three least-altered basalts.

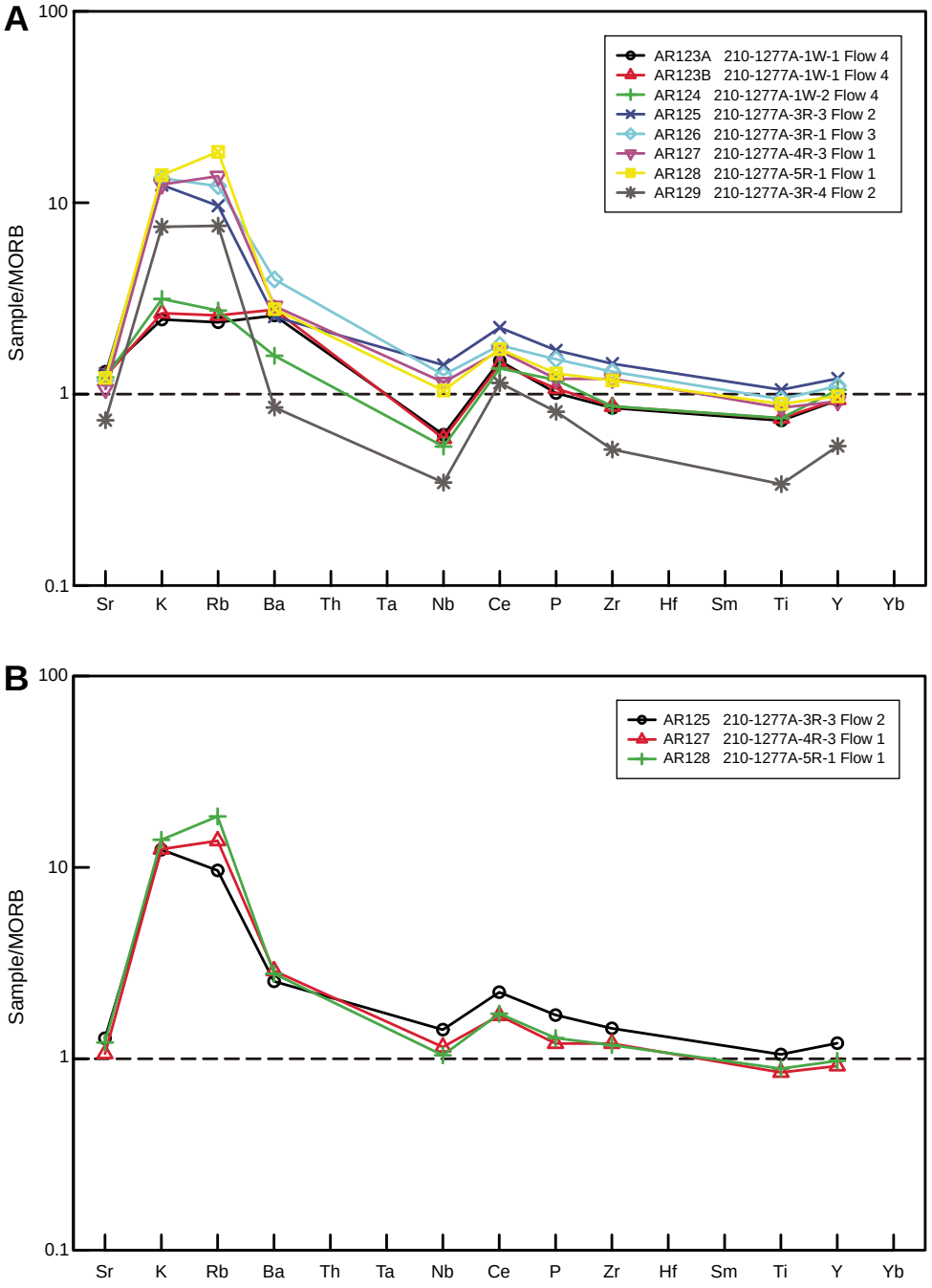

Figure F10. Selected geochemical plots using ICP-MS whole-rock basalt data. These plots supplement the data shown in Figure F8, p. 57. TiO_2 is recalculated as Ti ppm. **A.** Zr/Y vs. Zr (Pearce, 1982). **B.** Ti vs. V (Shervais, 1982). ARC = volcanic arcs, OFB = ocean floor basalt. (Continued on next page.)

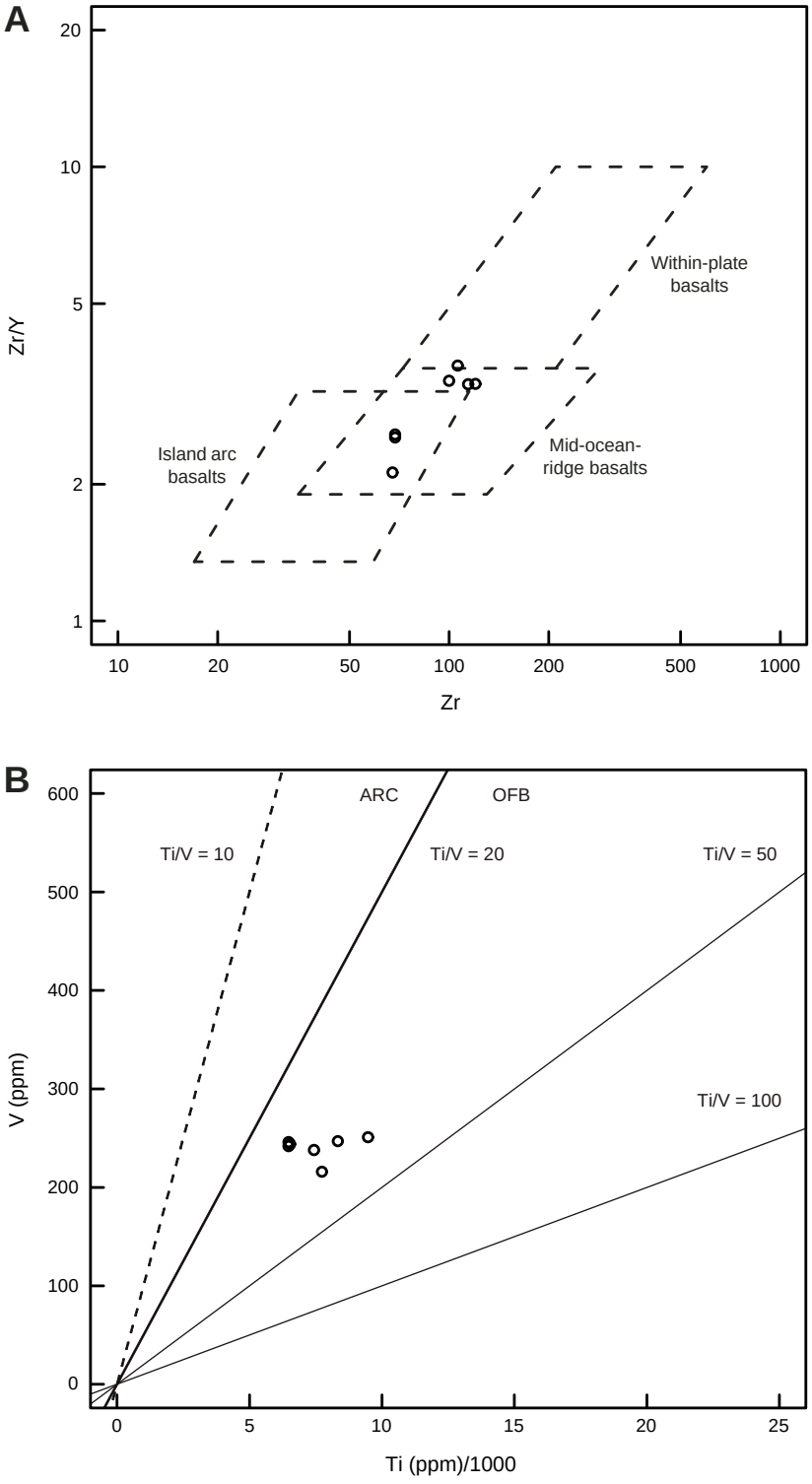

Figure F10 (continued). **C.** Ti/100 vs. Zr vs. 3Y (Pearce and Cann, 1973). IAT = island arc tholeiite, MORB = mid-ocean-ridge basalt, CAB = calc-alkali basalt, WPB = within-plate basalt. **D.** Hf/3 vs. Th vs. Ta (Wood, 1980). N-MORB = normal MORB, E-MORB = enriched MORB, WPT = within-plate tholeiite, WPA = within-plate alkaline basalt.

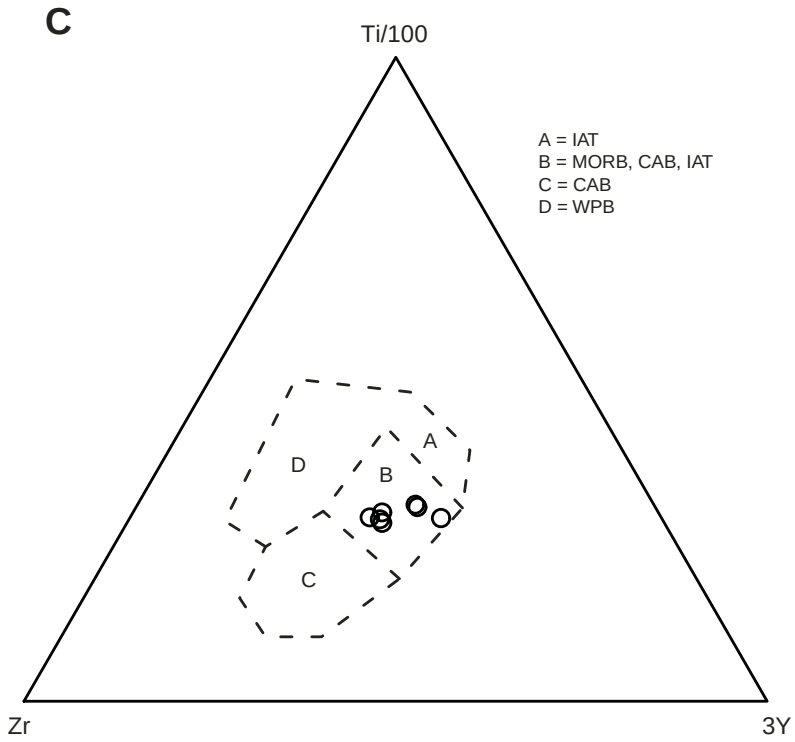

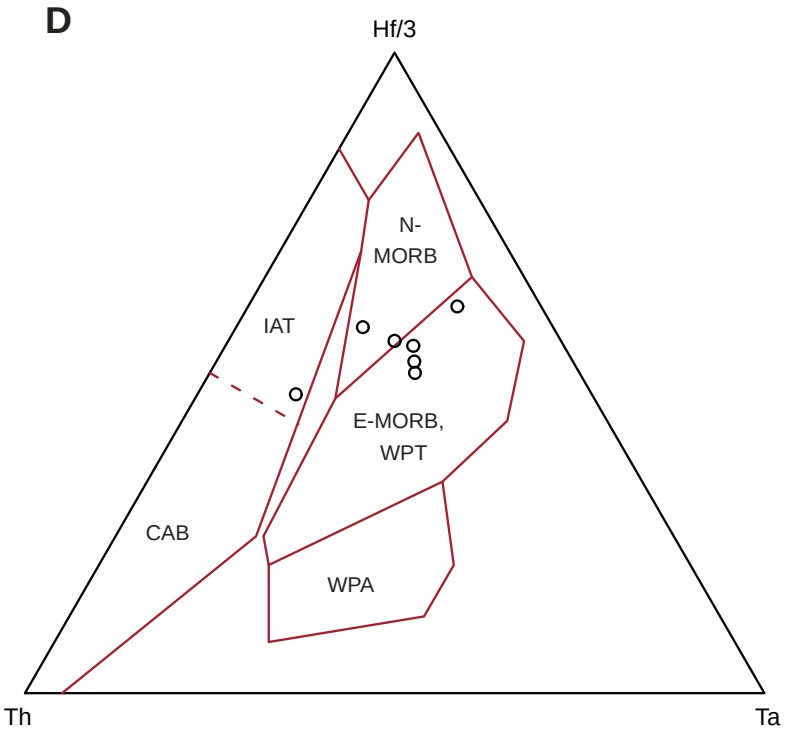

Figure F11. A. Normal mid-ocean-ridge basalt (MORB) normalized multielement diagram using ICP-MS whole-rock basalt data. These plots supplement the data shown in Figure F9, p. 59. Normalizing values in parts per million: La = 0.31, Ce = 0.808, Pr = 0.122, Nd = 0.6, Pm = 1, Sm = 0.195, Eu = 0.0735, Gd = 0.2590, Tb = 0.0474, Dy = 0.322, Ho = 0.0718, Er = 0.21, Tm = 0.0324, Yb = 0.209, Lu = 0.0322 (from Pearce, 1982). **B.** Chrondrite-normalized rare earth element (REE) patterns. Normalizing values from Boynton (1984).

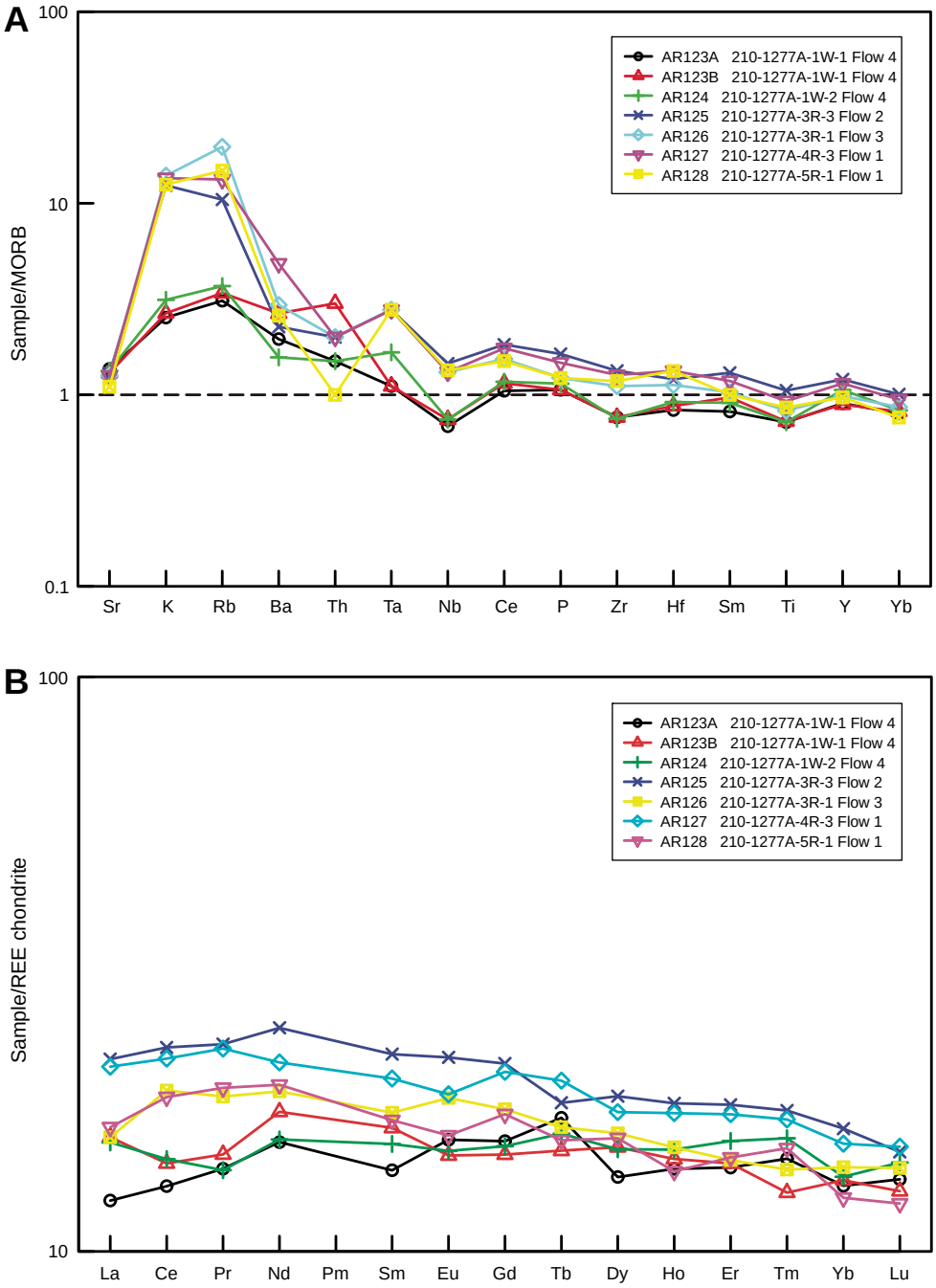

Figure F12. Nb/Y vs. Zr/Y plot using XRF data comparing the Site 1277 basalts (solid circles) with basalts from several other oceanic settings. Comparative data are from Kempton et al. (2000), other than for the Iberia margin basalts, which are from Cornen et al. (1999).

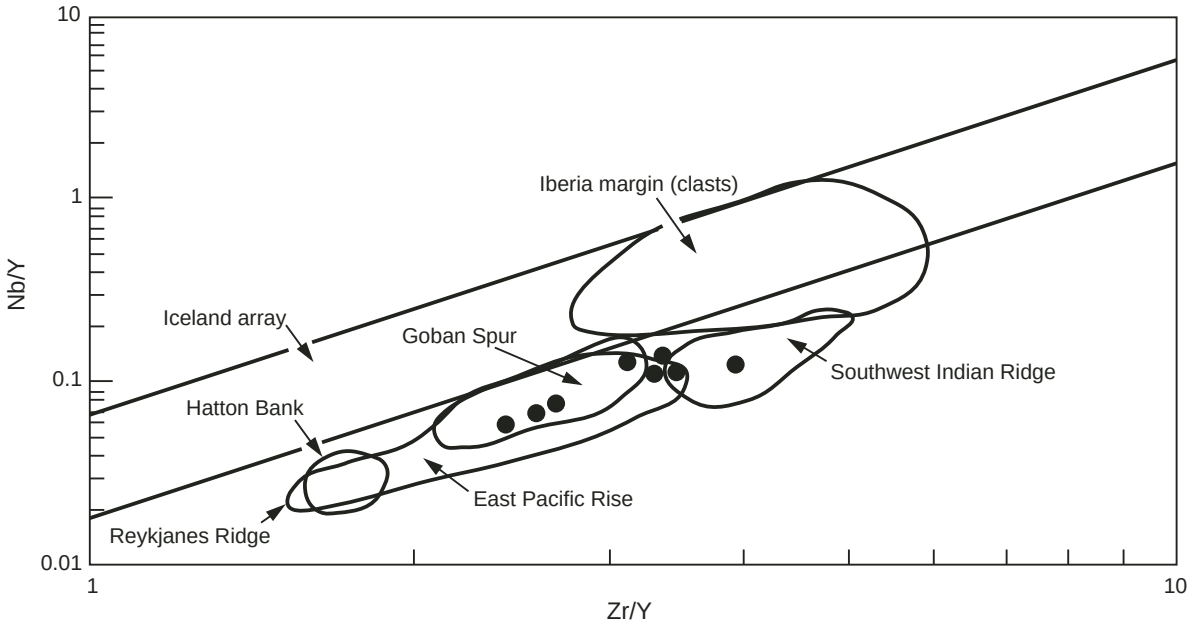

Figure F13. Comparison of the tectonic and stratigraphic relations at the top of basement, as indicated by drilling at Site 1277, the Iberia margin at Site 897C, and by outcrop evidence from the Alps (e.g., Le Chenaillet ophiolite).

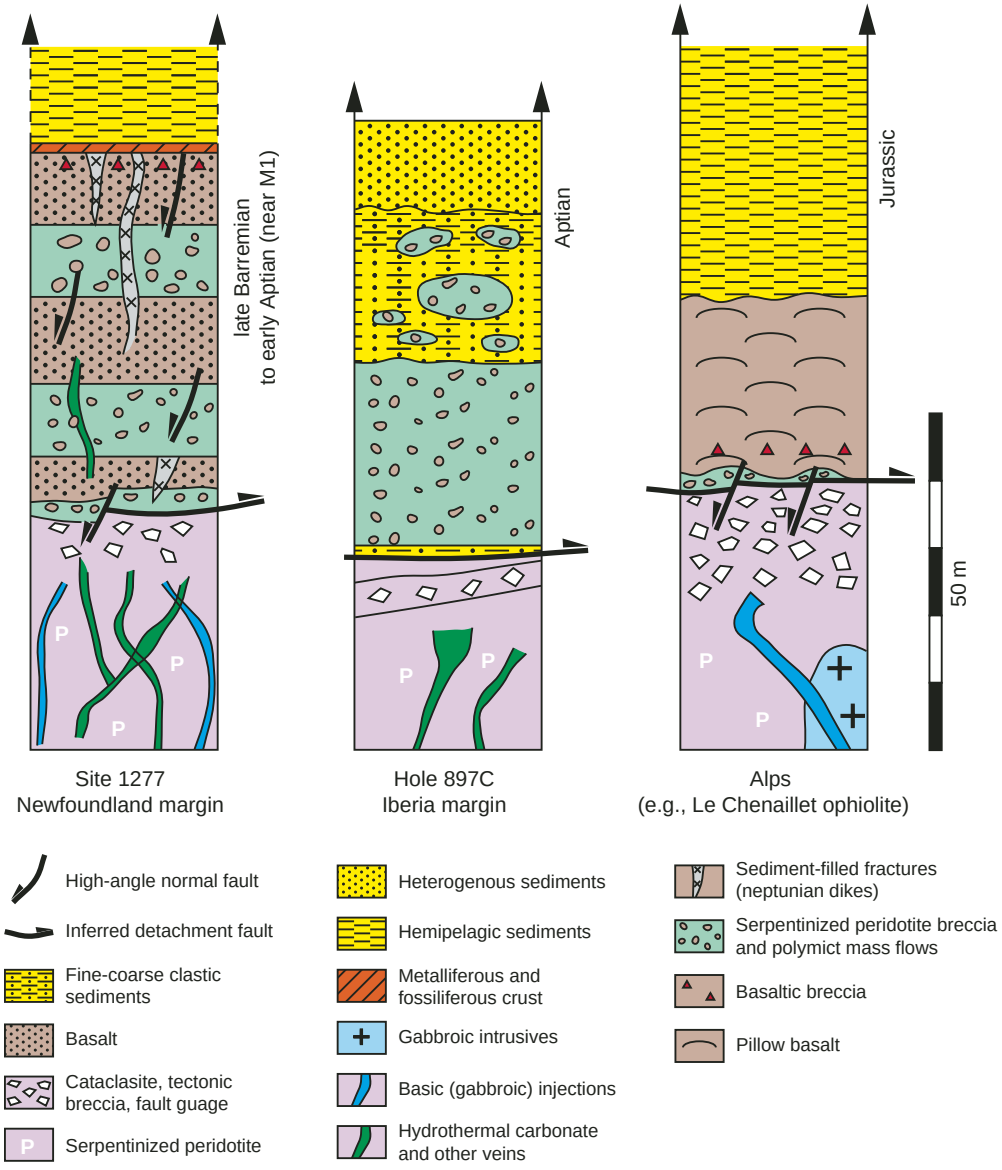

Figure F14. Interpretation of local seafloor relations at Site 1277. MOR = mid-ocean ridge.

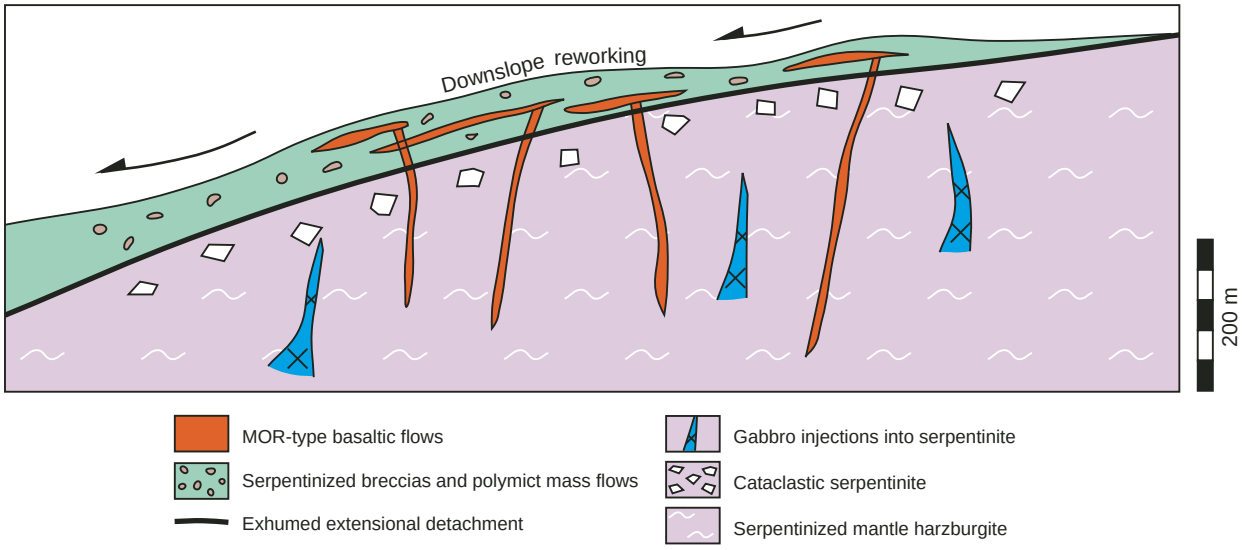

Figure F15. Tectonic model for the final stages of continental breakup documented on the distal Newfoundland margin at Site 1277, also taking account of evidence from the Iberia margin and the Alps-Apennines. A–C are seen as a continuum of processes that culminated in "normal" seafloor spreading, possibly around the Aptian/Albian boundary. Later (Albian–Cenomanian) intrusion of alkaline sills in the vicinity of Site 1276 (west of Site 1277) was probably associated with the activity of a postbreak-up thermal plume (Hart and Blusztajn, 2006; not shown here). **A.** Exhumation of subcontinental mantle lithosphere, coupled with submarine erosion of the low-angle extensional detachment and episodic eruption of mid-ocean-ridge basalt (MORB). Seismic reflection evidence indicates strong crustal thinning along the Newfoundland margin, but the westward-dipping detachment beneath continental crust is hypothetical. **B.** With continued in-plane extension, the exhumed mantle was dissected to form serpentinite ridges and intervening basins. Evidence from the Alps suggests continuing mid-ocean-ridge (MOR)-type volcanism during this stage. **C.** Final separation of brittle subcontinental mantle lithosphere and massive influx of magma to initiate "normal" seafloor spreading. (**Figure shown on next page.**)

Figure F15 (continued). (Caption shown on previous page.)

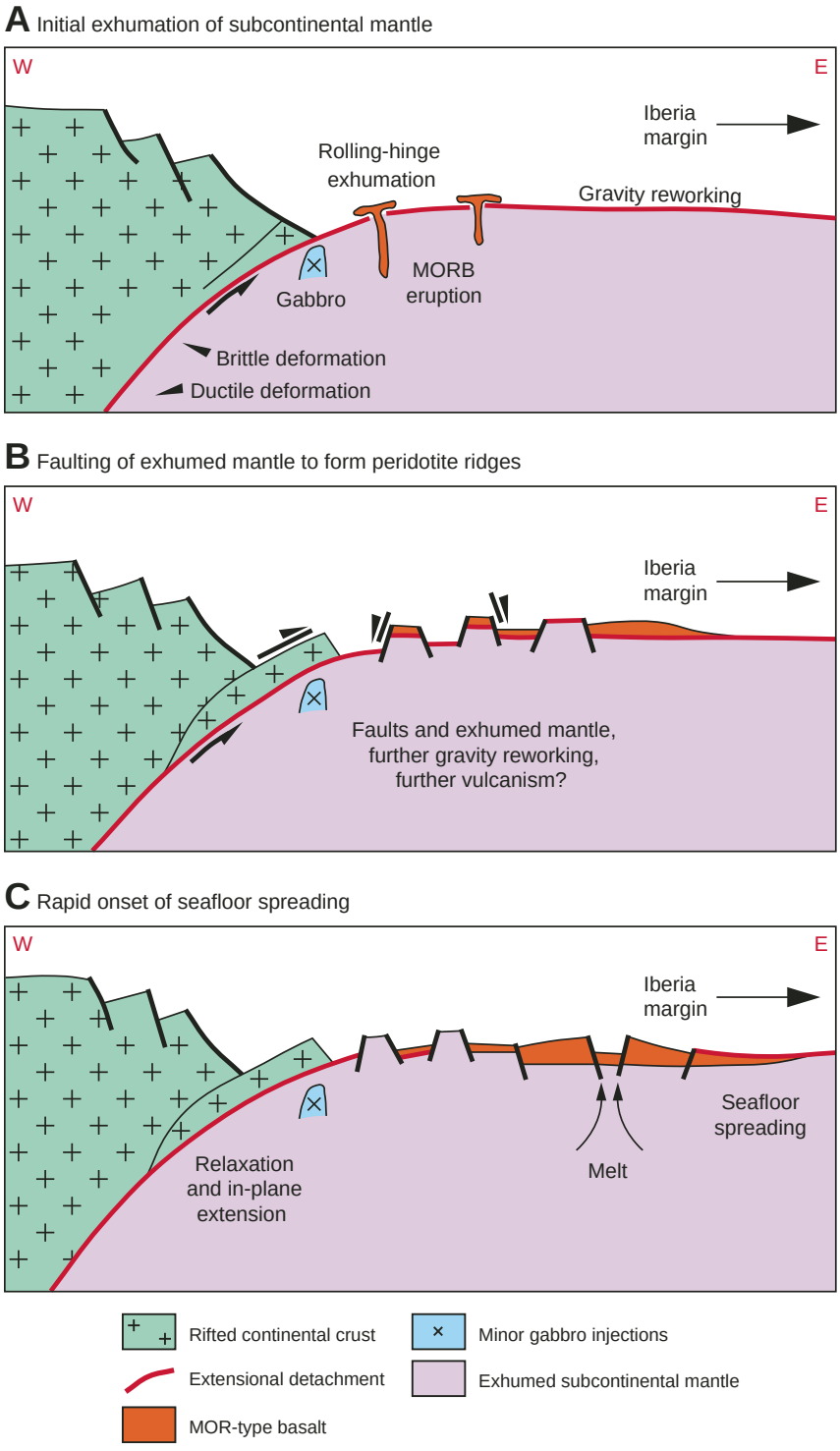

Table T1. Major and trace element analyses, Site 1277.

Core, section, interval (cm)	Depth (mbsf)	Sample number	Major element oxides (wt%)											
			SiO_2	Al_2O_3	Fe_2O_3	MgO	CaO	Na_2O	K_2O	TiO_2	MnO	P_2O5	LOI	Total
210-1277A-														
1W-1,36–39	0.93	AR123A	39.89	16.59	5.6	3.11	18.98	2.97	0.368	1.092	0.23	0.124	10.31	99.26
1W-1,36–39	0.93	AR123B	40.97	16.91	5.88	3.24	18.68	3.06	0.397	1.122	0.228	0.131	9.69	100.31
1W-2, 62–66	1.98	AR124	43.15	16.41	7.71	4.31	15.82	3.22	0.471	1.124	0.239	0.145	7.49	100.09
3R-1, 84–87	114.40	AR126	44.24	14.56	10.3	4.4	13.73	2.67	2.015	1.411	0.135	0.186	6.79	100.24
3R-3, 46–49	116.97	AR130	35.77	11.16	8.15	5	20.42	2.15	1.919	1.126	0.124	0.196	14.37	100.29
3R-1, 84–87	114.40	AR126	44.24	14.56	10.3	4.4	13.73	2.67	2.015	1.411	0.135	0.186	6.79	100.24
3R-3,131–135	117.82	AR125	48.68	15.89	9.08	5.93	9.92	2.97	1.856	1.581	0.124	0.207	3.59	99.83
3R-4, 61–65	118.57	AR129	21.55	5.47	5.63	6.51	32.12	0.86	1.123	0.507	0.152	0.099	26.37	100.29
4R-3, 2–6	125.96	AR127	48.66	15.22	8.35	8	7.49	2.77	1.865	1.273	0.097	0.147	3.45	99.01
5R-1, 52–55	133.12	AR128	49.12	15.79	9.34	6.34	9.64	3.12	2.091	1.334	0.113	0.157	3.43	100.38

Notes: LOI = loss on ignition. X-ray fluorescence analyses performed at the Institute of Earth Science, University of Edinburgh (United Kingdom), using the method specified by Fitton et al. (1998).

Table T1 (continued).

Core, section, interval (cm)	Depth (mbsf)	Sample number	Trace elements (ppm)													
			Nb	Zr	Y	Sr	Rb	La	Ce	Nd	Zn	Cu	Ni	Cr	V	Ba	Sc
210-1277A-																	
1W-1,36–39	0.93	AR123A	2.1	76.2	27.9	157.1	4.7	3.6	14.9	11.6	92.1	84.4	134.1	403.7	317.3	51.5	50.4
1W-1,36–39	0.93	AR123B	2.1	77.6	28.1	148.6	5.2	5.0	14.3	10.1	90.6	83.7	146.0	411.9	325.8	55.2	48.8
1W-2, 62–66	1.98	AR124	1.9	77.7	31.6	146.9	5.5	5.2	13.6	9.6	76.8	76.1	145.7	381.2	308.4	31.7	48.3
3R-1, 84–87	114.40	AR126	4.4	117.9	33.1	141.5	24.4	6.1	18.0	15.1	117.0	51.8	121.8	191.7	275.2	79.4	39.4
3R-3, 46–49	116.97	AR130	3.1	91.9	27.7	127.3	25.7	6.4	19.7	14.6	117.1	26.9	157.9	239.9	263.3	44.4	34.4
3R-1, 84–87	114.40	AR126	4.4	117.9	33.1	141.5	24.4	6.1	18.0	15.1	117.0	51.8	121.8	191.7	275.2	79.4	39.4
3R-3,131–135	117.82	AR125	5.0	129.8	36.2	153.7	19.3	5.7	22.3	17.5	116.7	33.7	133.2	155.1	263.0	50.8	37.7
3R-4, 61–65	118.57	AR129	1.2	46.3	16.1	87.7	15.2	6.3	11.4	10.0	71.3	28.0	451.3	810.0	150.6	17.0	25.0
4R-3, 2–6	125.96	AR127	4.0	108.2	27.5	127.5	27.5	4.9	16.8	12.6	85.4	54.4	290.3	209.2	228.5	57.6	31.5
5R-1, 52–55	133.12	AR128	3.7	106.1	29.3	145.9	36.9	5.3	17.2	12.2	76.6	40.5	152.2	232.0	249.4	55.6	34.1

Table T2. Major, trace, and rare earth element analyses, Site 1277.

Core, section, interval (cm)	Depth (mbsf)	Sample number	*N*	Major element oxides (wt%)														Trace and rare earth elements (ppm)				
				SiO_2	Al_2O3	Fe_2O_3	MgO	CaO	Na_2O	K_2O	TiO_2	P_2O_5	MnO	Cr_2O3	Total C	Total S	Total	Ni	Sc	Be	Co	Cs
210-1277A-																						
1W-1,36–39	0.93	AR123A	65	39.13	16.52	5.58	3.13	18.84	2.92	0.38	1.08	0.13	0.22	0.044	3	0.05	99.99	119	37	<1	45.8	0.3
1W-1,36–39	0.93	AR123B	66	39.75	16.66	5.82	3.28	18.52	2.97	0.4	1.09	0.13	0.21	0.044	2.83	0.06	100	129	37	<1	48.9	0.3
1W-2, 62–66	1.98	AR124	67	42.22	16.61	7.49	4.42	15.76	3.11	0.47	1.08	0.14	0.23	0.045	2.04	0.06	100	136	36	<1	55.2	<0.1
3R-1, 84–87	114.40	AR126	70	42.83	14.83	9.92	4.46	13.31	2.59	2.03	1.39	0.18	0.13	0.023	1.58	0.02	100.01	98	33	<1	35.5	0.5
3R-3,131–135	117.82	AR125	68	47.25	16.14	8.95	6.08	9.83	2.82	1.86	1.58	0.2	0.12	0.021	0.54	0.01	99.87	108	36	1	46.3	0.2
4R-3, 2–6	125.96	AR127	71	49.65	15.65	8.38	8.35	7.52	2.75	1.88	1.29	0.15	0.1	0.037	0.18	0.01	100	280	32	<1	50.1	1.4
5R-1, 52–55	133.12	AR128	69	47.86	15.77	9.03	6.37	9.53	2.99	2.09	1.24	0.15	0.11	0.034	0.48	0.01	100	140	33	1	42.9	3.4

Notes: *N* = ACME laboratory sample number. Whole-rock inductively coupled plasma–mass spectrometry analyses performed at the ACME Analytical Laboratories, Ltd., Vancouver (Canada), utilizing an in-house method.

Table T2 (continued).

Core, section, interval (cm)	Depth (mbsf)	Sample number	*N*	Trace and rare earth elements (ppm)																		
				Ga	Hf	Nb	Rb	Sn	Sr	Ta	Th	U	V	W	Zr	Y	La	Ce	Pr	Nd	Sm	Eu	Gd	Tb
210-1277A-																								
1W-1,36–39	0.93	AR123A	65	15.5	2	2.4	6.2	3	163.9	0.2	0.3	3.1	242	30.7	68.7	27.1	3.8	10.5	1.7	9.3	2.7	1.15	4.03	0.81
1W-1,36–39	0.93	AR123B	66	14.4	2.1	2.6	6.8	1	156.1	0.2	0.6	3.2	244	15.4	68.7	26.7	4.9	11.5	1.8	10.5	3.2	1.08	3.82	0.71
1W-2, 62–66	1.98	AR124	67	15.4	2.2	2.6	7.4	<1	160.5	0.3	0.3	2.2	246	36.1	67.5	31.8	4.8	11.7	1.69	9.4	3	1.1	3.95	0.76
3R-1, 84–87	114.40	AR126	70	15.8	3.2	4.6	26.6	1	150.8	0.5	0.4	0.2	247	11.6	114.2	34.4	6.5	17.5	2.75	12.8	3.9	1.38	5.32	0.94
3R-3,131–135	117.82	AR125	68	17.7	2.9	5.1	20.9	1	155.5	0.5	0.4	0.2	251	27.7	120.1	36.1	6.7	18.3	2.8	14.7	4.3	1.6	5.5	0.86
4R-3, 2–6	125.96	AR127	71	15.9	3.2	4.7	29.6	1	132.1	0.5	0.2	0.3	216	18.2	106.2	29.1	5.1	15	2.35	11.7	3.3	1.17	4.49	0.74
5R-1, 52–55	133.12	AR128	69	15.8	2.7	4.6	39.4	1	151.6	0.5	0.4	0.4	238	35.7	100	29.6	4.9	15.4	2.27	11.4	3.4	1.36	4.58	0.78

Table T2 (continued).

Core, section, interval (cm)	Depth (mbsf)	Sample number	*N*	Trace and rare earth elements (ppm)																		
				Dy	Ho	Er	Tm	Yb	Mo	Cu	Pb	Zn	Ni	As	Cd	Sb	Bi	Ag	Au	Hg	Tl	Se	Lu
210-1277A-																						
1W-1,36–39	0.93	AR123A	65	4.34	1	2.94	0.47	2.72	0.6	77.1	2.1	72	102.7	5.3	0.2	0.1	<0.1	<0.1	<0.5	0.01	0.1	<0.5	0.43
1W-1,36–39	0.93	AR123B	66	4.89	1.04	2.99	0.41	2.78	0.7	79	1.8	72	113.2	5.1	0.2	0.1	<0.1	<0.1	2	<0.01	0.1	<0.5	0.41
1W-2, 62–66	1.98	AR124	67	4.85	1.08	3.27	0.51	2.82	0.2	72.2	0.8	53	124.9	1.7	0.1	0.1	<0.1	<0.1	2.5	0.02	0.1	<0.5	0.46
3R-1, 84–87	114.40	AR126	70	5.63	1.25	3.64	0.55	3.22	20.2	43.2	0.7	79	94.7	2.7	0.1	<0.1	<0.1	<0.1	<0.5	<0.01	<0.1	<0.5	0.49
3R-3,131–135	117.82	AR125	68	6	1.3	3.78	0.57	3.42	0.2	26.2	0.5	78	104.9	<0.5	0.1	<0.1	<0.1	<0.1	1.8	0.01	<0.1	<0.5	0.48
4R-3, 2–6	125.96	AR127	71	5.07	0.99	3.06	0.49	2.59		48.1	0.4	63	245.2	1.5	<0.1	<0.1	<0.1	<0.1	0.7	<0.01	0.1	<0.5	0.39
5R-1, 52–55	133.12	AR128	69	5.17	1.09	3.03	0.45	2.93	0.1	37.3	0.3	56	125.3	2.4	0.1	<0.1	<0.1	<0.1	<0.5	0.01	<0.1	<0.5	0.45